UNIVERSITÀ DEGLI STUDI DI PALERMO
Dottorato di ricerca in Biomedicina e Neuroscienze – indirizzo Oncobiologia Sperimentale
Dipartimento di Biomedicina Sperimentale e Neuroscienze Cliniche (BioNec)
SSD BIO/10

Development of different nanosystems for *drugs* and *siRNA delivery*

IL DOTTORE
SIMONA CAMPORA

IL COORDINATORE
PROF. RENZA VENTO

IL TUTOR
PROF. GIULIO GHERSI

CO TUTOR
PROF. PETER GRIFFITHS

CICLO XXVI
ANNO CONSEGUIMENTO TITOLO 2016

Ministero dell'Istruzione dell'Università e Ricerca

UNIVERSITA' DEGLI STUDI DI PALERMO

Department of Biomedicina Sperimentale e Neuroscienze Cliniche (BioNeC)

PhD programme in Biomedicine and Neuroscience- Experimental tumour biology

SSD BIO/10

Development of different nanosystems for *drugs* and *siRNA delivery*

Director of PhD programme
Prof.ssa Renza Vento

PhD Thesis by:
Simona Campora

Supervisors
Prof. Giulio Ghersi

Co-supervisor
Prof. Peter Griffiths

CICLO XXVI: 2013-2015

Summary

Abstract 5
Introduction 7
Nanoscience and Nanotechnology 8
Nanoparticles 9
Inorganic nanoparticles 10
Organic nanoparticles 11
Drug Delivery system 14
Project of nanoparticles 16
Nanoparticles targeting 18
Passive targeting 19
Active targeting 21
Cellular uptake 27
Controlled drug release 29
Extended release 31
Stimuli-Responsive Release 32
Aim of the project 38
Materials And Methods 40
Cell culture 41
Nano-conjugates 41
INULIN and PHEA nanosystems 44
Cytotoxicity studies 44
Quantitative uptake by flow cytometry 45
Qualitative uptake by fluorescence microscopy 46
Co-culture experiments 46
Analysis of PHEA-EDA-P,C-FITC-Doxo internalization mechanisms. 47
Lysosomal-specific PHEA-EDA-P,C-Doxo localization studies 48
PVP nanogels 49
Small interference RNA (siRNA) 49
Transfecting siRNA into mammalian cells using Lipofectamine 49
Conjugation of siRNA to PVP nanogels 50
Treatment with PVP-siRNA complex 51
Treatment with PVP-AEDP-siRNA complex 51
Extraction of soluble proteins 51
Western Blot assay 52

RGO, RGOY and RGOY-siRNA systems 54
Sterilization of RGO, RGOY and RGOY-PVP 54
Characterization of RGO and RGOY 54
Biocompatibility of RGO and RGO-PVP 55
Uptake studies by confocal microscopy 56
Results and discussion 57
INU-EDA-P,C-DOXO 58
Cytotoxicity of INU-EDA-P,C-Doxo 59
Qualitative uptake by fluorescence microscopy 61
Quantitative uptake by flow cytometry 63
PHEA-EDA-P,C-DOXO 67
Cytotoxic studies of cells treated with PHEA-EDA-P,C-DOXO 67
PHEA-EDA-P,C-FITC-Doxo localization studies by fluorescence microscopy 69
PHEA-EDA-P,C-FITC-Doxo localization studies by flow cytometry 71
Co-culture experiments. 74
PHEA-EDA-P,C-FITC-Doxo internalization mechanisms. 76
Specific localization studies 79
PVP nanogels 83
Egr-1 pathway and Egr-1 silencing by siRNA 84
Bcl-2 silencing by siRNA 89
GRAPHENE 92
Sterilization and characterization of RGO systems. 92
Biocompatibility of sterile RGO systems 94
RGO conjugated to an antibody: RGOY 95
Cellular biocompatibility and uptake studies of RGOY-AF 98
RGOY-siRNA systems 101
RGOY-PVP systems 103
Conclusion 105
Bibliography 113

Abstract

Cancer is one of the leading causes of death in the world. Over the past several decades, the development of engineered nanosystems for targeted drug delivery have received great attention thanks to their possibility to overcome the limitations of classical cancer chemotherapy including poor solubility, targeting incapability, nonspecific action and, consequently, systemic toxicity.

In this contest, four different models of nanocarriers have been analysed and compared for their capacity to target tumour tissue and to release the therapeutic agent in a controlled way: **INU-EDA-P,C-DOXO**; **PHEA-EDA-P,C-DOXO**; **PVP-siRNA** and **RGO-siRNA.**

Inulin and PHEA were conjugated to the antineoplastic drug doxorubicin through a citraconylamide bridge used as a pH sensitive spacer and their different action in normal and tumour cells was compared by viability assay, fluorescence microscopy and flow cytometric analysis. The data revealed a higher effect against the cancer cells probably due to the higher capability to enter the cancer cells respect to the healthy ones, but also due to a partial drug release in tumour microenvironment, that presents a lower pH (6.5) respect to normal tissue (7.4). Because of the better efficiency of PHEA-EDA-P,C-DOXO, its preferential uptake into tumour cells was further demonstrated through co-culture experiments. Moreover, cellular internalization mechanism studies suggested a model in which the polymer would enter the cells through a caveolae-mediated endocytosis and would be steered toward lysosomal compartment where the drug would be released and become free to go into the nucleus.

On the other hand, siRNA delivery was investigated comparing other two kind of nanosystems: PVP and Graphene nano-complexes conjugated with siRNA against Egr-1 (a transcription factor involved in the progress of the tumour) and Bcl-2 (a protein related with the apoptotic pathway in cancer cells). They are very different complexes, each with specific properties that would influence differently their ability as siRNA delivery system.

Data relative to PVP nanogel showed it as a good candidate for siRNA delivery because it binds siRNA without any functional alteration or degradation. Moreover, the addition of a glutathione sensitive linker permitted a higher amount of siRNA released through a controlled way. Even graphene nanosystems have displayed good features as nanocarriers

thanks to their biocompatibility and their ability to be internalized by cells. Furthermore, their bidimensional nature would permit to conjugate a large amount of oligonucleotides.

All the complexes analysed showed specific features that make them good candidates for drug or siRNA delivery. The choice of the best nanosystem is depending on the target site and on the therapeutic agent conjugated. PHEA nanopolymers present better characteristics for doxorubicin delivery compared with those of Inulin. On the other hand, the hydrogel nature of PVP and the bidimensional structure of graphene can minimize the typical degradation problems of the oligonucleotides and, therefore, offer the best conditions for siRNA delivery.

Moreover, the possibility to release biological molecules in controlled way (mediated by pH or Glutathione) and to recognize the specific tumour target allow to overcome the typical limits of the classic cancer therapy.

Introduction

Nanoscience and Nanotechnology

Nanoscience represents one of the most interesting field of modern science, with a highly interdisciplinary character, indeed it develops by the mix of different doctrines like chemistry, biology, physics and engineering, taking advantage of their principles and of their processes. It is based on understanding and knowledge of the matter properties on nanometric scale (between 1 and 100 nm). The realization of materials, systems and apparatuses on this size scale determines the nanotechnology (Ahmad Gatoo *et al.*, 2014).

The term "nanotechnology" was first defined by Norio Taniguchi of the Tokyo Science University in 1974 (Taniguchi, 1974). In the 1980s, the idea of nanotechnology as deterministic, rather than stochastic, handling of individual atoms and molecules was conceptually explored in depth by Dr. K. Eric Drexler that called it Molecular Nanotechnology (MNT) (Drexler, 1986). It is a constantly evolving field that finds application in many productive sectors, in fact, it is widespread the use of nanoparticles for cosmetics, coating and paints, but also for high tech with the production of nano-hard disks or memory chips. One of the major applications concerns the biomedical environment (Nanomedicine) principally for tissue engineering (Van Vlierberghe *et al.*, 2011) and drug delivery system (DDS) (Ranganathan *et al.*, 2012; Tiwari, 2012). Nanosystems (1-100nm) can be design as vehicles for biological molecules like drugs capable of going inside cells with a size between 1 and 100 µm (Figure 1). The size comparison between all the cellular components and the nanoparticles (NPs) can give an idea of their potentiality especially for the cure of many diseases like tumours. Furthermore, their very small size confers them specific properties, because they are subjected to physical laws that are in the middle between classical and quantum physics (Papazoglou, 2007).

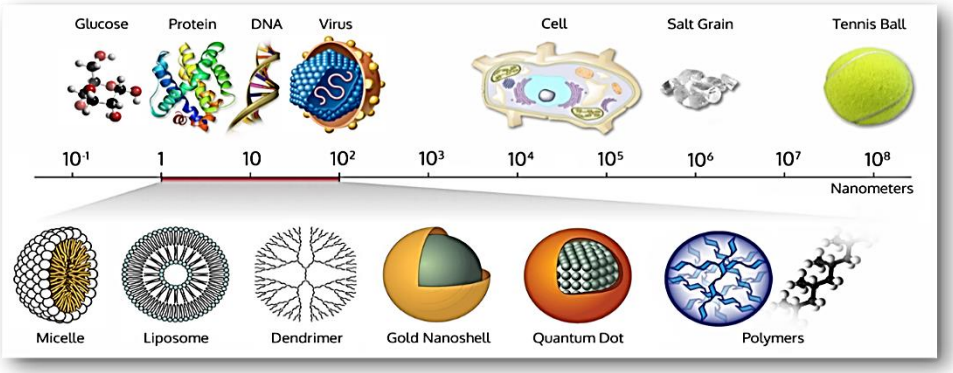

Figure 1. Dimensional scale from nanoscopic to macroscopic. Cell presents a diameter between 1 and 100 µm, while nanoparticles between 1 and 100 nm.

The engineered nanomaterials can be synthetized by two different approaches that can be also used in complementary way (Figure 2):

- Top down: it is a physical approach that consists on the reduction of macrostructures named *bulk materials* through procedures of incisions, grindings and cuttings (Nagavarma *et al.*, 2012).
- Bottom up: it is a chemical approach that brings to NPs production starting from atoms or molecule aggregates. This is the typical synthesis mechanism adopted in biomedical field because it permits a specific control of the process in order to obtain nanostructures with the desired properties.

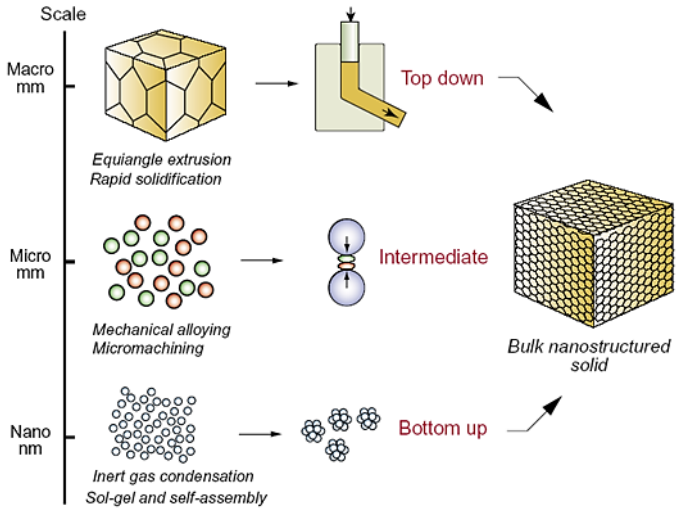

Figure 2. Representation of Top-down and Bottom-up processes for the nanomaterials synthesis.

Nanoparticles

Nanoparticles (NPs) are dispersion solution of atomic aggregates or solid particles with a size between 1 and 300 nm. They can be constituted by different materials and can assume both irregular of regular shapes like cube, sphere, rod or plate (Salata, 2004).

The possibility to engineer their surface permits multifunctional applications especially in clinical environment for diagnosis and therapies (Siddiqui *et al.*, 2015; Haun *et al.*, 2010; Srikanth *et al.*, 2012), but also for bio-localization studies (*bioimaging*) through conjugation with fluorescence probes (Xing *et al.*, 2014).

Depending on the nanoparticles' nature, it is possible to classify them in inorganic or organic NPs (Jesus and Grazu, 2012) (Figure 3).

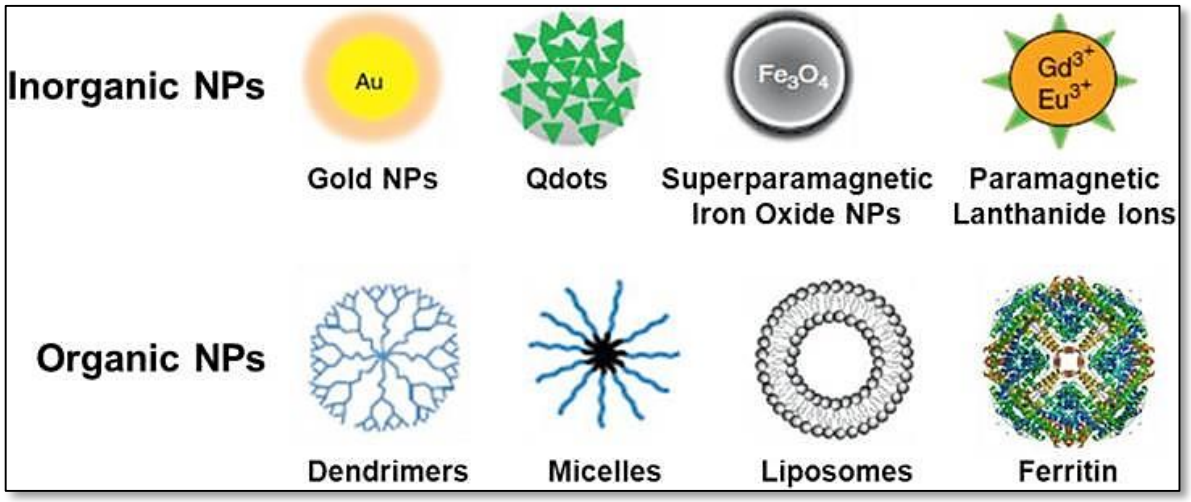

Figure 3. Schematic representation of inorganic and organic nanoparticles.

Inorganic nanoparticles

Inorganic nanoparticles play a fundamental role in modern materials science due to their unique physical characteristics like size-dependent optical, magnetic, electronic, and catalytic properties. They can be easily and cheaply synthesized and mass produced, and for this reason, they can also be more readily used for many applications. These inorganic nanoparticles include iron oxides, gold, silver, silica, quantum dots (QDs) and second harmonic generation (SHG) particles (Ladj *et al.*, 2013). The Quantum dot is a crystal of semiconductor material whose diameter is about several nanometers (from 1 to 100 nm). Its optical properties vary depending of its size so that it can emit different fluorescence (Ryman-Rasmussen *et al.*, 2006). Indeed, when the metallic nanoparticles (MNPs) are lit up with a beam of light, the oscillating electric field induces the movement of the electrons with consequent special optical phenomena (Siddiqui *et al.*, 2015).

The more used metals for the development of NPs are those noble like gold, silver or copper with a diameter around 100 nm (Okuzaki *et al.*, 2013). In recent years, gold nanoparticles (AuNPs) have been object of interest for cancer research because of their easy synthesis and surface modification, and tunable optical properties (they show strong surface plasmon resonance bands in the visible region) as well as excellent biocompatibility with the

biological systems (Huang et El-Sayed, 2010). On the other hand, silver NPs can be exploited for their antibacterial and antifungal properties (Prucek *et al.*, 2011), while magnetic NPs are largely used for applications in site specific treatments such as targeted drug delivery, localized heating of cancerous cells (hyperthermia), and magnetic resonance imaging (MRI) contrast enhancement (Frey NA *et al.*, 2009).

Organic nanoparticles

In the last years, many researchers have focused their studies on the possible use of organic nanoparticles (ONPs) in different sectors especially in the biomedical ones. The organic nature of these systems, indeed, highly reduces their toxicity and therefore side effects. There are different types of ONPs depending on heir composition and structure like liposomes and micelles, dendrimers, polymeric NPs and nanogels.

Liposomes and micelles

Liposomes are vesicles constituted by self-assembled phospholipid bilayer that delimits an aqueous core in which can be encapsulated hydrophilic molecules like some drugs (Figure 4, Panel A). They can transport also hydrophobic molecules in the lipid bilayer (Conniot *et al.*, 2014). For this reason, they are largely employed in drug delivery system because they can fuse with the plasmatic membrane and release the drug inside the cell (Catalina *et* Pérez, 2005). Their chemical-physical properties can be accurately modified by mixing different lipid molecules and therefore changing the superficial charge, the size and functionalization. Even if they have a good distribution in the organism, they present some advantages like the possibility to change lipid components with High or Low-density lipoprotein (HDL and LDL respectively) and thus modify their size and composition, but also their accumulation into the tissues (De *et al.*, 2008). Micelles, instead, are characterized by a single lipid layer that defines a spherical structure with a hydrophobic core, fundamental for the transport of lipophilic molecule like many antitumor drugs (Prabhu *et al.*, 2015) (Figure 4, Panel B).

Dendrimers

Dendrimers are nanovectors with a spherical shape constituted by polymeric macromolecules that are capable of self- assembling. They present three different parts: a central hydrophobic core, ramification units and hydrophilic functional groups at the external side that can be conjugated with specific molecules for a targeting activity (Figure 4, Panel B). Their synthesis is based on a polymerization process of the ramification units from the surface to the core (convergent synthesis) or vice versa (divergent synthesis) and it can be patterned to control the drug release (Nanjwade *et al.*, 2009).

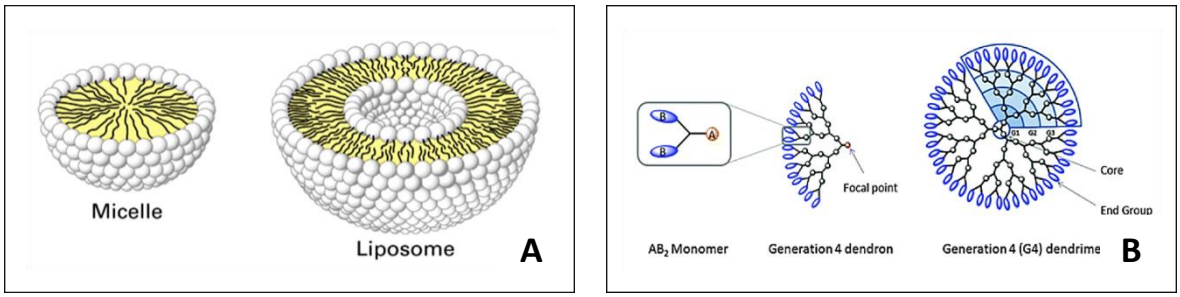

Figure 4. Representation of Micelles and liposomes (Panel A) and of Dendrimers (Panel B): Polymeric structures constituted by monomeric units (ABn).

Polymeric nanoparticles

Polymeric nanoparticles (PNPs) are solid colloidal systems formed by a polymeric matrix with a range size from 10 to 500 nm. Depending on the synthesis process, the resulting structure can be nanospheres (the drug is dispersed in the matrix) or nanocapsules (the drug is confined in an aqueous core surrounded by a polymeric membrane) (Figure 5, Panel A). This particular structure protects drugs from the enzymatic and hydrolytic degradation, so that they are optimal candidate as drug delivery systems. In details, therapeutic agent can be dissolved, trapped, encapsulated or absorbed by the polymeric matrix and therefore can be released with different mechanisms like desorption, diffusion or erosion. The natural mostly used polymers for the PNPs synthesis are Chitosan, Gelatin, Sodium Alginate and Albumin. Instead, the synthetic ones are Polylactic acid (PLA), poly(lactic-co-glycolic acid) (PLGA), Polyvinylpyrrolidone (PVP), Polyethylene glycol (PEG), Poly(methyl acrylate) (PMA), Poly(acrylic acid) (PAA) and Polyacrylamide. In particular, PLA and PLGA are amply used for drug delivery system thanks to their biocompatibility and their ability to slowly dissolve

in solution. For this reason, they have been approved by Food and Drug Administration (FDA) for the parenteral injection (Alexis *et al.*, 2009). Indeed, PNPs present higher stability respect to other NPs, and they can be functionalized for a controlled drug release and to have a prolonged action; finally, they can be administered with a multitude of methods.

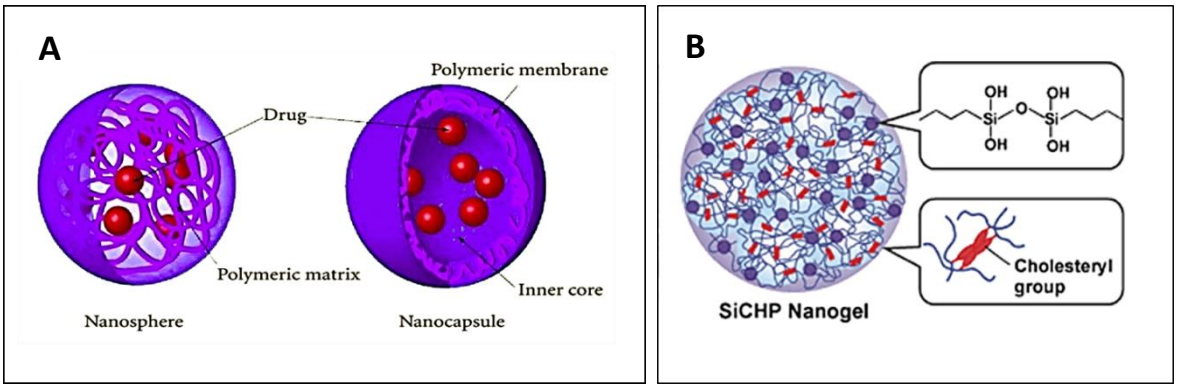

Figure 5. Representation of: polymeric nanoparticles [nanospere and nanocapsule] (Panel A) and nanogel (Panel B).

Nanogels

Nanogels (NGs) are hydrogels of nanometric size, constituted by polymer chains that form a network able to absorb and retain high quantity of aqueous solution (swelling capacity) (Kabanov *et al.*, 2009) (Figure 5, Panel B). The hydration capacity is due to basic or acid groups of the polymers that facilitate the retention of water molecules in the inner regions (Dispenza *et al.*, 2012). Their size (form 10 to 300 nm) and their shape are determined by the equilibrium between the osmotic pressure generated by the aqueous component and the elastic force of the polymer (Alexander *et al.*, 2009). Nanogels can be classified in function of their chemical composition (synthetic, natural or hybrid NGs) or in function of their surface charge (neutral, anionic or cationic NGs) (Miyata *et al.*, 2002).

Thanks to their characteristics, they are largely used as vectors for small molecules like fluorescence probes (bioimaging) or drugs (drug delivery system) (Yamane *et al.*, 2008). Indeed, they present many vantages like stability, a large flexible surface for the conjugation with a big amount of cargo that is protected in an aqueous environment. The biological

molecules can be loaded through spontaneous interactions (like hydrophobic, electrostatic or van der Waals interactions) with the polymer. Furthermore, it is possible also a specific binding of proteins, nucleic acids, drugs or other molecules, with the functional groups (like -OH, -CONH-, -CONH2) on the NGs surface (Yun, *et al.*, 2012). In this way, it is possible a specific cargo release induced by ionic force, pH, temperature or chemical stimuli (Gibas *et al.*, 2010; Miyata *et al.*, 2002).

Natural polymers like alginic acid, chitosan, collagen, fibrin and hyaluronic acid (HA) or synthetic polymers like polyacrylic acid (PAA), polyvinylpyrrolidone (PVP), polyvinyl alcohol (PVA) and polypeptides can be used for the synthesis process.

Drug Delivery system

Classical pharmacological treatments (parenteral, oral, cutaneous or topic) for diseases and, in particular, the cancer chemotherapy can induce side effects because of their nonspecific action: indeed, they act both on normal and tumour cells. Furthermore, the drug dilution in the bodily fluids limits its absorption in the target tissue so that it is necessary to administer substantial doses to have a high local concentration. Moreover, Conventional Drug Administration Systems (CDASs) present pharmacological-kinetic limitations: the therapy requires periodic doses of therapeutic agent that, in a short time, overpasses the "therapeutic band" reaching very high levels and consequently resulting toxic; soon after, instead, its concentration decreases at a level in which it is ineffective (Figure 6, Panel A) (Leroux *et al.*, 1996; Audumbar and Ritesh, 2015). In such cases, a method of continuous administration of therapeutic agent is desirable in order to maintain fixed plasma levels as it happens using nanoparticles for Drug delivery system. Therefore, the use of nanoparticles for drug delivery system, can resolve all these problems (Ranganathan *et al*., 2012; Tiwari, 2012). Figure 6, panel B, shows the drug trend when it is administered through a NPs system: the drug level, after only one dose, is maintained constant over time and then decreases slowly.

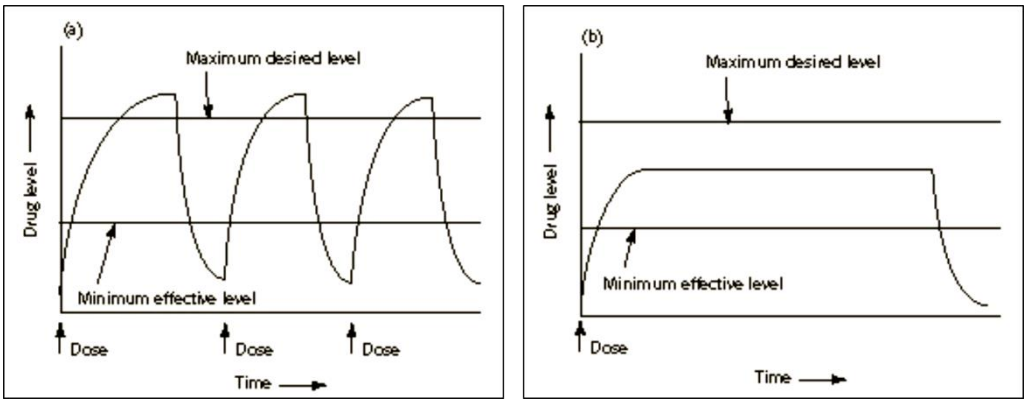

Figure 6. Drug levels in the blood with a) Traditional drug dose systems and b) Drug delivery system.

The use of nanosystems permits a controlled release of the conjugated drug, depending on physiological conditions of the targeted site (site specific-targeting) and a modulation during the release time (temporal modulation), in function of the physical properties of the microenvironment (Swami *et al.*, 2012).

The Drug Delivery System develops from the coordination of three components (Figure 7):

- Cargo i.e. drug
- Targeting molecule
- Nanocarrier

In a unique system, these components permit to carry and then release the drug in a specific tissue and in a controlled way and, at the same time, to increase the drug therapeutic effect.

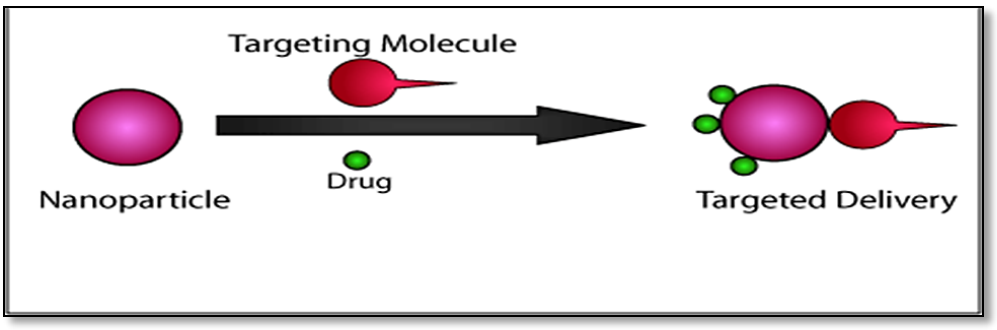

Figure 7. Representation of targeted delivery mediated by a nanoparticle.

Project of nanoparticles

Nanoparticles have to be synthetized, engineered and optimized in order to raise the circulating half-life and to obtain a site-specific release of drugs at therapeutically optimal levels and dose regimes. The composition, size, shape, surface properties, biocompatibility and degradation profile should be carefully considered for the optimal design of the NPs for therapeutic therapy (Figure 8) (Tianmeng Sun *et al.*, 2014).

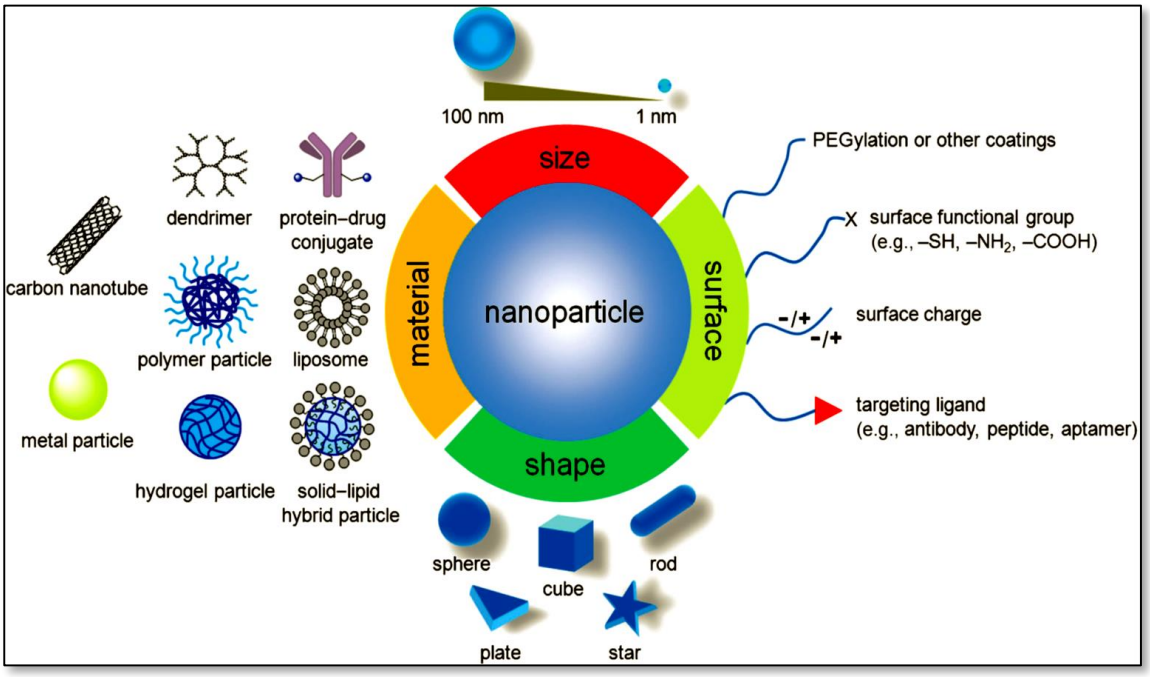

Figure 8. Schematic representation of the principal characteristics to project the NPs.

Size and shape

The size is a fundamental characteristic of the nanoparticles especially for their long circulation, biodistribution and clearance. Generally, their size is between 1-100 nm to permit a longer circulation half-life *in vivo* and a reduced hepatic filtration. Additionally, their small size consents a higher cellular internalization compared with microparticles, as described by Desai *et al*.. They performed uptake studies in a Caco-2 cell line by comparing

100 nm nanoparticles with 1 μm and 10 μm microparticles: NPs had a 2.5 and 6-fold higher uptake level than microparticles (Desai *et al.*, 1997). In particular, very small NPs (size smaller than 10 nm) can easily cross the blood vessels and be cleared by kidneys, while bigger nanoparticles can be intercepted by cells of the mononuclear phagocyte system (MPS).

NPs can be also adopted for the therapy of some brain diseases such as Parkinson, Alzheimer or glioma. Indeed, they can across the blood brain barrier (BBB) through the opening of tight junctions (TJ) if treated with a hyperosmotic mannitol solution (Kroll *et al.*, 1998). Finally, their size can also concern the drug release because the smallest particles present a larger surface area so that the majority of the conjugated drug would be at or close to the particle surface, facilitating a fast drug release.

The shape of nanoparticles (sphere, cube, rod, plate) plays, also, a key role in uptake and drug release processes. Many studies have demonstrated that, for example, spherical particles are good candidates for drug delivery because they are internalized with higher likelihood and faster than rod-shaped NPs (Chithrani *et al.*, 2006). On the other hand, even the rod NPs orientation to the cellular membrane is important for the cellular uptake, indeed this kind of particles have a higher probability of internalization when their major axis is perpendicular to the cell membrane (Champion and Mitragotri, 2006). Shape can also influence their tissue-specific accumulation: for example, cylindrical and regular spherical NPs gather in the liver; discoidal-shaped NPs in the heart and irregular spherical NPs in the spleen (Park *et al.*, 2009; Devarajan *et al.*, 2010).

Surface proprieties

The hydrophobic character of NPs can shorten their circulation time *in vivo* because of the opsonization process in which small molecules, called opsonins, adhere to NPs surface facilitating their phagocytosis by the cells of the immune system. In this contest, even the NPs surface charge is implicated in their uptake by the MPS cells. Indeed, positively charged NPs induce higher complement activation compared to negatively and neutrally charged NPs. The charge is important also to determinate the NPs zeta potential and therefore the

aggregation state in solution: nanoparticles with a zeta potential above (+/-) 30 mV have been shown to be stable in suspension and prevent the aggregation process.

In order to prolong the circulation time of the particles it is possible directly synthetize them from block polymers presenting both hydrophobic and hydrophilic fragments (Harris 2001, Adams 2003) or to coat them with hydrophilic protective layer like polyethylene glycol (PEG) (Mohanraj 2006, Kamaly 2012, Xia 2012). The PEG conformation on the nanoparticles surface is fundamental in repelling opsonins, for example a brush-like configuration of PEG limits phagocytosis and complement activation, while, a mushroom-like arrangement favours both processes (Yang 2010). On the other hand, the presence of PEG shell on the NPs can interfere with the target cells interaction and prevent the endosomal escape, as demonstrated by many studies in which it has been compared the effect of the same nanoparticles PEGylated or not (Du 1997). For these reasons, in the last years, many studies have focused on the development of new strategies to increase the circulation life of NPs, including the use of synthetic or natural polymers, or the coating with biomimetic molecules, or red blood cell (RBC) membranes to evade the immune response cascade (Sambruy 2001).

The coating process can also increase the NPs uptake: Chitosan, for example, can help to disrupt the integrity of intracellular TJs involved in paracellular transport, thus facilitating the delivery of higher amount of nanocarriers to the targeted site (Luk2014).

Nanoparticles targeting

The physicochemical characteristic of nanoparticles like size, shape, surface charge, surface proprieties and their possible conjugation with specific biological molecules, can improve the delivery of drugs to the target tissue through to two different ways: passive and active targeting (Figure 9 and 10).

Passive targeting

In the passive targeting, the localization of the particle depends only on morphological, chemical and physical features of the nanoparticle and on the anatomical and physiological characteristics of the target site.

Normally, small molecules, including NPs, are retained in the bloodstream because they cannot cross the tight junctions between endothelial cells of normal vascular linings. By contrast, tumour tissue needs of extensive vascularization to receive sufficient supplies of nutrients and oxygen; therefore, the rapid growth lends itself to a leaky and defective architecture. Differently from healthy tissue, tumour microvasculature is characterized by abnormal branching and enlarged interendothelial gaps due to damage of TJs between endothelial cells and a disrupted basement membrane (Figure 9) (Martin, 2014). In this contest, small particles, with opportune size, can easily cross through the large gaps and extravasate from the surrounding vessels to the malignant tissue by means of a passive targeting mechanism named EPR (Enhanced Permeation and Retention) effect. Therefore, this phenomenon depends not only on the NPs size but also on the gaps size that can be dissimilar between several tumours and even between different parts of the same tumour (100-800 nm).

In the malignant tissue, it is evident also a dysfunction of the lymphatic system that, sometimes, can be even totally absent inducing the NPs accumulation. In this way, the concentration of the drug released from vectors in tumour microenvironment can reach levels from 10 to 100 times higher than those obtained from the administration of free drug through the classical pharmacological treatments.

In 1986, Matsumara and Maeda have described, for the first time, the ERP Effect. They have carried out localization experiments by comparing two complexes of different sizes: a polymer conjugated with an anticancer molecule named poly(Styrene-co-Malei Acid)-Neo Carrzino Stain (SMANCS) (16 kDa) and a system formed by its non-covalent bind with labelled Albumin (SMANCS-Albumin) (80 kDa). In particular, they have noted that the proteins larger than 30 kDa had preferentially accumulated into tumour interstitium and had lingered there for a prolonged period of time (Matsumura and Maeda, 1986).

Therefore, nanoparticle's size plays a key role in EPR-based tumour targeting. On one hand, the NPs need to be not too much big: different studies have shown that particles with a diameter smaller than 200 nm are more effective than the larger ones that could be more rapidly cleared from the bloodstream by the spleen (Aruna *et al.*, 2013). On the other hand, the NPs need to be not too much small because they would travel back to the blood vessels: nanoparticles with size range of 30-200 nm present an excellent retention by the tissue resistance that shifts the equilibrium toward the extravasation and therefore induces their accumulation in the tumour site.

The passive targeting efficiency is influenced also by the NPs shape associated with tumour interstitial pressure in the malignant interstitium that takes position against the extravasation process (Ferrari, 2005). For example, nanosystems with a spherical shape tend to follow a laminar flow pattern so that, when they are in close contact with the vessel wall, they can cross the gaps and go into the tumour microenvironment. Instead, rod or bar-shaped nanoparticles are hydro-dynamically more unstable and so they have more difficulty to follow a laminar flow pattern and to linger into the bloodstream (Decuzzi *et al.*, 2005)

EPR effect is due to the high permeability of tumour vasculature, therefore many vascular mediators such as Nitric Oxide (NO), Carbon Monoxide (CO), Vascular Endothelial Growth Factor (VEGF), can increase this phenomenon. NO is a signalling messenger involved in different pathways and produced by NO synthase that is more expressed in cancer cells than in healthy ones, suggesting that there is a higher NO production in tumours. Indeed, NO is probably involved in their growth as demonstrated by NOS knockout mice experiments: by inhibiting the NO synthesis, there is an intense reduction of the extravasation process, demonstrating its involvement in EPR effect (Kisley *et al.*, 2002). In cancer microenvironment, alsoCO induces angiogenesis thanks to its action as vasodilator: experiments in which the production of CO is induced by a CO donor showed an increase of vascular permeability and blood flow thus determining an higher EPR effect.

Although often EPR effect promotes nanoparticles targeting in tumour site and it is widely exploited for cancer therapy, passive targeting efficiency can be rather limited because of the nature of the tumour. For example, small tumour or metastatic lesion does not present strong and diffused angiogenesis, so that vessels are not evenly distributed and size of gaps can be different in several part of the same malignant site (Aruna *et al.*, 2013). Hence, it is

necessary to improve specific targeting by conjugating specific molecules for an active targeting.

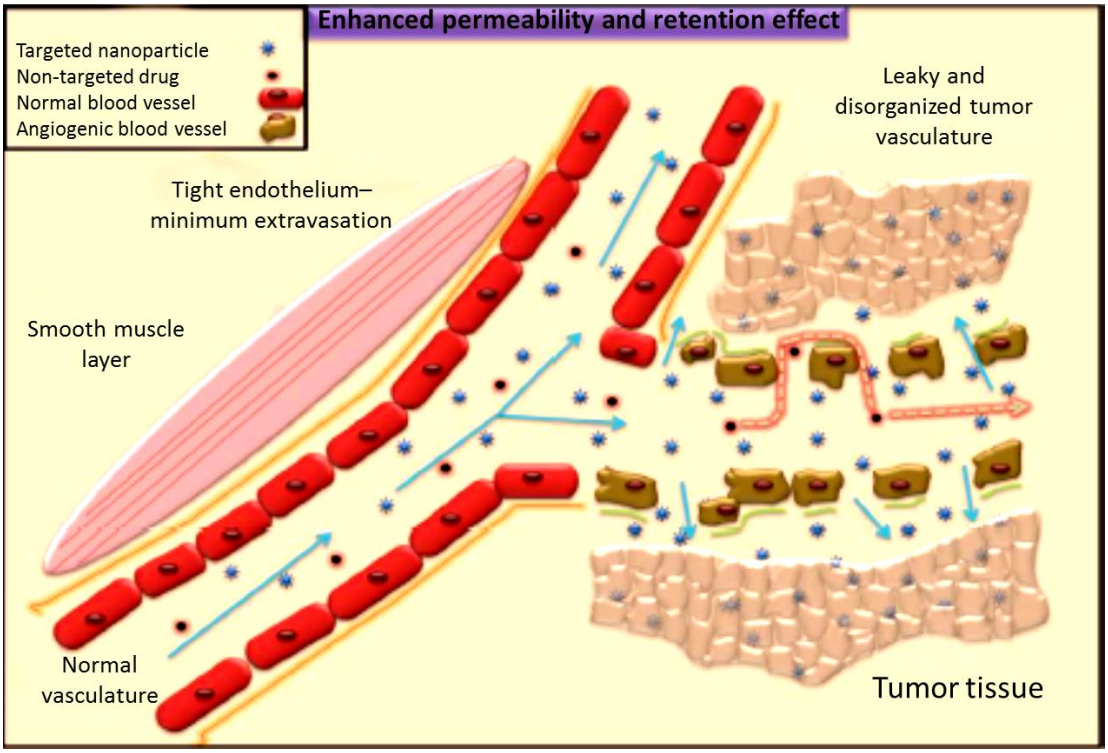

Figure 9. Passive targeting: EPR Effect.

Active targeting

Tumour cells overexpress many characteristic molecules into their membrane that can bind antigens like growth factors and induce various tumorigenic pathways such as angiogenesis or growth metabolic ones. Active targeting, named also ligand-mediated targeting, is based on this feature: nanoparticles can be conjugated to a targeting moiety that purposely bind to the surface of a definite type of cells, like tumour cells. Therefore, active and passive targeting can be independent or, sometimes, combined in order to improve the nanoparticles efficiency.

The active targeting can be formulated not only to directly recognise tumour cell, but also other cellular types involved in cancer progression. An example is the active vascular targeting (Neri *et al.*, 2005) in which the molecules conjugated to NPs recognise

angiogenetic endothelial cell surface receptors including fibronectin (extradomain B), integrins, annexin A1 and grow factors or their receptors like VEGFs and VEGFR. Once internalized, the nanosystems can release specific drugs or biological molecules able to induce apoptotic events in the endothelial cells that, in this way, cannot supply oxygen and nutrients to tumour: in this manner cancer mass is eradicated.

Beyond the function in the specific identification, the active targeting increases also cellular uptake as result of receptor-mediated endocytosis when the NPs are in tumour microenvironment. In this contest, density and orientation of ligands and their affinity for the substrate, result to be fundamental, because the multiple interactions of the NPs with the target cell membrane determine the clustering of receptors and so the improvement of the endocytosis. By contrast, high ligand density can facilitate the macrophage phagocytosis and consequently can sequester them to tumour cells; therefore, the identification of the antigen optimal concentration needs to be well investigated.

It is fundamental to keep unchanged the efficiency and physicochemical properties like size and shape of nanomaterials during the conjugation process, because the NPs can be modified by density, orientation or charge of ligands (Bertrand *et al.*, 2014). In particular, the attachment strategies depend on NPs' nature: usually the ligand is linked by a covalent bond, but, in some cases, it is preferable a physical adsorption like it is for liposomes in which the ligands require of a bulkier hydrophobic anchor to insert them into the lipid bilayer in order to increase their stability, especially *in vivo*. Moreover, some inorganic polymers need the interposition of functional groups like NH_2 or OH to link targeting ligands, dye molecules for localization studies or drugs.

Independently of conjugation approaches used, nanoparticles can be functionalized using targeting ligands of different nature like aptamers, small molecules, peptides, antibodies, carbohydrates or glycoproteins in function of the characteristic of the target cells (Figure 10).

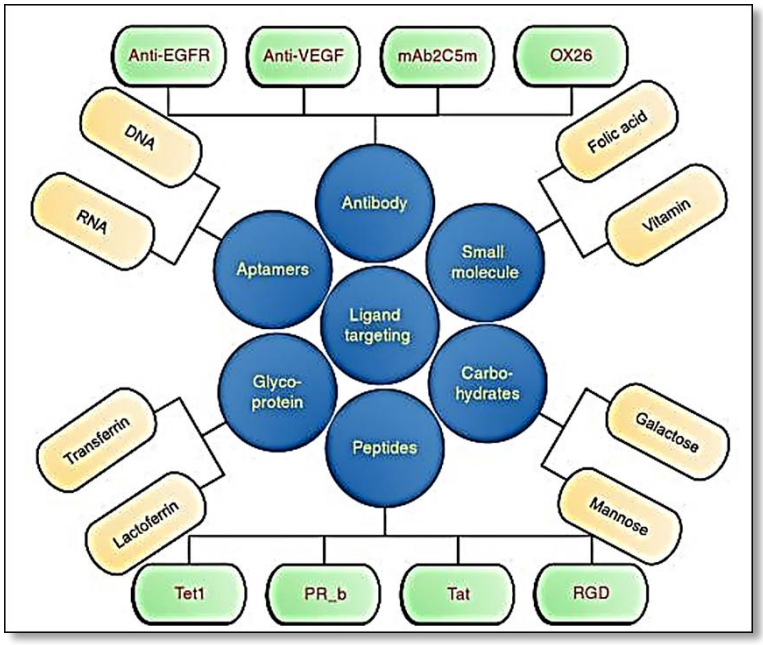

Figure 10. Ligands for a nanoparticles' active targeting.

Aptamers

Aptamers (Apts) are small single-stranded DNA or RNA oligonucleotides (20-80 nucleotides) that can fold into unique tertiary configuration capable of binding proteins, phospholipids, acid nucleic or carbohydrates expressed by target cells. When they are conjugated to NPs, they are optimal candidates for tumour targeting, thanks to many features like very low immunogenicity and stability and capacity to tolerate small variations of temperature or pH. Moreover, a specific chemical process named "Systemic evolution of ligands by exponential enrichment" (SELEX) permits to select and amplify the aptamers with higher binding affinity for the target molecules, starting from a random library of single-stranded DNA or RNA (Daniels *et al.*, 2003). Furthermore, their functionalization with

molecules such as PEG or cholesterol improves half-life of aptamer-NPs in bloodstream and delay their clearance by the kidneys (Nimjee *et al*., 2005).

It has been identified even an Apts role as pharmaceutical agents because some of them can inhibit proteins involved in pathological pathways (i.e. the Pegaptanib Sodium aptamer recognise VEGF protein) (Bates *et al*., 2009). However, because of their expensive cost of production, it is preferable employ Apts only as targeting agents.

Small molecules

Organic small molecules, with a molecular weight less than 500 Da, can be used for active targeting because they present high stability, chemical management, low cost production and especially a high binding affinity for different substrates of interest. The most famous example is Folic Acid (FA), named also Vitamin B9: it is involved in many metabolic pathways like cellular proliferation and DNA or RNA synthesis and it can link, with very high specificity and affinity, to its receptor (Folate Receptor-FR) that is over-expressed in the majority of human tumours (brain, colon, ovarian, breast, renal and lung cancers). Some studies have suggested a higher uptake of FA-NPs compared with NPs alone (Zhang *et al.*, 2015) and a higher cytotoxic effect, when the nanosystem is conjugated also with an anticancer drug. Another small molecule abundantly adopted for active targeting, is TPP (triphenyl-phosphonium) that is a positively charged molecule able to cross the mitochondria membrane and so it accumulates inside this cellular compartment (Smith *et al.*, 2003). Furthermore, TPP can partially confer positive charge on NPs (zeta-potentia more than +22mV) that, in this way, can escape the endosomal compartment and accumulate in mitochondria more than NPs alone (Marrache *et al.*, 2012).

Peptides

Peptides are linear or cyclic sequence of amino acids (not more than 50 residues) that can fold into three-dimensional structures acquiring high stability and resistance against the immune system, so that they can be used as targeting moieties unlike proteins.

cRGD (cyclic RGD), a member of peptide family RGD (arginine- glycine- aspartic acid), is largely studied because of its capacity to recognise and bind the $\alpha_V\beta_3$ integrin receptors, overexpressed on both tumour and angiogenetic endothelial cells. It is partially expressed also on normal or inflamed tissues even though at low levels and some data has demonstrated

that cyclic form presents 10-fold higher anti-cancer activity (Colombo *et al.*, 2002). Furthermore, cRGD can upregulate VEGF signal through its receptor VEGFR-2 that is typically associated to $\alpha_V\beta_3$; indeed by inhibiting the $\alpha_V\beta_3$ binding site, there is a reduction of VEGF signalling, resulting in an anti-angiogenic mechanism (Ruoslahti *et al.*, 2002).

In this contest, the use of cRGD conjugated with NPs induces two advantages: it can improve specific targeting but it can also, indirectly, downregulate VEGF pathway and induce an anti-angiogenetic effect (Blanco *et al.*, 2010). Several types of nanosystems were synthetized using RGD as targeting molecule and a variety of moieties as therapeutic agents among which drugs like doxorubicin or paclitaxel, but also siRNA to block mRNA involved in tumour growth pathways.

Dong Han and colleagues carried out studies using a system composed by RGD peptide-labelled chitosan nanoparticle (RGD-CH-NP) as a tumour targeted system for siRNA delivery (siRNA/RGD-CH-NP). They showed that the presence of cyclic peptide significantly increases selective intratumoral delivery in orthotopic animal models of ovarian cancer that overexpress integrin $\alpha_V\beta_3$ (Han *et al.*, 2010).

Antibodies and their fragments

The most important class of targeting moieties used is certainly composed by monoclonal antibodies (mAb), thanks to their very high specificity and capacity to strongly bind the corresponding (complementary) antigen expressed by targeted cells (Figure 11). Because of mAb role in the immune response, they confer high immunogenicity to the NPs after conjugation; therefore, the use of engineered antibodies in order to obtain Ab-fragments that can escape the immune system is largely diffused. Some of them, like single-chain variable fragments (scFv), present only the Fab region able to recognize specific antigen (the Fc portion confers the immunogenic propriety). In particular, scFv are fusion proteins constituted by the variable regions of both heavy and light chains of the Ab linked with a short peptide of about 15 amino acids (Chen *et al.*, 2010).

MCC-465 and STG-53 are two examples of Ab-fragment-targeted NPs: the first one shows excellent results in preclinical studies in doxorubicin delivery for stomach tumour cells (Jain

et al., 2010); while the second one is able to bind transferrin receptors (Tf-R) on cancer cell membrane and to release into the cytoplasm a p53 inhibitor (Nemunaitis *et al.*, 2008).

Thanks to their properties, since the 1980s, more than 30 different types of mAb and their derivatives have been accepted for clinical use like cetuximab, rituximab, bevacizumab or trastuzumab.

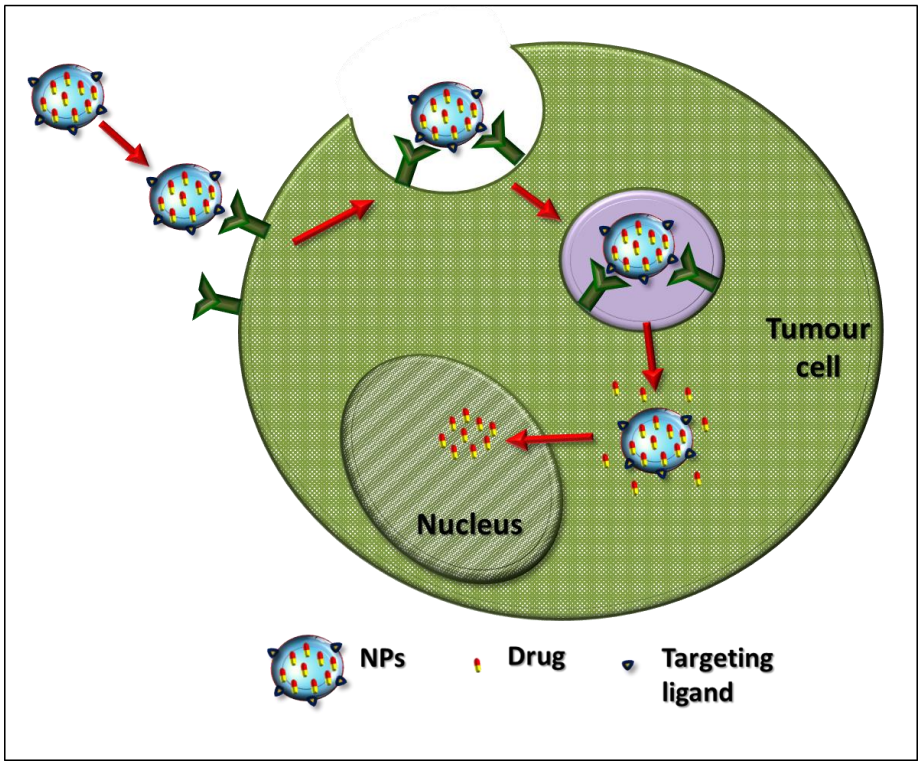

Figure 11. Active targeting antibody-mediated (submitted data).

Carbohydrates and Glycoproteins

Carbohydrates (CHs) are very important mediators of cell-cell interactions so that they are involved in many mechanisms such as cellular differentiation, cell signalling regulation and immune response. Even if they can bind lectins ubiquitously expressed, many studies have reported the presence in tumour cells of proteins similar in size and sugar-binding specificity to the lectins of the normal cells. Therefore, carbohydrates can be used as targeting ligands (Lotan *et al.*, 1988). Different kinds of CHs can be involved in nanoparticles' active targeting. For example, galactosamine binds specific membrane receptors into primary and

metastatic liver cancer cells. In this way, if conjugated to NPs, galactosamine permits their uptake via Receptor-mediated endocytosis only in tumour cells (Seymour *et al.*, 2002). Beyond galactose, it has also been documented an active targeting by exploiting other carbohydrates moieties like mannose or glucose and their derivatives. Nevertheless, CHs are not good targeting ligands because of their difficult synthesis and their labile glycosidic linkages that can be easily degraded by enzymes.

On the other hand, glycoproteins like Lactoferrin (Lf) and Transferrin (Tf) are widely employed for this purpose and in particular, Lf- NPs have higher targeting efficiency for tumour cells than Tf-NPs (Choe *et al.*, 1998).

An important limit of the use of classical chemotherapeutic agents is the transport across the blood brain barrier (BBB) to act against neural cells for neural pathologies like Alzheimer, Parkinson or glioma. In this contest, both Lactoferrin and Transferrin can be conjugated to nanosystems to act in a complementary way. In depth, since many transporters, like the transferrin receptor, are expressed at the BBB, it is possible to use them for active targeting, so that Tf-NPs would cross the barrier and reach the target site in the brain. Once there, NPs functionalized also with Lf can recognise, for example, glioma cells that over-express Lf receptors as reported by two very similar studies about glioma treatment with Lf- liposomes (Pang *et al.*, 2010; Chen *et al.*, 2011).

Cellular uptake

Once arrived in the target site, nanosystems must first cross the cell plasma membrane through endocytosis, an energy-depending internalization process. This mechanism can be induced by a specific highly selective interaction between the targeting molecules associated to the NPs and their receptors on the membrane or by an unselective binding based on hydrophobic or electrostatic interactions. In this contest, size, shape and surface properties of NPs play a key role determining the specific internalization pathway (Mao *et al.*, 2013) (Figure 12):

- Clathrin-mediated endocytosis [receptor-mediated endocytosis (RME)]: the interaction between cellular receptor and its ligand on the NPs, induces the inward

budding of plasma membrane vesicles containing both receptor and ligand and coated by specific cellular proteins named clathrins.

- Caveolae-mediated endocytosis: the membrane internalization occurs in correspondence of lipid rafts rich of cholesterol and caveolin that facilitate the vesicles formation.
- Phagocytosis: cells internalize very big molecules (larger than 500 nm) or opsonized nanoparticles. This process is typical only of some cellular types like macrophages, monocytes and neutrophils.
- Simple diffusion: molecules can cross the membrane without the vesicles formation.

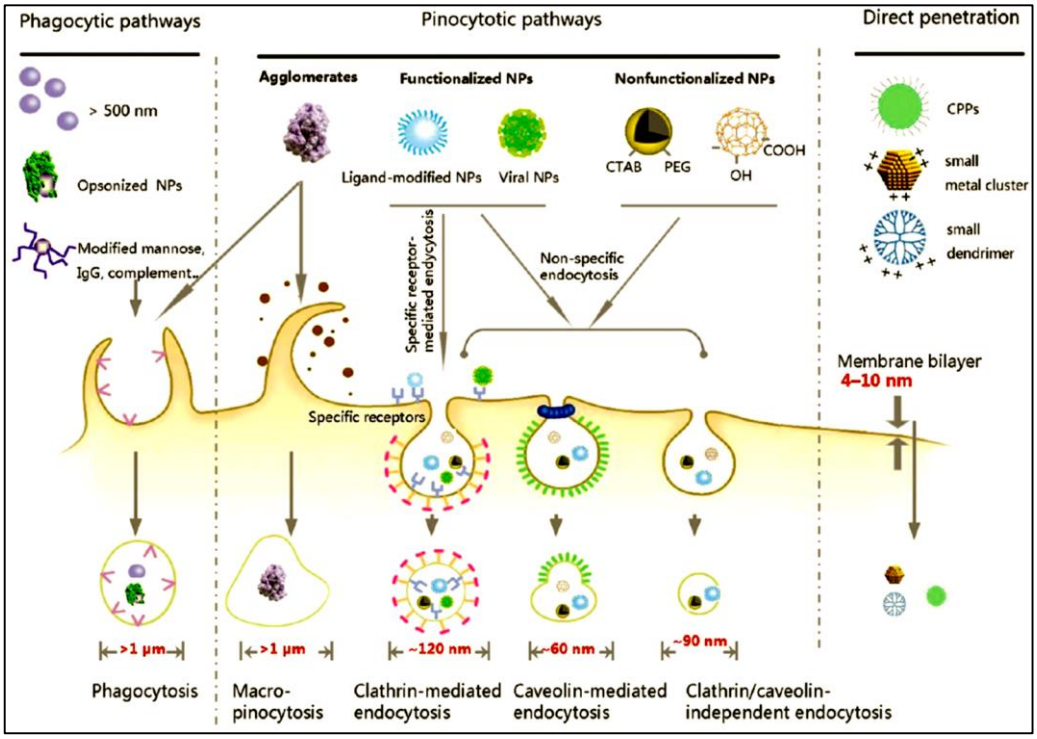

Figure 12. Pathway for the cellular internalization of different types of nanosystems.

The endocytic mechanism is also influenced by the type and physiological condition of the cells as it has been demonstrated by many experiments comparing the uptake mechanism of the same nanosystem in different cellular lines (Chan *et al.*, 2007). Moreover, the internalization process is a temperature-dependent mechanism: at 4°C, all the energy-

mediated endocytic pathways are halted with the consequent reduction of the uptake level compared with the regular cultures performed at 37°C.

When NPs are inside the cells, they can follow different ways: they can be transported along the endolysosomal network to other organelles or they can be exocytosed (Figure 13). Many cytoplasmic complexes are involved in this process, especially the cytoskeletal structures. It is also possible to direct the nanoparticles to a specific cellular compartment by conjugating them with a target sequence. For example, many studies have shown that a nuclear localization signal (NLS) peptide motif can be added to the NPs for a nuclear targeting (Mao *et al.*, 2013).

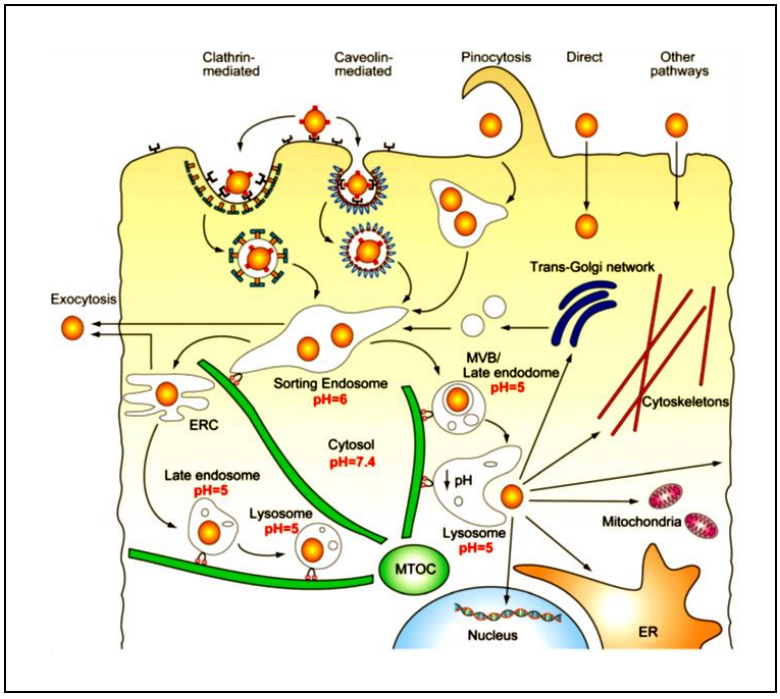

Figure 13. Intracellular transport of nanoparticles.

Controlled drug release

One of the most important aspects of drug delivery system is the possibility to control the conjugation process of therapeutic molecules and therefore also their release mechanism. In this contest, the nature and the physicochemical properties of both drug and nanosystem, but also the NPs synthesis process, play a key role, so that biological cargo can be adsorbed or covalently attached to the NPs surface or encapsulated inside (Liu *et al.*, 2006). In this way,

the drugs are also protected from harsh environments like the highly acidic environment of the stomach, the blood stream rich of high levels of proteases or other enzymes, and even, at cellular level, the lysosomes that present a very low pH (Couvreur *et al.*, 2013). All these factors determine an extended half-life of the drug and its higher concentration in the target site.

There are many therapeutic agents used for tumour treatment that differ for chemical or physical properties (hydrophobicity or hydrophilicity and surface charge) (Sun *et al.*, 2014). Hydrophobic drugs such as paclitaxel, methotrexate, cisplatin and doxorubicin, can aggregate in an aqueous solution like the extracellular environment or the bloodstream, inducing side effects such as embolisms and local toxicity (Owen *et al.*, 2012). Their conjugation with vectors, especially micelles and polymeric NPs composed of hydrophobic or amphiphilic materials can prevent these complications.

On the other hand, also the hydrophilic drugs increase their efficiency if conjugated with nanosystems. Indeed, the action of free hydrophilic drugs, including macromolecules such as proteins, peptides, and nucleic acids and many small molecules, can be impeded by the rapid MPS (mononuclear phagocyte system) clearance and kidney filtration (Ku *et al.*, 2014). Moreover, they are subjected to proteolytic and hydrolytic degradation and therefore they have a short half-life in bloodstream; additionally, they are unable to cross the hydrophobic lipid bilayer of cell membranes (Torchilin *et al.*, 2003). The most important example is represented by siRNA, micro-RNA and DNA, with high charge density, highly used in gene therapy (Dispenza *et al.*, 2014); even though they are not stable, their instability can be overtaken when they are transported by a nanosystem. Their conjugation occurs through electrostatic interactions between the nucleic acids (negatively charged) and nanocarriers (positively charged) (Woodrow *et al.*, 2009) or through direct binding to functional groups on the NPs surface.

Independently of the drug nature, the drug controlled release from the nanosystems can be enclosed into two major categories: extended and stimuli-responsive release (Figure 14).

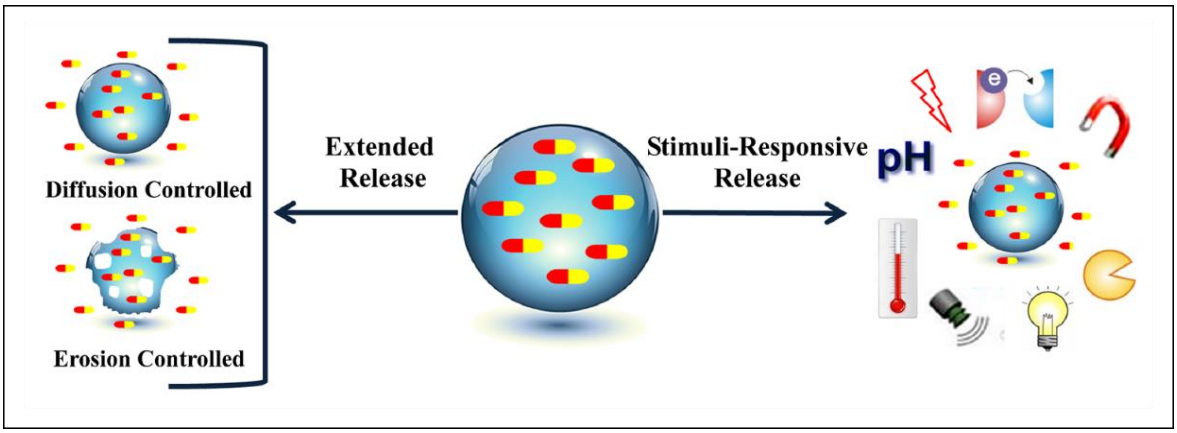

Figure 14. Controlled drug release mediated by nanoparticles.

Extended release

Extended drug release permits to deliver drugs over a sustained period and to maintain constant their concentration in the plasma or target tissue by matching the rate of release and clearance of drugs (Robitzki *et al.*, 2010). It is a model adopted especially for drugs rapidly metabolized and eliminated from the body and it can be realized through a diffusion or an erosion controlled mechanism (Figure 14).

Diffusion-controlled release

Diffusion-controlled release is typical of the nanosystems in which the drug is localized into their core delimited by an insoluble barrier usually made of an organic polymer. In this manner, the drug is protected from the aqueous environment and can be released by diffusion process at determined rate, depending by its physicochemical properties, such as porosity or thickness (Cheng *et al.*, 2009). This kind of nanosystems are based on a water-insoluble matrix polymer such as poly(methyl methacrylate) (PMMA) and polyurethane (PUA) that are characterized by a two-phases release. In particular, there is an initial substantial detachment of therapeutic molecules from the NPs surface ("burst release"), and a second release of the other molecules from the core up to the surface thanks to their diffusion across the polymer matrix (Ma *et al.*, 2011).

Erosion-controlled release

Some nanocarriers are made of erodible or degradable polymers so that the drug is released by an erosion-controlled mechanism and therefore does not require additional clearance processes (Chen *et al.*, 2006).

Biodegradable polymers can be natural or synthetic. Poly (lactic acid) (PLA), poly(glycolic acid) (PGA), and poly(lactic-co-glycolic acid) (PLGA) are examples of synthetic polymers largely used for erosion controlled drug delivery. They can be easily metabolized by a hydrolytic process, through cleavage of the ester bond between lactic and glycolic acid so that they are subsequently eliminated as carbon dioxide and water (Göpferich *et al.*, 1996).

Polymer erosion can happen through a surface or bulk mechanism (Zuleger *et al.*, 2001). The surface erosion occurs when the rate of erosion is faster than the rate of water permeation into the bulk of the polymer. On the other hand, bulk erosion happens when the water molecules can quickly penetrate into the polymer before that the erosion can take place and the chain scission occurs throughout the matrix.

Stimuli-Responsive Release

Some nanosystems can release the conjugated drugs in response to specific stimuli that can be broadly classified as either internal (i.e. pH variation, enzymes or redox state) or external (i.e. light, ultrasound, heating) (Figure 14). On one hand, chemical, biochemical, or physical stimuli can induce a modification of the structural composition or conformation of the nanocarriers with the consequent release of the drug entrapped within them (complexation approach). These modifications include isomerization, polymerization, decomposition, activation of supramolecular aggregation (Fleige *et al.*, 2012). On the other hand, the release mechanism can involve the cleavage of a linker between the carrier and the drug (nanocarrier-conjugate approach).

pH-responsive nanocarriers

One of the most important features of the pathologic tissue (like those inflamed, infected, or cancerous) is the alteration of the pH values. The extracellular pH registered in solid tumours is more acid (pH 6.5–6.8) than those recorded in the healthy tissue (pH 7.4), probably because of the different vasculature and the consequent altered anaerobic conditions (Vaupel *et al.*, 1989). The pH difference concerns also the intracellular compartments like endosomes

or lysosomes so that NPs following the classical endocytic pathway, can proceed through compartments with different pH (early endosome with pH about 5–6 and late lysosome with pH around 4–5) (Mura *et al.*, 2013). In this way, a two-phase drug-release is possible: an initial delivery outside the cells so that free drug can diffuse through the plasmatic membrane, and a subsequent phase inside the cellular organelles.

Several synthetic polymers have been developed as pH-sensitive nanocarriers, such as poly(acrylamide) (PAAm), poly(acrylic acid) (PAA), poly(methyl acrylate) (PMA), and poly(diethylaminoethylmethacrylate) (PDEAEMA), able to perceive the pH-variation and consequently to modify their structure and hydrophobicity as result of protonation or deprotonation of inner functional groups or of cleavage of the shell (Bawa *et al.*, 2009). For example, concerning the nanogels, it has been broadly reported that pH-responsiveness is based on the change of their ionization state that induces a swelling/deswelling and therefore the release or the entrapment of various molecules. (Oishi *et al.*, 2007).

Another approach largely adopted is the conjugation of drugs through pH-sensitive linkers (Figure 15), which can be incorporated into nanocarrier structure. The conjugation protocol is based on the activation of functional groups of both nanocarriers and linkers (i.e. imine, ketal, oxime, citraconylamide, hydrazone, hydrazide, and acetal) (Lee *et al.*, 2006).

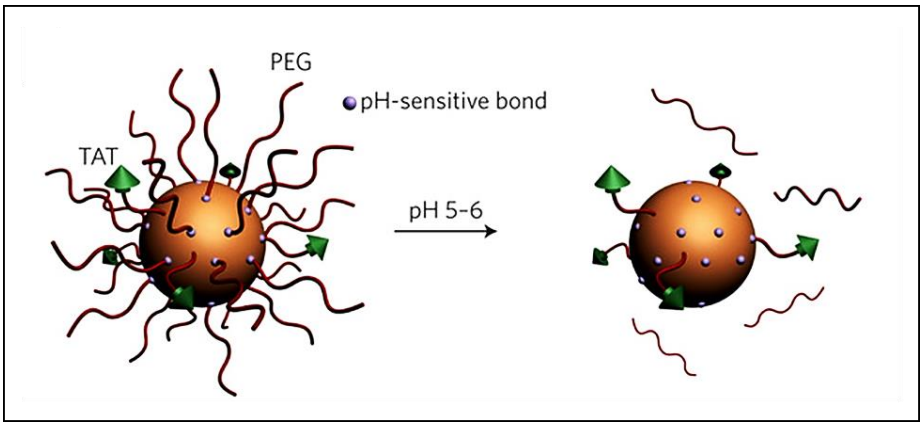

Figure 15. Representation of pH-dependent drug release from nanoparticles.

Redox-responsive nanocarriers

Redox-responsive nanocarriers are based on the difference of redox potential (~100–1000 fold) existing between extracellular (oxidative state) and intracellular (reductive state)

environments. Principally, this is due to a diverse glutathione (GSH) concentration, indeed, the cytosolic concentration of GSH is higher (1-10 mM) than those registered in the tissues or in the plasma (2μM). Moreover, the cytosolic GSH level in cells with an enhanced oxidative stress (like tumour cells) is 7–10 fold higher than in normal cells (West and Otto 2005).

Therefore, NPs can be functionalized with a redox-sensitive linker, which can be conjugated to the drug. In this way, a high GSH concentration can cleave the spacers like those that, for example, presents a disulphide bridge (Adamo, Campora *et al.*, 2014) (Figure 16).

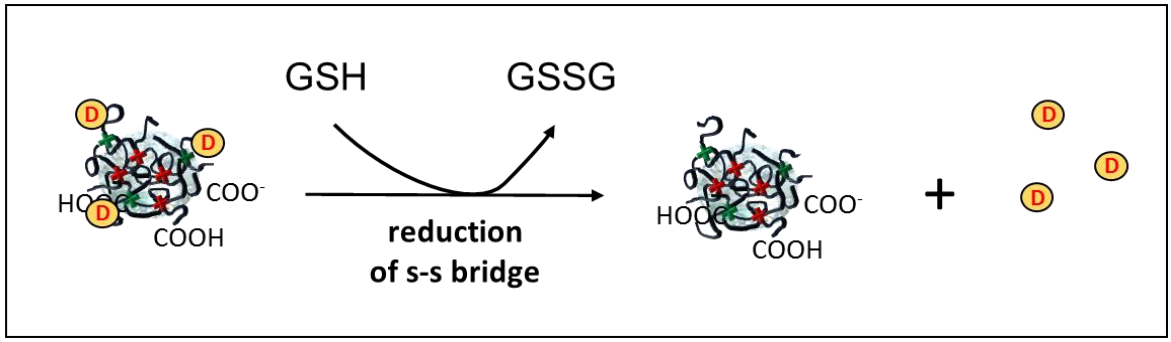

Figure 16. Glutathione (GSH) drug (D) release from PVP nanoparticles (Adamo, Campora *et al.*, 2014).

This controlled release system is especially effective for gene (DNA or siRNA) delivery, because it is necessary to protect the oligonucleotides outside the cell and to release them after their cellular internalization. The presence of a linker with a disulphide or a thioester bond permits a very high (until to 40–100-fold higher) transfection efficiency if compared with the same complex without the spacer (Neu *et al.*, 2007).

Even if the disulphide bridge is the most used linkage to generate redox-sensitive nanocarriers, there are some disadvantages concerning their *in vivo* stability. Indeed, GSH and cysteine are also present outside the cells and they can induce an early breakdown of the nanoparticles. This problem can be overcome by using multiple disulphide bonds and by controlling the amount of disulphide cross-links (Miyata *et al.*, 2004).

Enzyme-responsive nanocarriers

Enzymes are involved in a wide range of biochemical important functions and some of them can be overexpressed in some pathological conditions like in tumours. Therefore, it is possible to take advantage of this feature by introducing specific enzyme substrate sequences either directly into the nanocarrier or in the linker segment by which the drug is conjugate to the nanocarrier (Law *et al.*, 2009).

One of the most used linker is the tetrapeptide Gly–Phe–Leu–Gly, which can be cleaved by the cathepsin B enzyme that degrades proteins in lysosomes and is overexpressed in tumour cells (Duncan *et al.*, 2009).

Extracellular proteases, such as the matrix metalloproteases, are considered specific biomarkers of tumour tissues because of their capacity of proteolysis of extracellular matrix (ECM) and basement membranes, required for tissue remodelling and angiogenesis.

For instance, some studies have reported the use of short peptides, with sequences cleavable by MMPs, as linkers between PEG chains and liposomes, polymeric nanoparticles, or iron oxide nanoparticles (Zhu *et al.*, 2012). On the other hand, Haba and colleagues have developed a so-called "self immolative dendrimer": after the enzymatic cleavage of the substrate, a complete dendrimer degradation occurs along with the simultaneous release of three different drug molecules (Haba *et al.*, 2005).

Thermo-sensitive nanocarriers

Some nanocarriers are constituted by temperature-sensitive materials able to change their physical properties and to trigger drug release following up a local variation of the temperature. They are largely used to contrast some pathological conditions like tumours, inflammations, or infections that are characterized by a local temperature increase.

In most cases, the nanosystems are produced to respond to variation of temperature in the range between 37 and 42°C, because higher or lower values could cause protein denaturation or loss of function (Aluri *et al.*, 2009). In this contest, many research have been carried out using liposomes as thermo-responsive systems, because of the properties of their constituent lipids, that, following up heating, can undergo to conformational structural changes associated with variations of the lipid bilayers permeability. For example, doxorubicin

loaded to thermo-sensitive liposomes (ThermoDox, Celsion Corporation) are in phase II trial for the treatment of breast and colorectal cancers, and have reached phase III trial for the treatment of hepatocellular carcinoma (Al-Ahmady *et al.*, 2012).

Moreover, some nanogels alter their swelling state in response to a temperature alteration of the aqueous media in which they are. Depending on the reaction, they can be classified in two categories: negative and positive nanogels. Negative temperature-sensitive hydrogels have a *lower critical solution temperature* (LCST) and contract upon heating above the LCST; while positive temperature-sensitive hydrogels have an *upper critical solution temperature* (UCST) and contract upon cooling below the UCST (Peppas *et al.*, 2000).

Photo-responsive nanocarriers

The use of light as an external stimulus to induce the drug release offers many advantages, including ease of application and the spatial and temporal control. The photo-responsive properties are conferred to functional groups or linkers that, upon light irradiation with the proper wavelength, can alter their conformations or destabilize the nanoparticles structure through a molecular switch.

The possibility to irradiate a specific area with a light source from outside of the body permits a space-temporal control. By contrast, one of the major obstacles of photodynamic therapy is the necessity to put the patient in the dark for a definite period, named "dark toxicity", in order to prevent an early drug release (Jiang *et al.*, 2005).

Despite many advantages of this light-sensitive systems, the low penetration depth (<200 mm) caused by the strong scattering of soft tissues has limited the use of these UV-based systems for *in vivo* applications (Wang *et al.*, 2014). Moreover, even for *in vitro* applications, the UV light causes genetic damages to the cells. An alternative may be the near-infrared (NIR, 700–900 nm) irradiation, that can penetrate more deeply into soft tissues, without significant damage of the area of application.

Sonic and ultrasonic-responsive nanocarriers

Another method that permits a spatial and temporal control is based on the ultrasound application to trigger drug release. Usually, the most used ultrasonic-responsive nanocarriers are liposomes constituted mainly by PEG-lipids. Moreover, ultrasound-mediated delivery of genetic material from microbubbles has been used as a method for gene delivery to vascular

smooth muscle cells *in vitro*, using ultrasound that triggers the delivery of a plasmidic DNA, linked by electrostatic interactions. These microbubbles are acoustically ruptured near smooth muscle cells, under a range of acoustic pressures (0 to 950 kPa) and pulse durations (0 to 100 cycles) (Phillips 2010).

Other stimuli-sensitive nanocarriers

Even if the stimulus-responsive nanocarriers mentioned above are the most used for tumour therapy, there are also other nanocarriers able to respond to other stimuli and to trigger a controlled release.

Electrical field-responsive nanocarriers: in most cases, they contract when exposed to an electric pulse and this effect persists for all the stimuli duration (Schmidt 2010).

Magnetic field-responsive nanocarriers: they generate heat when a high-frequency magnetic field (HFMF) is applied to them (Lee 2010).

Competitive ligands or ions-responsive nanocarriers: their interaction with the drug is based on coordinative bonds, so that the presence of a competitor with higher binding affinity can induce the drug release.

Metabolic-responsive nanocarriers: They (for example nanogels) can be conjugated with an enzyme like glucose oxidase (GOD). In this case, in presence of glucose, the GOD–glucose reaction produces an acid with consequent pH reduction and collapse of the NGs that can release the therapeutic molecules (insulin) (Peppas and Bures, 2004).

Nowadays it is largely adopted the possibility to have dual-responsive nanocarriers for design of stimuli-sensitive DDS. These systems can respond to two different stimuli, such as pH and ionic strength or thermo-responsiveness. Most often, these dual-responsive systems are produced by the combination of two monomers having responsiveness to different stimuli. However, the complexity of dual-responsive systems increases and certainly complicates the phase of the synthesis and the clinical approval of these systems.

Aim of the project

Traditional chemotherapeutic agents are unable to discern the specific tumour target so, in order to be effective, they are administered in high doses, thus leading to a diffused toxic effect. The drug delivery nanosystems can solve this problem, because they can be functionalized to recognize a specific target and, therefore, to release the therapeutic agent in controlled way.

In this contest, the research project has been focused on the analysis and the comparison of four different nanosystems for *drug and siRNA delivery*: **INU-EDA-P,C-DOXO**; **PHEA-EDA-P,C-DOXO**; **PVP-siRNA** and **RGO-siRNA.** Two different therapeutic agents have been investigated in details: doxorubicin (Doxo) and siRNA for EGR-1 and Bcl-2.

Doxorubicin has been taken into account as a drug model thanks to its features. It is a potent antineoplastic agent able to intercalate DNA and to induce apoptosis. Moreover, it is characterized by a red auto-fluorescence that permits to localize it very easily. The drug has been conjugated to two different polymeric systems through the same pH- sensitive citraconic anhydride linker (**INU-EDA-P,C-DOXO** and **PHEA-EDA-P,C-DOXO**), in order to compare their effects both in normal and tumour cells of the same tissue.

Both nanoconjugates were synthesized in collaboration with Professor Giammona research group (University of Palermo); firstly, the cytotoxic effect inducted by the released drug was evaluated and, secondly, their specific localization inside the cells was analysed through fluorescence microscopy and flow cytometric analysis. Moreover, the specific action of PHEA-EDA-P,C-DOXO for tumour cells was further investigated through co-culture experiments with both kind of cellular lines, and their specific internalization mechanism was clarified by inhibiting different endocytosis pathways and by conducting lysosomal-specific localization studies.

On the other hand, siRNA delivery studies have been carried out comparing two very different systems: **PVP** nanogels and Graphene oxide reduced (**RGO**).

PVP nanogels (NGs) have been largely characterized and studied by Dr. Adamo (from Ghersi research group) in collaboration with Prof. Dispenza research group.

Due to the intention of conjugating Egr-1 siRNA to the NPs, the Egr-1 pathway was studied in order to individuate the optimal condition for silencing experiments. In parallel, it was developed a protocol for the conjugation of Egr-1 siRNA to PVP nanogels. Once established the optimal condition for Egr-1 expression, silencing experiments using PVP-siRNA complex were carried out in order to investigate the role of NGs as siRNA delivery system.

Furthermore, another siRNA (siRNA for Bcl-2, an important anti-apoptotic protein) was conjugated through a Glutathione sensitive spacer to obtain a controlled siRNA release: pre-treating cells with the inductor of GSH (GSH-Oet), it was possible to perform silencing assays.

In order to explore if a two-dimensional nanosystem would conjugate a bigger amount of siRNA respect to three-dimensional PVP nanogels, the use of RGO (reduced graphene oxide) as a possible vector for siRNA delivery was investigated.

In collaboration with Professor Peter Griffiths research group (University of Greenwich), the nanosystem was investigated for its capability to link biological molecules like antibody and siRNA through Dynamic Light Scattering (DLS), Differential Scanning Calorimetry (DSC) and Raman Spectroscopy. Furthermore, Transmission Electron Microscopy (TEM) had underlined the planar conformation of RGO that would offer a larger surface available for the siRNA attachment through stacking interactions. In order to evaluate if the complex is a good candidate for cellular therapy, its biocompatibility and its ability to be internalized by cells were performed in cells treated with different amount of the complex.

The use of nanosystems for tumour therapy can offer a large variety of advantages respect to the classical drug administration technics. The possibility to link higher amount of drugs or biological molecules, like siRNA, to a vector and to release them in a controlled way, strongly limits the typical side effects of the chemotherapy. In this way, all the therapeutic agents are released in the same time, amplifying the signal and inducing a better effect. Therefore, the optimization of systems with these characteristics can offer the bases for an innovative therapeutic approach.

Materials And Methods

Cell culture

Human mammary epithelial cell line **HB-2** was grown in Low-glucose Dulbecco's Modified Eagle Medium (LG-DMEM, Sigma) supplemented with 10% (v/v) Fetal Bovine Serum (FBS) (Euroclone, Celbar), 100 units per ml penicillin G, 100 µg ml^{-1} streptomycin (Euroclone, Celbar), 2 mM l-glutamine (Euroclone, Celbar), 5 µg ml^{-1} hydrocortisone (Sigma Aldrich) and 10 µg ml^{-1} Bovine Insulin (Sigma Aldrich).

Human cervical cancer cell line **HeLa,** human breast cancer cell line **MDA-MB231,** human Hepatic Adenocarcinoma Cell Line **SK-HEP-1,** Human liver hepatocellular carcinoma cell line **HepG2** and Human normal bronchial epithelial **16HBE** cells were grown in Dulbecco's Modified Eagle Medium (DMEM, Sigma) containing 10% (v/v) FBS (Euroclone, Celbar), 100 units per ml penicillin G, 100 µg ml^{-1} streptomycin (Euroclone, Celbar) and 2 mM L-glutamine (Euroclone, Celbar).

ECV-304 (Endothelial Cell Vein) was grown in M199 medium (Sigma) with 10% (v/v) FBS (Euroclone, Celbar), 100 units per ml penicillin G, 100 µg ml^{-1} streptomycin (Euroclone, Celbar) and 2 mM L-glutamine (Euroclone, Celbar).

Human colon cancer **HCT-116** cells were grown in RPMI-1640 medium added of 10% fetal bovine serum (FBS), 100 U/ml penicillin, 100 µg ml^{-1} streptomycin and 2 mM L-glutamine.

All the cells were cultivated at 37°C, in a humidified atmosphere of 5% CO_2 and maintained in sterile conditions.

Nano-conjugates

INU-EDA-P,C-DOXO, PHEA-EDA-P,C-DOXO and **RGO** systems and all their variants were developed and characterized by Professor Gaetano Giammona research group (Laboratory of Biocompatible Polymers, Department of "*Scienze e Tecnologie Biologiche, Chimiche e Farmaceutiche*" (STEBICEF)) of the University of Palermo.

- Inulin-pentyne,citraconate-doxorubicin **(INU-EDA-P,C-DOXO)** was a pH sensible system synthetized first combining pentynoic acid to an amine functionalized inulin derivative (INU-EDA) through amidic link. Later, it was functionalized with citraconic anhydride to obtain pH-sensitive citraconate pendants, which were partially functionalized with doxorubicin (Figure 17). A fluorescence variant was

obtained by conjugation to Fluorescein Isothiocyanate (FITC) green probe (**INU-EDA-P,C-DOXO-FITC**).

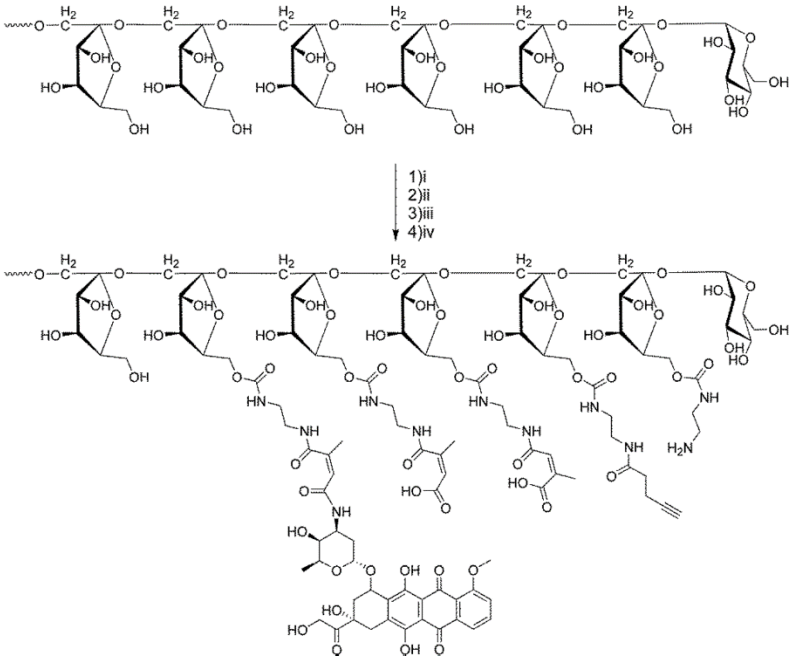

Figure 17. Schematic representation of the INU-EDA-P,C-DOXO synthesis. i) Bis(4-nitrophenyl) carbonate, 4h, 40°C, 40'; EDA; ii) EDC HCl, NHS, pentynoic acid, pH 6.8, r.t., 18h; iii) Citraconic anhydride, NaOH, pH 8-9, 2h; iv) EDC HCl, NHS, doxorubicin hydrochloride, pH 6.8, r.t., 18h.

- α,β-poly(N-hydroxyethyl)-D,L-aspartamide **(PHEA)** was a multifunctional polymer that was coupled to doxorubicin though cis-citraconic acid to form **PHEA-EDA-P,C-DOXO (**α,β-poly(N-hydroxyethyl)-D,L-aspartamide- pentyne,citraconate-doxorubicin) (Figure 18).

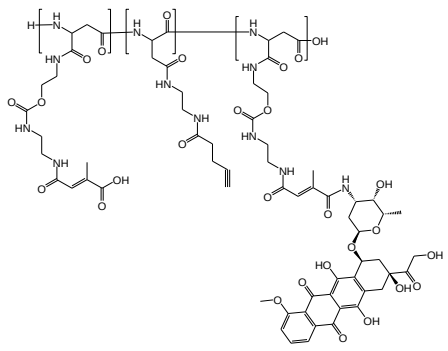

Figure 18. Schematic representation of PHEA-EDA-P,C-DOXO

- Graphene was a single-atom thick, two-dimensional sheet of hexagonally arranged carbon atoms isolated from its three-dimensional parent material, graphite. The oxide reduced form (**RGO**) was a highly oxidized form of chemically modified graphene; their structure consisted of single-atom-thick carbon sheets with carboxylate groups on the periphery, where they provided pH dependent negative surface charge and colloidal stability. The basal surfaces contain hydroxyl (-OH) functional groups, which were uncharged but polar. The basal planes also included unmodified graphenic domains that were hydrophobic and capable of π-π interactions relevant to adsorption of dye molecules or some drugs (Figure 19).

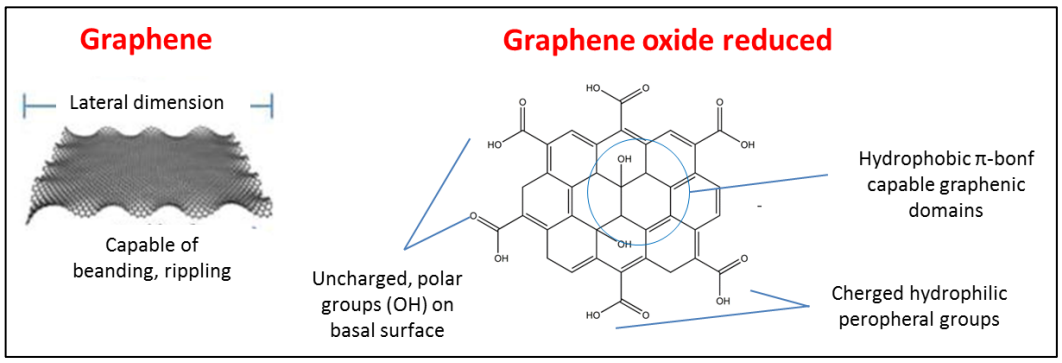

Figure 19. Representation of Graphene and RGO

Graphene variants were obtained by conjugating Seprase antibody alone (**RGOY**) or with Polyvinylpyrrolidone (PVP) (**RGOY-PVP**) in order to reduce the stacking interaction between the graphene sheets.

RGOY and RGOY-PVP were also conjugated to the red fluorescence probe Alexa Fluor 647 (RGOY-AF and RGOY-PVP-AF respectively) for the uptake studies.

Polyvinylpyrrolidone (**PVP**) nanogels (NGs) were synthetized in collaboration with Professor Clelia Dispenza research group (Department of "*Ingegneria Chimica, Gestionale, Informatica, Meccanica* (DICGIM))" of the University of Palermo. This nanoparticles were synthesized by high-energy radiation (e-beam irradiation), starting from a dilute aqueous solution of a commercial polyvinylpyrrolidone (PVP), that can be simultaneously grafted with a variety of functional monomers like acrylic acid (AA). In this way, it was possible to obtain carboxyl functionalized PVP nanogels, named K60-0.5AA50E40, in only one-step of

synthesis. (Figure 20). The resulting NGs are formulated with appropriate size, shape, surface properties and specific chemical functionality. A variant of PVP nanogels was obtained by conjugating (3-[(2 aminoethyl)dithio] propionic acid) AEDP to obtain PVP-AEDP nanoparticles.

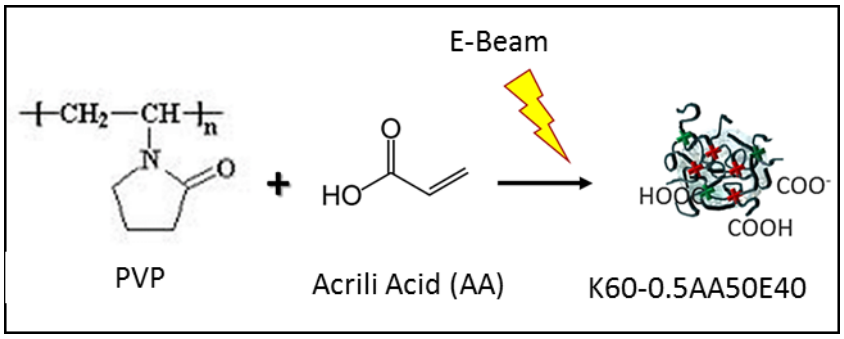

Figure 20. Schematic representation of the K60-0.5AA50E40 synthesis through electron beam (e-beam) irradiation. polyvinylpyrrolidone (PVP) e acrylic acid (AA) were used to obtain PVP carboxyl functionalized nanogels K60-0.5AA50E40.

INULIN and PHEA nanosystems

Cytotoxicity studies

Cells were seeded in 96-well plates at the density of 1 x 10^4 cells/well and grown in the appropriate medium for 24h at 37°C in a humidified atmosphere of 5% CO_2. Therefore, they were incubated with the opportune amount of conjugates as indicated in table 1. Cells treated with the same concentrations of free doxorubicin were considered as positive control, whereas untreated cells as negative control. Cytotoxicity assay was conducted using Cell Counting Kit-8 (CCK-8) (Sigma Aldrich). In particular, water-soluble tetrazolium salt (WST-8) was added to each samples (1:10 dilution in complete medium) and incubated at 37°C for 2h in order to permit its reduction by mitochondrial dehydrogenases of the living cells into soluble formazan dye that was so directly proportional to the number of living cells. The absorbance were determined at a wavelength of 460 nm by a microplate reader DU-730 Life Science spectrophotometer (Beckman Coulter). The viability was expressed as

percentage respect to the negative control (100% of cell viability). Each experiment was done in triplicate.

Nano-system	Cell culture	Doxorubicin concentration (µM)	Incubation time
INU-EDA-P,C-DOXO	HB-2	0.5; 5; 25; 50.	24
	MDA-MB231		
	16 HBE	0.05; 0.1; 0.5; 5; 25; 50.	24; 48
	HCT 116		
	SK-Hep 1		
PHEA-EDA-P,C-DOXO	HB-2	0.5; 2; 3.5; 5; 10; 15; 20; 25.	24
	MDA-MB231		
	SK-Hep 1	0.05; 0.1; 0.5; 5; 25; 50.	24; 48

Table 1. Schema of different cell lines treated with a variety of doxorubicin concentrations conjugated to INU-EDA-P,C-DOXO or PHEA-EDA-P,C-DOXO for 24 or 48h.

Quantitative uptake by flow cytometry

Cells were grown in 6-well plates at 37°C and 5% CO_2 until the confluence state. Afterwards, they were incubated with the specific conjugates at the doxorubicin concentration and times reported in table 2. Subsequently, the samples were washed with Phosphate Buffer Saline (PBS) without Ca^{2+} and Mg^{2+}, detached by Trypsin-EDTA 1X in PBS (EuroClone) and collected by centrifugation at 1000 rpm for 5'. The pellets were re-suspended in 500µL of PBS and analysed by FACS-Canto cytometer (Becton Dickinson, Germany) detecting the green (FITC) and the red (Doxo) fluorescence emission (530–585nm respectively). For each sample were collected 1 x 10^5 events investigated by BD FACS Diva software.

Nano-system	Cell culture	Doxorubicin concentration (µM)	Incubation time (hours)
INU-EDA-P,C-DOXO-FITC	HB-2	25	1; 2; 4; 6; 8; 24.
	MDA-MB231		
PHEA-EDA-P,C-DOXO-FITC	HB-2	25	0.5; 1; 2; 4; 6; 8; 24.
	MDA-MB231		

Table 2. Schema of quantitative uptake by flow cytometry assay

Qualitative uptake by fluorescence microscopy

Cells were seeded into 12-well plates containing sterile coverslips at a density of 5 x 10^3 cells per well with the opportune complete medium and grown for 24h at 37°C in a humidified atmosphere of 5% CO_2. Next, each sample was incubated with the specific FITC variant of the nanosystems over time (see table 3) and washed with PBS in order to remove the nanocojugates that were not taken up by the cells. After, they were fixed with 3.7 wt % formaldehyde for 15 minutes. Nuclei were labelled with DAPI (dilution of 1: 10000 in water) for 15 minutes at room temperature. The green fluorescence relative to the nano-conjugates and red auto-fluorescence of the doxorubicin were detected by fluorescence microscopy (Leica). Untreated cells were used to calibrate the background fluorescence.

Nano-system	Cell culture	Doxorubicin concentration (µM)	Incubation time (hours)
INU-EDA-P,C-DOXO-FITC	HB-2	25	1; 4; 24.
	MDA-MB231		
PHEA-EDA-P,C-DOXO-FITC	HB-2	25	1; 4; 6; 24.
	MDA-MB231		

Table 3. Schema of qualitative uptake by fluorescence microscopy assay

Co-culture experiments

The co-culture studies were conducted only for **PHEA-EDA-P,C-DOXO** nano-systems. Tumour cells MDA-MB231 (1 x 10^5 cells/mL) were stained with 25 µM Molecular Probe

CellTrace CFSE fluorescent stains (CellTrace CFSE Cell Proliferation Kit- Life technologies) by incubating for 30 minute at 37°C.

Labelled MDA-MB 231 and unlabelled HB-2 normal cells were mixed in ratio 1:1 and were grown at the final density of 8 x 10^4 cells/well into 12-well plates containing sterile coverslips in complete LG-DMEM for 24h at 37°C.

Afterwards, the samples were incubated with PHEA-EDA-P,C-Doxo or free Doxo as positive control (final Doxo concentration of 10 µM) for 15', 30', 1h, 2h, 4h, 6h, 24h. Following, the cells were washed twice with PBS, fixed with 3.7 wt % formaldehyde for 15 minutes and washed again with PBS. Additionally, nuclei were stained with DAPI (1: 10000) for 15 minutes at room temperature. Untreated cells were considered as negative control to set the auto fluorescence. The samples were analysed by fluorescence microscopy (Leica).

Analysis of PHEA-EDA-P,C-FITC-Doxo internalization mechanisms.

Internalization studies was carried out both on tumour cells (MDA-MB 231) and normal ones (HB-2) through flow cytometry and confocal microscopy. In both experiments, the cells were pre-incubated for 10 minutes with PBS-G buffer (PBS with 5mM 2- deossi-D-Glucose) and subsequently with different endocytosis inhibitor. The endocytosis inhibitors used are 75 µM ethyl-isopropyl amiloride (EIPA); 40 µM nystatin and 5 µM Phenylarsine oxide (PAO). EIPA and Nystatin were incubated 10' at 37°C while PAO for 5' at 37°C. Therefore, PHEA-EDA-P,C-FITC-Doxo (final Doxo concentration of 25 µM in PBS-G buffer) mixed with EIPA or Nystatin and without PAO were added and incubated for 1 h at 37°C. Samples incubated only with PHEA-EDA-P,C-FITC-Doxo for the same time were considered as positive control, while cells incubated at 4°C for 20' and then treated with conjugates for 1h were used to estimate the passive internalization.

- For flow cytometry studies, the cells were maintained in 6-well plates with the appropriate medium until the cell confluence. After the mentioned treatment, they were washed with PBS without Ca^{2+} and Mg^{2+}, detached by Tripsin 1X (EuroClone) and centrifuged at 1000 rpm for 5 minutes. The cell pellet obtained was re-suspended with 0.5 mL of PBS and analysed by FACS-Canto cytometer (Becton Dickinson, Germany) in order to detect the green (FITC) and the red (Doxo) fluorescence

emission (respectively 530–585nm). For each sample were collected 1 x 10^4 events investigated by BD FACS Diva software.

- For confocal microscopy studies, the cells were seeded on 12-well plates containing sterile coverslips at a density of 5 x 10^3 cells per well and grown for 24h at 37°C. Therefore, the cells were treated only with Nystatin inhibitor as described above and, after washing twice with PBS, were fixed with 3.7 wt % formaldehyde for 5 minutes. Nuclei were labelled with DAPI (1: 10000 in water) for 15 minutes at room temperature and the samples were detected by FLUOVIEW FV10i-LIV (Olympus). Cells treated with PHEA-EDA-P,C-FITC-Doxo were consider as positive control and cells inhibited by 4°C treatment as negative control.

Lysosomal-specific PHEA-EDA-P,C-Doxo localization studies

MDA-MB231 cells were grown at a density of 5 x 10^3 cells/well into 12-well plates containing sterile coverslips in complete medium for 24h at 37°C. Therefore, they were incubated with 10µM of PHEA-EDA-P,C-Doxo for 30', 1h, 2h, 4h, 6h and 24h. At the end of each time, samples were incubated with 60nM of LysoTracker® Red DND-99 (Thermo Fisher scientific) for 1h at 37°C, washed twice with complete phosphate buffer saline (PBS) and fixed with 3.7 wt % formaldehyde for 5 minutes. After different washing with PBS, nuclei were labelled with DAPI (1 : 10000) for 15minutes at room temperature. The samples were detected by confocal microscopy (FLUOVIEW FV10i-LIV, Olympus).

PVP nanogels

Small interference RNA (siRNA)

The siRNA employed for the silencing experiments are reported in Table 4.

siRNA	siRNA sequence (sense strand)	Modification	Strand of modification
Egr-1	5'-CAAUUACUAUUCCCUUUGATT-3'	/	/
Egr-1	5'-CAAUUACUAUUCCCUUUGATT-3'	5'-AminoC6linker	sense
Bcl-2	5'-GGGAGAACAGGGUACGAUATT-3'	/	/
Bcl-2	5'-GGGAGAACAGGGUACGAUATT-3'	5'-AminoC6linker	sense

Table 4. siRNA characteristics.

Transfecting siRNA into mammalian cells using Lipofectamine

SK-HEP-1 or HeLa cells were seeded into 6-well plates and growth at 37°C with 5% CO_2. Hela cells were transfected with Bcl-2 siRNA; while SK-HEP-1 were treated with Egr-1 (Early growth response-1) siRNA. The expression of Egr-1 was regulated by Hepatocyte growth factor (HGF) and could be influenced by the factors presented into the serum. For this reason, the samples were first subjected to a gradual FBS starvation (5% FBS for 48h; 2.5% FBS for 24h; 0.2% FBS for 24h and 0% FBS for 24h) and then to HGF treatment (10 mM HGF at 37°C for 30', 1h, 2h, 3h,and 5h).

In all assays, 24 hours before transfection, the culture medium was substituted with medium without antibiotics so they were at 50% of confluence at the time of transfection.

The appropriate amount of unmodified siRNA (Table 5) was diluted in Opti-MEM® Reduced Serum Medium (Thermo Fisher) without serum and mixed gently. On the other hand, Lipofectamine 2000 (Invitrogen) was also diluted in the same medium and incubated for 5 minutes at room temperature. The diluted siRNA and the diluted Lipofectamine were mixed and incubated for 20 minutes at room temperature in order to form the complex

siRNA-Lipofectamine that, after appropriate dilution in culture medium without serum and antibiotics, was added to the cells. In all cases, the transfection was conducted for 48 hours. Untreated cells were used as negative control.

siRNA	siRNA (pmol)	Lipofectamine (µL)	Opti-MEM (µL)
Unmodified Egr-1	75	3.75	187.5
Unmodified Bcl-2	100	5	250

Table 5. Schema of Transfecting siRNA assays.

Conjugation of siRNA to PVP nanogels

First of all, PVP nanogels were sterilized using a 0.2µM filter and the samples were always treated in sterile conditions. They were dialysed (14 kDa) against NaOH 0.2M for 24h in order to deactivate Ribonuclease (RNAse) that could degrade the siRNA. After that, NGs were dialysed against H_2O RNAse free.

0.5mg/ml of PVP nanoparticles (108.04 pmol) were mixed with:

- 0.09 mM of EDC (1-Ethyl-(3-dimethylaminopropyl) carbodiimide) diluted in MES (4-Morpholineethanesulfonicacid) 2% (pH of 6.5)
- 0.18 mM of Sulfo-NHS (N-hydroxysulfosuccinimid)

The blend was incubated for 30 min in agitation at room temperature.

Therefore, 720 pmol of 5'-AminoC6linker siRNA were mixed and incubated for 3 hours in agitation at 4°C and then dialyzed against H_2O RNAse free to eliminate the excess of unlinked siRNA.

For the cell colure, the samples were then dialyzed against the appropriate medium.

The amount of siRNA conjugated to NGs was determined by reading the absorbance values at 260 nm employing the NanoDrop 1000 Spectrophotometer. Different concentrations of free siRNA were used for a Standard Assay.

Treatment with PVP-siRNA complex

Hepatocellular carcinoma cells (SK-HEP-1) were seeded in 6-well plates and maintained at 37°C in in a humidified atmosphere of 5% CO_2. Cells were subjected to FBS starvation and HGF treatment as reported above and subsequently were treated for 48h with 150 pmol of Egr-1 siRNA conjugated with PVP NGs. Cell treated with the same amount of PVP alone were used as negative control.

Treatment with PVP-AEDP-siRNA complex

HeLa cells were seeded in 6-well plates and grown at 37°C with 5% CO_2. Some samples were incubated for 2 hours at 37°C with 10mM of GSH-Oet (Glutathione reduced ethyl ester, Sigma Aldrich) in complete medium. After the opportune washes with PBS, PVP-AEDP or PVP-AEDP-siRNA (300pmol of siRNA) complex were added for 48h.

Extraction of soluble proteins

Cells were seeded in 6-well plates maintained at 37°C in a humidified atmosphere of 5% CO_2. After the appropriate treatment, the samples were washed with PBS without Ca^{2+} and Mg^{2+}, detached by Trypsin-EDTA 1X in PBS (EuroClone) and collected by centrifugation at 1000 rpm for 5'. The pellets were re-suspended in an appropriate volume (depending of the pellet size) of RIPA Buffer 1X (50mM Tris-HCl pH 7.5; 0.5% sodium deoxycholate; 150 mM NaCl; 1% Triton X-100) supplemented of proteases inhibitors:

- 1 mM of phenylmethylsulfonyl fluoride (PMSF) against serine proteases
- 1 µM of Pepstatin A against aspartyl proteases
- 100 µM Leupeptin against cysteine, serine and threonine peptidases
- 10 mM Ethylenediaminetetraacetic acid (EDTA) against metallopeptidases

At this point, the samples were incubated in ace for 15 minutes and constantly subject to micro vortex mixer treatments and then centrifuged at 10,000 rpm for 20 minutes.

The amount of proteins extracted presented into the supernatant were calculated by the Bradford assay (Bradford Reagent, Sigma), using different concentrations of bovine serum albumin (BSA) as Standard Assay.

Western Blot assay

20 µg of proteins were mixed with sample buffer 1X (62.5 mM Tris-HCl pH 6.8; 2.5 % SDS; 0.002 % Bromophenol Blue; 0.7135 M (5%) β-mercaptoethanol; 10 % glycerol) and incubated at 100°C for 5 minutes and immediately situated in ice. The proteins were separate by sodium dodecyl sulfate Polyacrylamide gel electrophoresis (SDS-PAGE) at the opportune SDS percentage, depending of the molecular weight of the interesting protein.

At the end, the gels and the nitrocellulose membrane (Hybond, *Amersham*) were washed in transfer buffer (20% methanol; 10% Running buffer 1X: Tris base 3 g/L-Glycine 14.4g/L) and the proteins were transferred from the gel to the membrane through electroblotting at 100V e 300 mA for 90 minutes at low temperature. Blocking of non-specific binding was achieved by placing the membrane in a solution of non-fat dry milk (3%) overnight a 4°C. Therefore, the specific primary antibody (IgG produced in mouse) (see table 6) was incubated again overnight at 4°C; after washing with TBS-T solution (0.6% Trizma base; 0.87% NaCl; 0.05% Tween 20), the peroxidase-linked anti-mouse secondary antibody (Sigma) was incubated for 2h at room temperature. After other TBS-T washes, the presence of the target protein was identify using "SuperSignal West Femto Maximum Sensitivity Substrate" (Thermo Scientific) and the chemiluminescence signal was reveal using the ChemiDoc XRS (Biorad). The intensity of the discovered bands was analysed by Image J program and β-actin was used to normalize each sample.

Proteins	% SDS PAGE	Primary Antibodies (IgG) produced in mouse	Peroxidase-linked secondary Antibodies Anti-mouse
Egr-1 (Sigma)	12	1 µg/ml	0.04 µg/ml
Bcl-2 (Sigma)	15	1:1,000	0.04 µg/ml
β-actin (Sigma)	12	0.4 µg/ml	0.04 µg/ml
	15		

Table 6. Schema of Western blot assays.

RGO, RGOY and RGOY-siRNA systems

Sterilization of RGO, RGOY and RGOY-PVP

In order to obtain sterile nanoparticles for *in vitro* studies, sterilization protocols with Ethanol (EtOH) 70% (Konios D. *et al.,* 2014) was performed:

- RGO was suspended in EtOH 70 % (0.05 mg/ml) and sonicated (3x120 sec) in order to reduce the aggregation of the sheets. At this point, they were first dialysed in sterile H_2O for 72h and they were dialysed in appropriate culture medium only for the biological studies.
- RGOY and RGOY-PVP was suspended in EtOH 70% (0.05 mg/ml) and put into a laminar flux hood to permit the Ethanol evaporation. The samples were suspended in culture medium without Fetal Bovine Serum (FBS) and subjected to sonication cycles in a 35kHz Ultrasonic Bath (3x10 minutes) alternating by micro vortex mixer treatments (3x5minutes).

Characterization of RGO and RGOY

RGO and RGOY systems were characterized in collaboration with Professor Peter Griffiths research group (Head of Department Pharmaceutical, Chemistry and Environmental Science, University of Greenwich -Medway Campus) through Dynamic Light Scattering (DLS), Transmission Electron Microscopy (TEM), Differential Scanning Calorimetry (DSC) and Raman Spectroscopy.

For the DLS analysis, the samples dispersed in water (0.05 mg/ml) were diluted 1:5 in bidistilled water and put into a quartz cuvette of 1mL. The size distribution were performed using a Malvern Zetasizer Nano-ZS (Malvern, UK). The measures were done in triplicate.

For the Transmission Electron Microscopy (TEM), the samples were diluted in bidilled water at the concentration of 20 mg/ ml and were placed on copper grids with films for observation. After 1 min of absorption, excess liquid was blotted off with filter paper. The dried specimens were examined by using a JEOL JEM200CX microscope. The electron beam was accelerated with a voltage of 1000V. The TEM images were captured using a Gatan, Inc.,ORIUS SC200CCD Camera.

DSC measurements were conducted using a Mettler Toledo DSC 823 instrument (Schwerzenbach, Switzerland). Approximately, 1-3 mg samples were accurately weighed in standard aluminium pans. An empty pan was used as a reference. A scan rate of 10 °C/min was employed to heat the samples from 25 to 350 °C. Analysis was performed under a nitrogen purge (60 ml/min). Calorimetric parameters were analysed using STARe Software.

Raman spectra were recorded with a LabRam Raman spectrometer (Horiba Jobin Yvon,Ltd), fitted with a Peltier-cooled CCD camera for detection and an Olympus BX40 microscope.

Biocompatibility of RGO and RGO-PVP

HepG2 and ECV-304 cell were seeded in 96-well plates at the density of 1 x 10^4 cells/well and maintained at 37°C in a humidified atmosphere of 5% CO_2. The day after, cells were treated with different amount of RGO or RGOY or RGOY-PVP systems for 24h, 48h and 72h as reported in table 7. At the end of each time, cells were incubated with 200µL/well of complete medium containing 0.25 mg/mL of MTT solution for 2h at 37°C. In living cell, the yellow tetrazole MTT is reduced to purple formazan that was solubilized with 100µL/well of DMSO solution and the relative absorbance was read at 490 nm wavelength on a DU-730 Life Science spectrophotometer (Beckman Coulter). The viability was expressed as percent values related to the untreated cells (100% of viability). Cells treated with Polyethylenimin (PEI) were used as positive control. Each experiment was repeated tree times.

Nano-systems	Cell culture	Nano-systems' concentration (µM)	Incubation time
RGO	HepG2	12.5; 25; 50; 100.	24, 48, 72
RGOY	ECV-304	0.25; 0.5; 1; 2.5; 5; 10; 15; 20; 25; 30; 50.	24, 48, 72
RGOY-PVP	ECV-304	0.25; 0.5; 1; 2.5; 5; 10; 15; 20; 25; 30; 50.	24, 48, 72

Table 7. Schema of different cell lines treated with a variety of concentrations of RGO, RGOY or RGOY-PVP for 24, 48 and 72h.

Uptake studies by confocal microscopy

ECV-304 cells were seeded on 12-well plates containing sterile coverslips at a density of $5x10^3$ cells per well and grown for 24h at 37°C. Therefore, cells were incubated with 50 µM of RGOY for 15', 30', 1h and 2h or with 5 µM of RGOY-PVP for 15', 30', 1h, 2h, 4h and 6h. At the end of each time, the samples were washed with complete phosphate buffer saline (PBS) and fixed with 3.7 wt % formaldehyde for 5 minutes. After other washings with PBS, nuclei were labelled with DAPI (1: 10000) for 15minutes and then the actin cytoskeleton were stained with phalloidin-FITC (1:500) per 15'. The samples were detected by confocal microscopy (FLUOVIEW FV10i-LIV, Olympus).

Results and discussion

In order to compare two different nano-system models for tumour therapy, inulin (INU) and α,β-poly(N-hydroxyethyl)-D,L-aspartamide (PHEA) were conjugated to the anti-cancer drug doxorubicin (Doxo), through a pH-sensitive link (Cytraconylamide). Both the nano-conjugates were synthetized in collaboration with Prof. Gaetano Giammona research group (Laboratory of Biocompatible Polymers, Department of "Scienze e Tecnologie Biologiche, Chimiche e Farmaceutiche" (STEBICEF)) of the University of Palermo.

INU-EDA-P,C-DOXO

Inulin is a natural, biocompatible and biodegradable (Van der *Zee et al.*, 1995) polysaccharide constituted by linear chains of β-(1-2) fructose units carrying a glucose unit as reducing end-chain. To obtain the nanosystem, inulin was firstly functionalized with ethylenediamine (EDA) and then coupled with pentynoic acid (P) and citraconic anhydride (C) used for the doxorubicin (Doxo) conjugation. The forming complex was named INU-EDA-P,C-DOXO and was characterized by Proton Nuclear Magnetic Resonance (^{1}H NMR) spectroscopy, UV spectrophotometry and Size-Exclusion Chromatography (SEC) analysis (Table 8). These analyses permit to individuate the specific nanopolymer composition and some properties like molecular weight and zeta-potential. Furthermore, the shape was investigated through by Scanning Electron Microscopy (SEM) and the amount of drug release at different pH values was determined by High Performance Liquid Chromatography (HPLC) (data not shown) (Mauro, Campora *et al.*, 2015).

Table 8. Characteristics of INU-EDA-P,C-Doxo and its precursors: molecular weight (Mw), polydispersity ζ-Potential and composition.

			Composition				
Sample	**[c]Mw**	**[c]Mw/Mn**	**[a]DDEDA (%)**	**[a]DDPentine (%)**	**[a]DDcitric (%)**	**[b]DDDoxo (%)**	**ζ-Pot (mV)**
INU-EDA	4	1.87	19	-	-	-	18.8±3.9
INU-EDA-P,C	4.3	1.7	19	4.1	16.1	-	24.8±4.1
INU-EDA-P,C-Doxo	13.3	1.62	19	4.1	16.1	8.57	18.2±7.0

[a] Calculated by means of ^{1}H NMR spectroscopy.

[b] Calculated combining ^{1}H NMR spectroscopy and UV spectrophotometry.

[c] Obtained by SEC analysis in 0.1 M LiBr DMF solution.

Cytotoxicity of INU-EDA-P,C-Doxo

In order to evaluate a specific cytotoxic effect of INU-EDA-P,C-Doxo, viability assay was performed in different cell lines including normal cells like 16HBE and tumour cells like HCT 116 and SK-Hep-1. After 24h of incubation looking at the lowest nanoconjugates concentrations (0.05; 0.1 and 0.5 μM) no differences in the viability were observed between normal and tumour cells (all the samples presented a viability of 100%); but at 5 μM and, more and more, at 25μM and 50μM, the viability of tumor cells strongly decrease respect to the control. Indeed, for example, at the concentration of 5 μM, 16 HBE presented a viability of 84.97%, while HCT 116 and SK-Hep-1cells showed respectively values of 49.95% and 44.44% (Figure 21, Panel A). After 48 hours (Figure 21, Panel B), the doxorubicin conjugated to the nano-systems started to kill also the normal cells, even though with a weaker effect (at 25 μM it was registered a viability of 39.40% *vs.* 12.12% *vs.* 3.07% for 16 HBE *vs.* HCT 116 *vs.* SK-HEP-1 respectively).

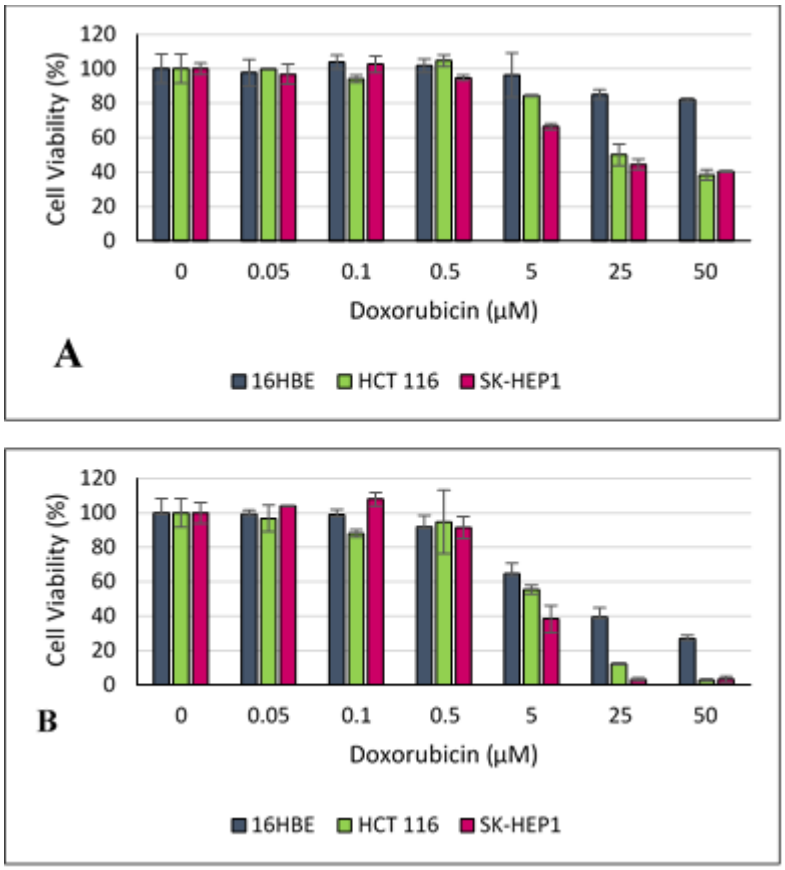

Figure 21. Cytotoxic assay on normal (16HBE) and tumour (HCT 116 and SK-Hep-1) cell lines treated with INU-EDA-P,C-Doxo for 24h (Panel A) and 48h (Panel B).

The specific effect of INU-EDA-P,C-Doxo was more evident comparing healthy and cancer cells from the same tissue. For this purpose, HB-2 and MDA-MB 231 cell lines were selected: they are normal and tumour cells of the breast tissue, respectively. Figure 22 shows the viability of both cells incubated for 24 h with different amount (0.5; 5; 25 and 50 µM) of INU-EDA-P,C-Doxo and free doxorubicin as positive control. In all the cases a dose-dependent reduction of viability was observed, but with some outstanding differences. It is evident that the viability of HB-2 treated with the conjugates was always higher, even if compared to free drug-treated samples. By contrast, INU-EDA-P,C-Doxo induced higher mortality level on tumor cells, especially when they were incubated with the doxorubicin concentration of 25 µM (52% vs 32% of viability for HB-2 and MDA-MB 231 respectively). Comparing the effects of doxorubicin alone and doxorubicin linked to Inulin on cancer cells, it is evident that at low concentrations, the nanosystem was significantly less efficient; but at higher concentrations (25 µM) the viability of tumor cells treated with INU-EDA-P,C-Doxo was lower than the one of tumor cells treated with plain drug (32% against 39%

respectively). These data suggested that the inulin would improve the specific action of the doxorubicin by conferring more selectivity for tumor cells respect to the normal ones independently of the EPR effect.

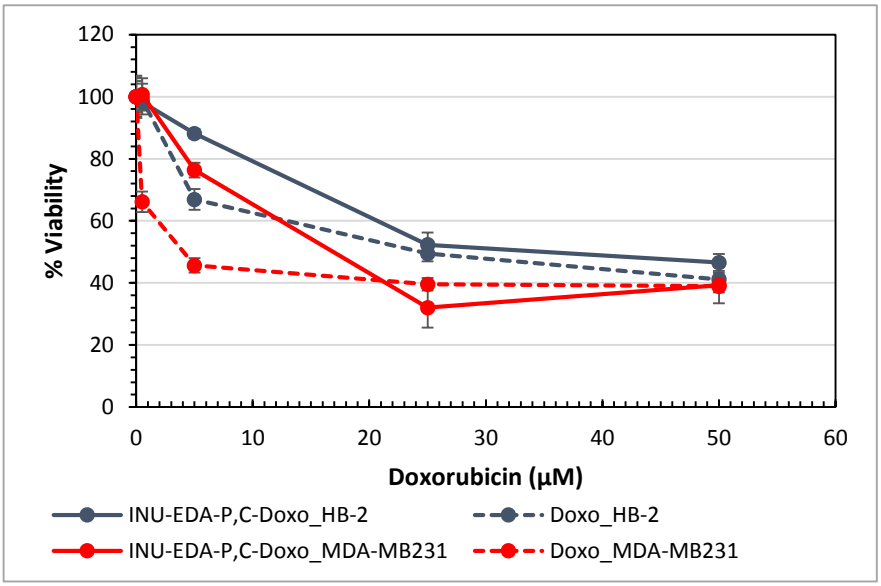

Figure 22. Cytotoxic assay on normal (HB-2) and tumour (MDA-MB 231) cell lines treated with INU-EDA-P,C-Doxo or free doxorubicin for 24h.

Qualitative uptake by fluorescence microscopy

To investigate, in greater detail, the different effect of the conjugates on normal and tumour cells, uptake studies were conducted using a variant of the system in which the polymer was stained with the green fluorescence probe FITC (INU-EDA-P,C-DOXO-FITC). In this way, fluorescence microscopy studies permitted to follow both Inulin and the drug released thanks to the FITC probe and the Doxo red auto-fluorescence. The Panel A of the figure 23 shows MDA-MB 231 cells incubated with the complex for different times (1h, 4h and 24h). After 1h of treatment, the co-polymer is localized in the cytoplasm and the drug is still linked to it, as demonstrated by the co-localization of the two fluorescence (a-a’’’). Four hours later, the green mark is still in the cytosol and, in particular, in the perinuclear region, while the red-doxo signal appears in the nuclear compartment, suggesting that the drug has been already released (b-b’’’). By contrast, in HB-2 normal cells (Panel B), after 1h of incubation, the green fluorescence appears muffled, punctuate and restricted in a peripheral cytosolic area and this organization persists even after 4h (e-e’’’). At 24h, the drug is totally confined

in the nuclei of MDA-MB 231 that looks damaged (c-c’’’), while it is barely presented in the nuclei of healthy cells that show a good morphology (f-f’’’).

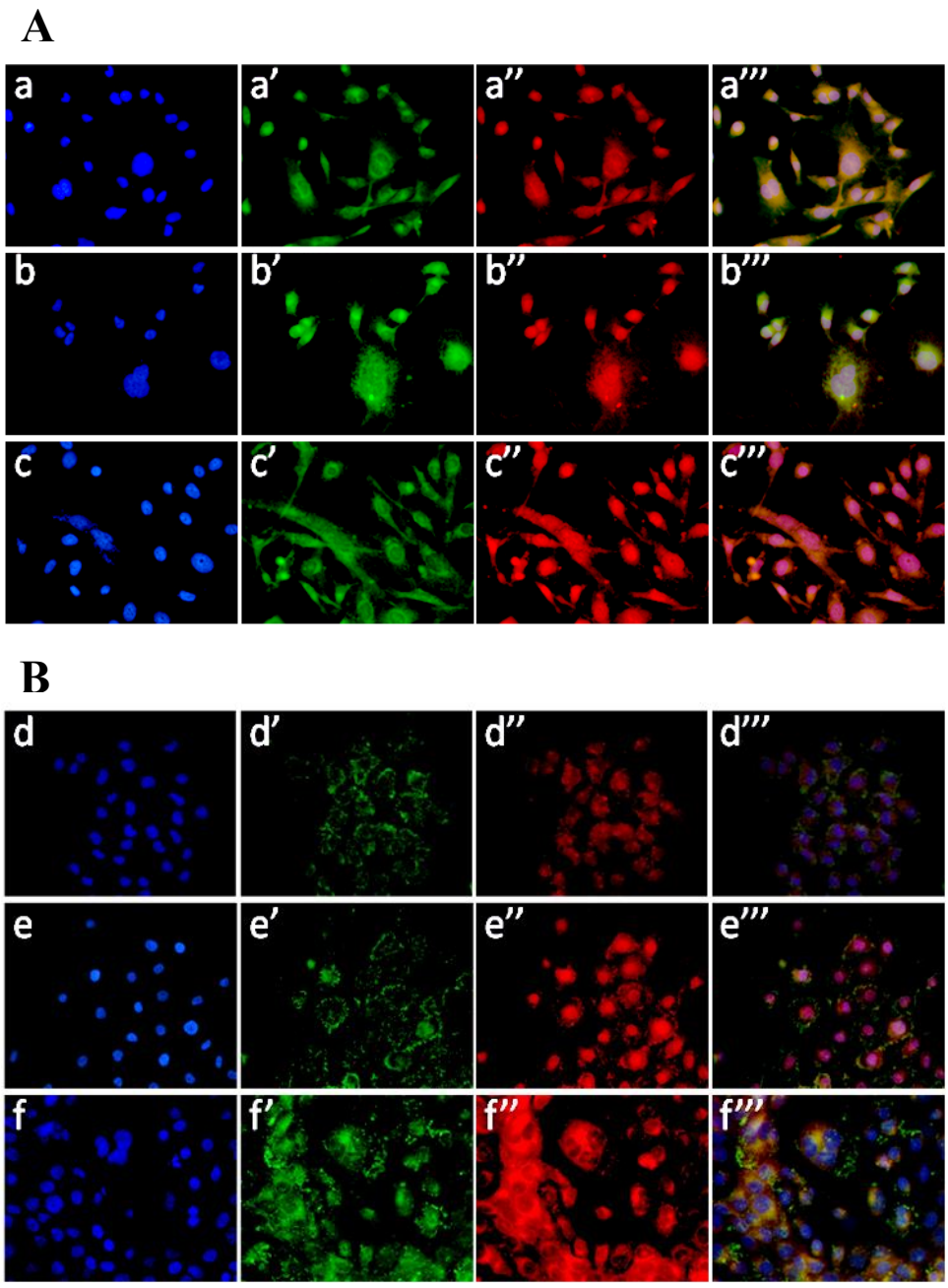

Figure 23. Fluorescence microscopy of MDA-MB 231 (Panel A) and HB-2 (Panel B) treated with INU-EDA-P,C-Doxo for 1h (a-a’’’ and d-d’’’), 4h (b-b’’’ and e-e’’’) and 24h (c-c’’’ and f-f’’’). Blue: nuclei; Green: Inulin; Red: doxorubicin; merge: overlay of three fluorescence. Magnificence 40X.

Quantitative uptake by flow cytometry

The INU-EDA-P,C-DOXO-FITC uptake was further investigated in the course of time (1, 2, 4, 6, 8 and 24h) both in normal (Figure 24, Panel A) and tumour cells (Figure 24, Panel B) by flow cytometry. These studies permitted to obtain also a quantitative information, following independently the FITC fluorescence relative to inulin (530 nm) and the autofluorescence of the doxorubicin (585nm). In each cytogram 1 x 10^5 events analysed were represented.

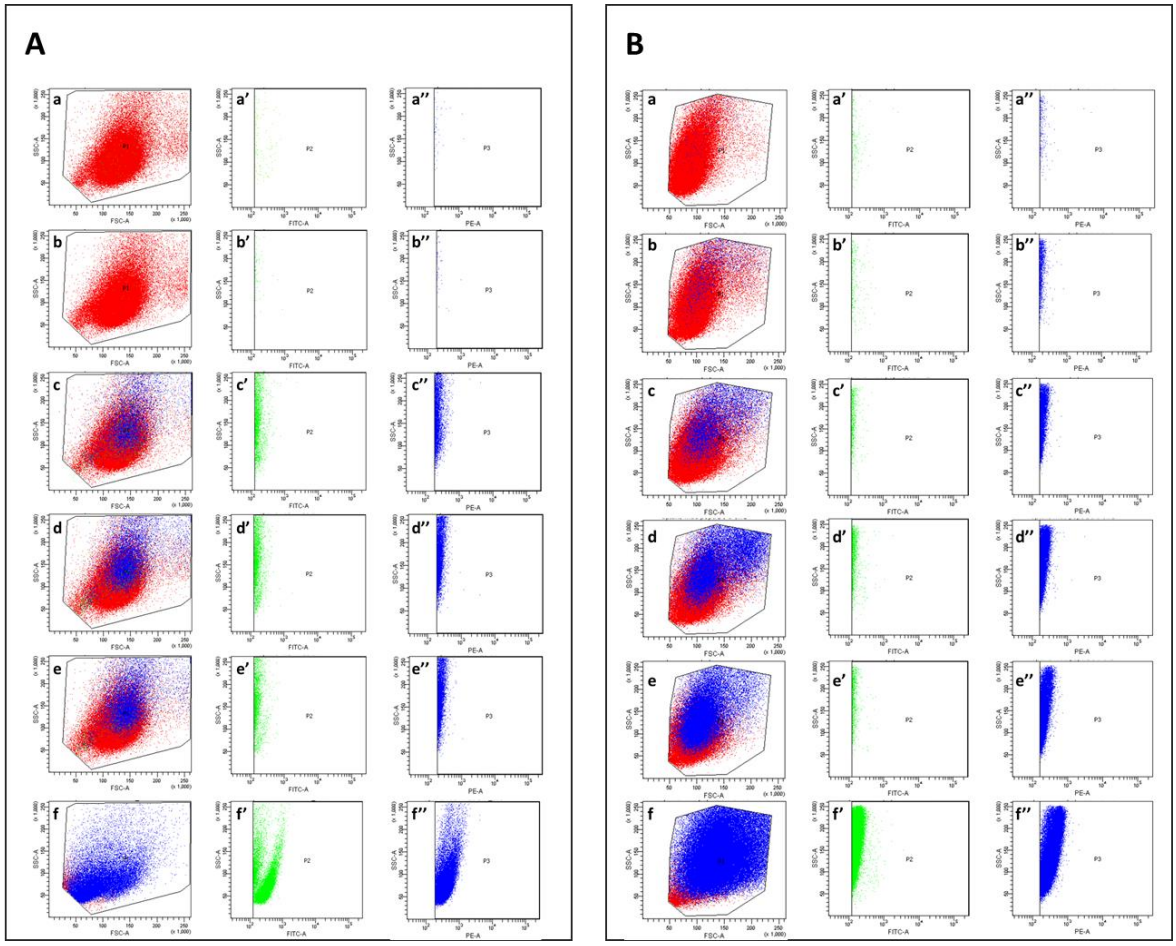

Figure 24. Representative cytograms for detection of INU-EDA-P,C-FITC (a'-f') and doxorubicin (a''-f '') in HB-2 cells (Panel A) and MDA-MB 231 (Panel B) after 1h (a-a''); 2h (b-b''); 4h (c-c''); 6h (d-d''); 8h (e-e''') and 24h (f-f '').

To better explain the uptake differences in both cellular lines, the same data are reported as percentages in fig. 25. Until 8h of treatment both normal and tumour cells present a similar inulin uptake profile (8.2% *vs.* 8.1% for HB-2 and MDA-MB 231 respectively) suggesting

that the polymer has been internalized in the same manner. After 24 hours, maximum internalization values are registered for both samples.

Moreover, comparing the doxorubicin uptake speed in both samples, it is notable that in cancer cells the red fluorescence increases proportionally over time reaching a maximum pick after 24h (92.7%); while, in healthy cells, the drug is internalized much more slowly, in a manner that resembled the copolymer until 8 hours. Indeed, from 4 to 8 hours, the doxorubicin and the inulin uptake percentages were about 8% and 3%, respectively. For longer time (24h), the drug was accumulated into the cells with a red internalization of 92.2%.

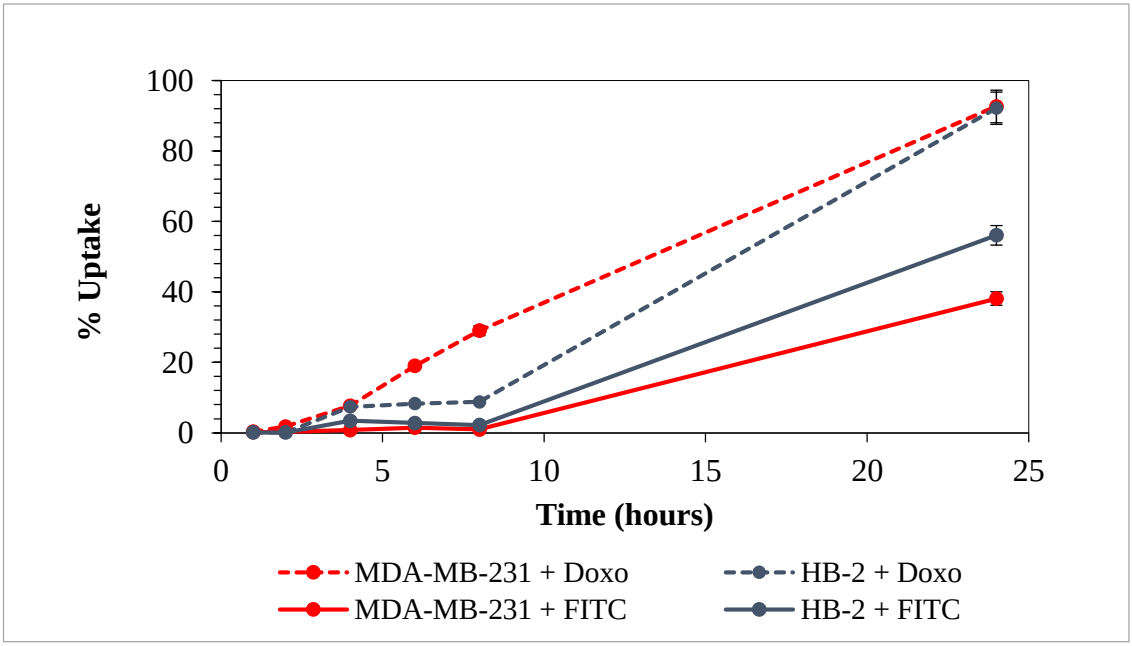

Figure 25. Quantitative uptake of INU-EDA-P,C-DOXO-FITC on MDA-MB 231 (Red) and HB-2 (Blue) cell lines: FITC: solid lines; Doxo: dashed lines.

The different trends of the drug uptake in the two cell lines, suggests an initial partial drug release in the tumour microenvironment and followed by the free doxorubicin independent diffusion across cell membrane. On the other hand, in healthy cells, the whole complex would enter the normal cells without any substantial chemical modification as demonstrated by the parallel increase of both green and red fluorescences. It is more evident in Figure 26, that shows the same data expressed like doxorubicin/FITC fluorescence ratio inside both cells. In HB-2 cells, the ratio is mostly constant (about 3) over time, proving that the

unmodified system enters the cells and remains intact. By contrast, a proportional increase of doxo/FITC ratio in tumour cells is observed until 8 hours of incubation, probably because of a faster break of the pH sensitive Cytraconylamide bridge and the consequent drug release in cancer microenvironment. At 24 hours, the fluorescence of the internalized conjugate return to 3, the normal Doxo/FITC ratio.

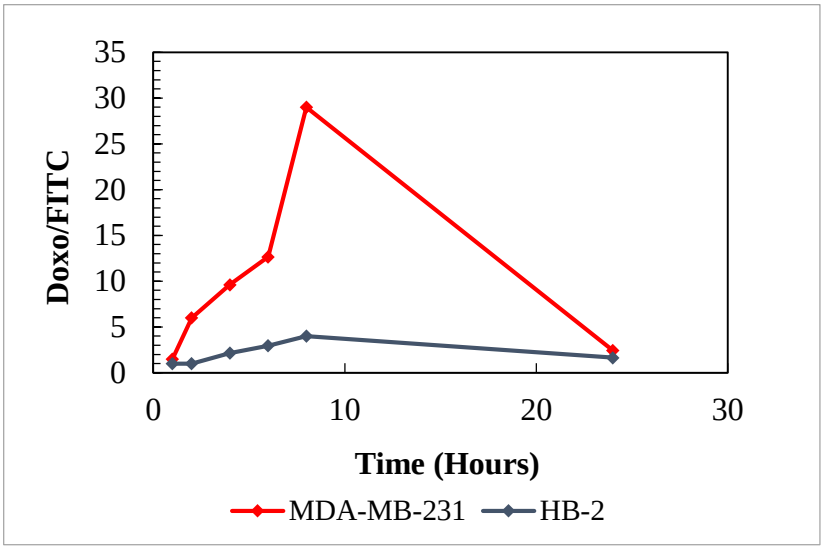

Figure 26. Relative uptake expressed as doxorubicin/FITC fluorescence ratio on MDA-MB 231 (Red) and HB-2 (Blue) cell lines.

All the data reported, suggest a specific model of action of INU-EDA-P,C-DOXO against tumour cells that is represented in figure 27. Tumour tissue is characterized by abnormal branching and wider interendothelial gaps due to damage of Tight Junctions (TJ) between endothelial cells and a disrupted basement membrane (Martin, 2014). Therefore, INU-EDA-P,C-DOXO in blood vessels would across through the large gaps and extravasate to the malignant tissue via EPR (Enhanced Permeation and Retention) effect. Tumour microenvironment presents a lower pH (6.5) respect to those of normal ones (7.4) (Gerweck and Seetharaman, 1996) so that the acidity would be able to reverse the conjugate charge from negative to positive. In this way, the doxorubicin would be partially released from the Cytraconylamide bridge and it would enter the cells through a simple diffusion mechanism, as demonstrated by flow cytometry studies. Inside the cells, the drug would be completely released and go into the nuclei to induce cell death, as demonstrated by cytotoxic assays.

Therefore, the different effects on normal and cancer cells is probably due to the difference of pH outside and inside the cells and to a different composition of the cell membranes.

The data relative to INU-EDA-P,C-DOXO, have been reported in the paper "Self-organized environment-sensitive inulin–doxorubicin conjugate with a selective cytotoxic effect towards cancer cells" published by Royal Society of Chemistry in March 2015 (N. Mauro, S. Campora, C. Scialabba, G. Adamo, M. Licciardi, G. Ghersi and G. Giammona).

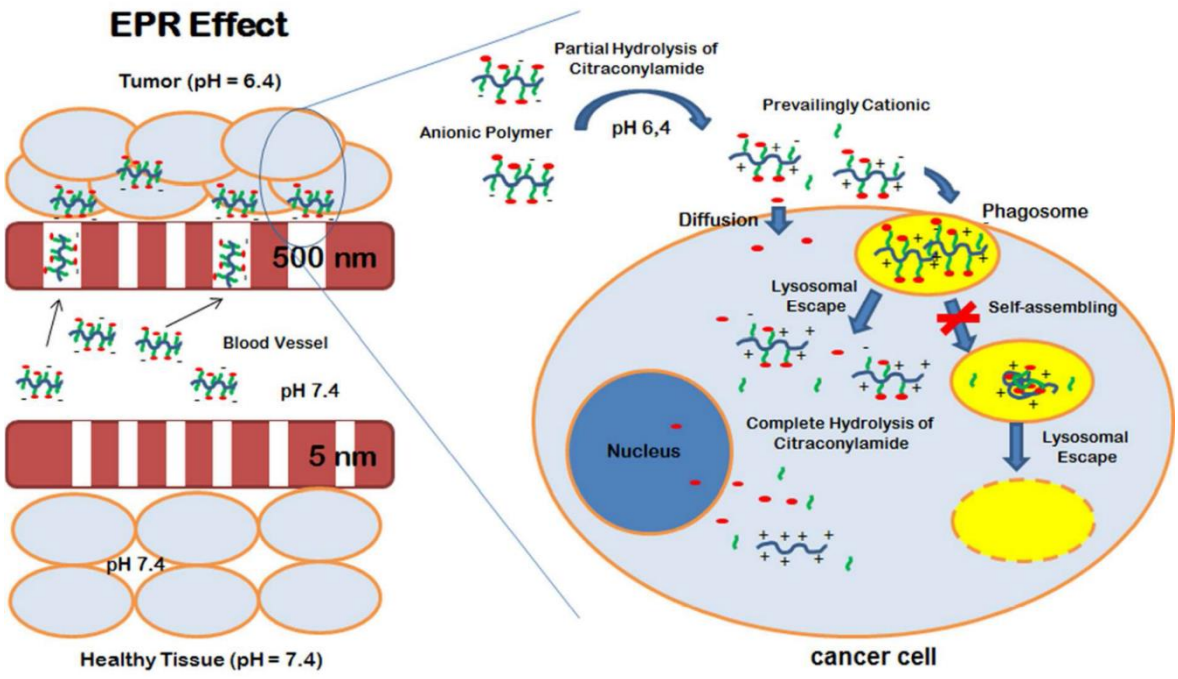

Figure 27. Representation of the model act of INU-EDA-P,C-DOXO.

PHEA-EDA-P,C-DOXO

PHEA (α,β-poly(N-hydroxyethyl)-D,L-aspartamide) is a multifunctional polymer endowed with high water solubility and biocompatibility. Aa for Inulin, the polymer was functionalized with EDA and pentynoic acid (P) and then conjugated to doxorubicin thanks to the pH-sensitive cis-citraconic linker acid to form PHEA-EDA-P,C-DOXO complex.

All the studies were carried out on MDA-MB 231 cancer cells and HB-2 normal cells to have a tumour and a normal model system of the same tissue (mammary tissue).

Cytotoxic studies of cells treated with PHEA-EDA-P,C-DOXO

The PHEA-EDA-P,C-DOXO cytotoxicity was assessed at 24h on the two cell models and compared with free doxorubicin as reported in figure 28. At low concentrations (0.5, 2 and 3.5 μM), all the samples presents similar trends, even with a slight difference from healthy and cancer cells treated with the conjugates (at 3.5 μM: 73.22% vs. 64.84% viability for HB-2 and MDA-MB 231 cells respectively). At 5 μM, HB-2 cells incubated with nanosystems show 75% of viability that is maintained also for higher concentrations (10, 15, 20 and 25 μM). On the other hand, in cancer cells, PHEA-EDA-P,C-DOXO induces a cytotoxic effect comparable to the one registered for the free drug. In particular, at 5 μM and 10 μM the viability is about 55%, but at 15 μM, as well as at higher concentrations (20 and 25 μM), it decrease till 30% suggesting a plateaux state in which the cytotoxic activity reaches the maximum level. The same trend of free and conjugated doxorubicin on MDA-MB 231 leads to hypothesize that the entire amount of conjugated drug would be released from the nanosystems at concentrations higher than 5 μM. By contrast, HB-2 cells present a different percentage of viability if treated with free or conjugates drug, thus suggesting that in healthy microenvironment or in the cells, are not optimal to permit the doxo release. Therefore, there is a selective activity of the polymer for tumour cells independently of the EPR effect, as it was supposed for inulin polymers.

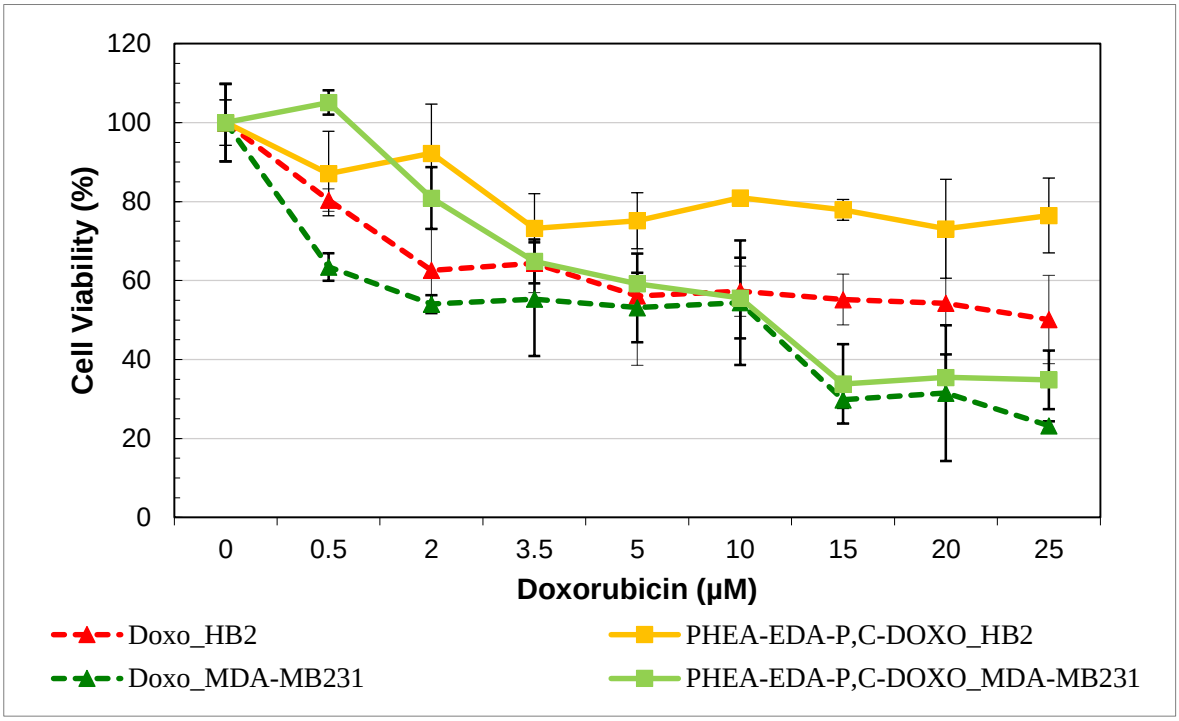

Figure 28. Cytotoxic assay on normal (HB-2) and tumour (MDA-MB 231) cell lines treated with PHEA-EDA-P,C-DOXO or free doxorubicin for 24h.

The cytotoxic activity of drug conjugated with the nanosystem was investigated also in another tumour cell line like SK-HEP-1 (human Hepatic Adenocarcinoma Cell Line) (Figure 29). The results obtained using MDA-MB 231 were confirmed: after 24 hours of treatment (Figure 29, panel A), there is not a significant drug inhibition in cell proliferation using low doxorubicin concentration conjugated with PHEA-EDA-P,C (viability around 100% at 0.05, 0.1 μM). Instead, at 5, 25 and 50 μM there is an evident reduction of the viability until a value of 40%. Stronger effect, but the same trend, is individuated also after 48 hours of incubation with the nanocomplex (Figure 29, panel A). Samples with free drug are used as control.

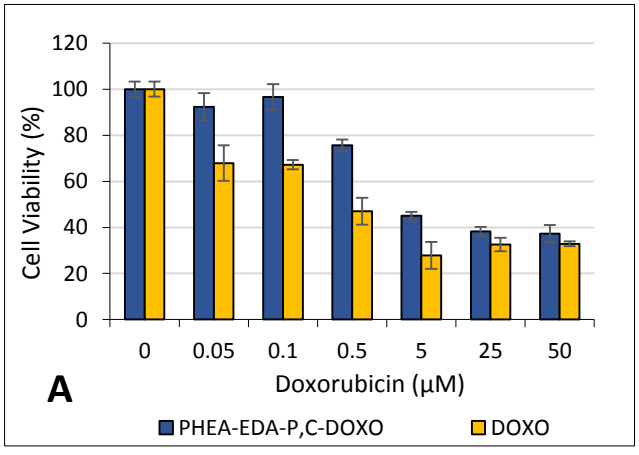

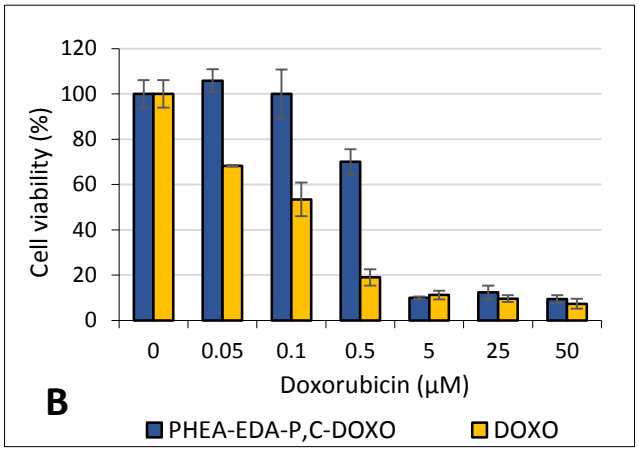

Figure 29. Cytotoxic assay on SK-Hep-1 tumour cell line treated with PHEA-EDA-P,C-Doxo or Doxo free for 24h (Panel A) and 48h (Panel B).

PHEA-EDA-P,C-FITC-Doxo localization studies by fluorescence microscopy

To investigate if the different cytotoxic effect of PHEA-conjugated doxorubicin between cancer and healthy cells is really due to a different release level, localization studies were conducted. In order to independently follow FITC-conjugated nanosystem and the released red auto-fluorescence doxorubicin, a fluorescent variant of PHEA, named PHEA-EDA-P,C-FITC-Doxo, is used. After 1 hour of incubation, the green fluorescence is lightly higher in tumour cells (Figure 30, Panel A, a') than in the normal ones, where it is feeble, around the cells and barely present inside them (Figure 30, Panel B, e'), suggesting a slight different uptake rate, probably because of the diverse composition of the cellular membranes. Anyway, in both cases, the two fluorescence signals co-localized, demonstrating that the drug is still bound to the polymer, even if, in cancer samples, doxorubicin is also partially inside the nuclei.

Like the inulin nanosystems, after 4h and much more after 6h, the polymer appears also inside the HB-2 cells, only in perinuclear region and, with a muffled and punctuates fluorescence (Panel B, f'), while in MDA-MB 231, the florescence is diffused (Panel A, b'). As at these time points, the drug release has already occurred, the red fluorescence appears into the nuclei of both cells. Finally, at 24h, all the systems are saturated, but the nuclei of MDA-MB 231 seem damaged and cell morphology is altered by the onset of apoptosis phenomena.

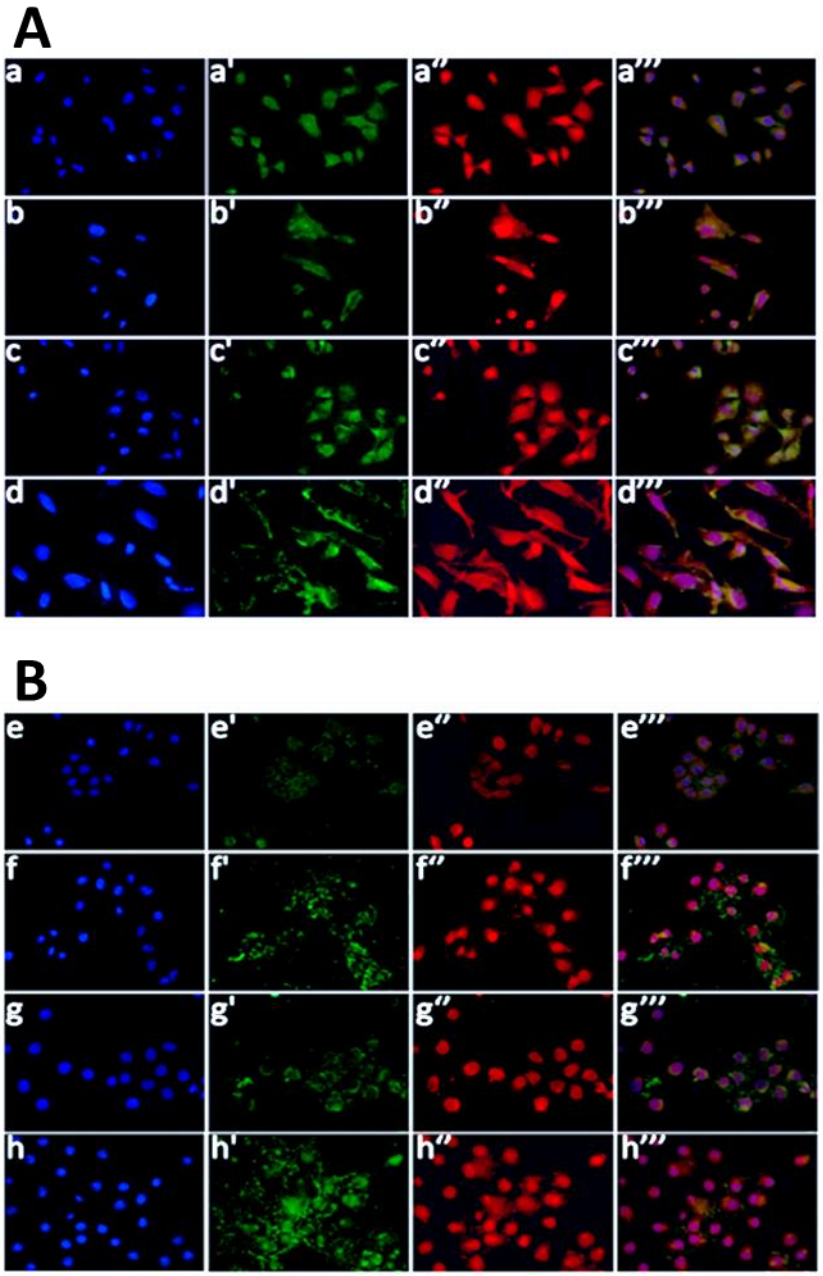

Figure 30. Localization studies of PHEA-EDA-P,C-FITC-Doxo on MDA-MB 231 (Panel A) and HB-2 (Panel B) after 1h (a-a''' and e-e''') , 4h (b-b''' and f-f'''), 6h (c-c''' and g-g''') and 24h (d-d''' and h-h''') of incubation. Blue: nuclei, green: PHEA-EDA-P,C-FITC, red: Doxo. Magnificence 40 X.

PHEA-EDA-P,C-FITC-Doxo localization studies by flow cytometry

The data were confirmed and examined in depth through flow cytometry following the FITC and the doxo fluorescence signals inside both healthy (Figure 31, Panel A) and tumour (Figure 31, Panel B) cells incubated with PHEA-EDA-P,C-FITC-Doxo over time (1, 2, 4, 6, 8 and 24 hours).

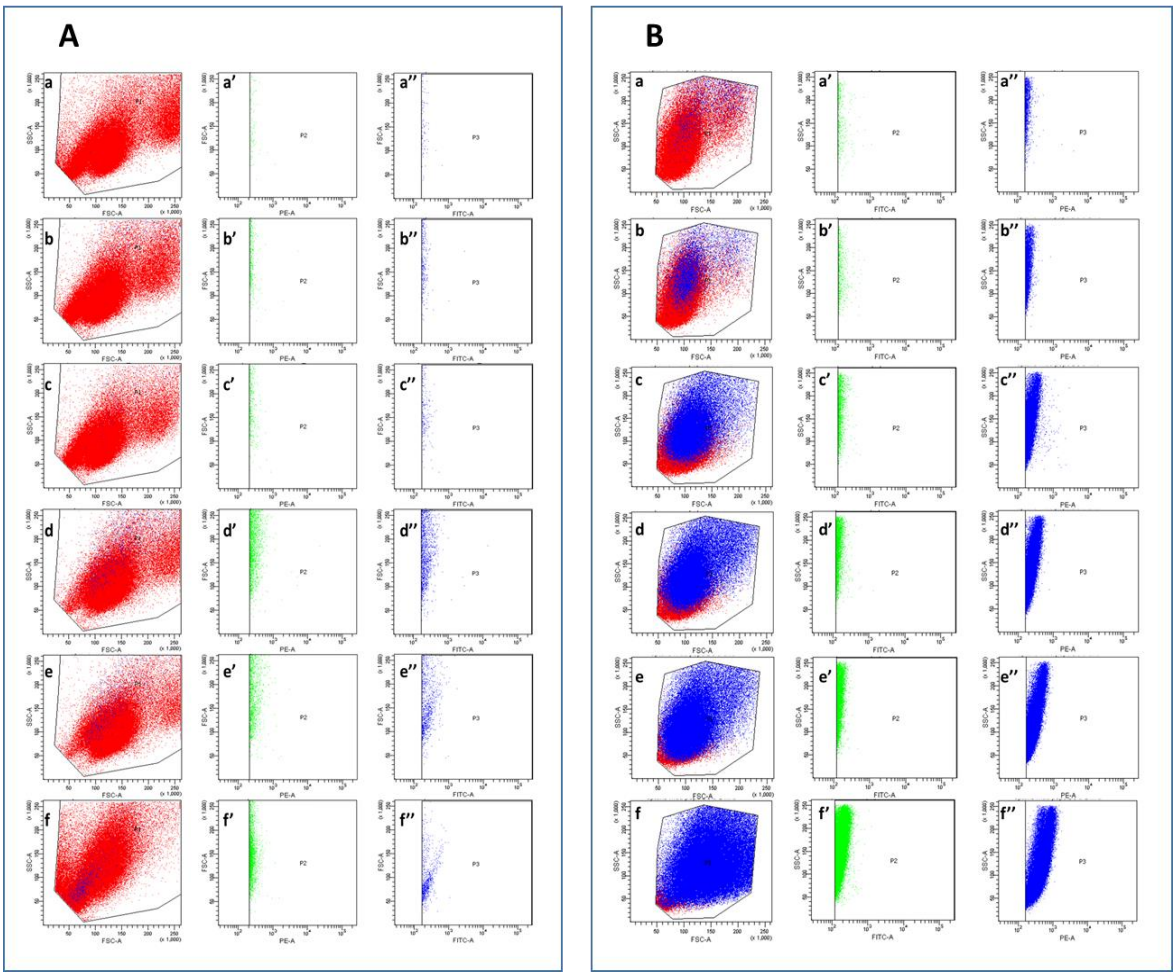

Figure 31. Representative cytograms for detection of PHEA-EDA-P,C-FITC (a'-f') and doxorubicin (a''-f'') in MDA-MB231 cells after 1h (a-a''); 2h (b-b''); 4h (c-c''); 6h (d-d''); 8h (e-e'') and 24h (f-f'').

The date reported in each cytogram were collected and re-elaborated in the graph in figure 32. An outstanding difference between normal and cancer cells is evident. The doxo signal in MDA-MB 231 very quickly increases over time (1, 2, 4 and 6 hours), reaching the plateau after 8 hours, which endures up to 24h. Even the green fluorescence increases over time, but very slightly at the beginning (until 8h) and then faster until 24h. On the other hand, in HB-2 cells, the two fluorescence present similar and very low uptake values for all the time points analysed. Comparing with cancer samples (light green line in the graph), the FITC mark relative to the PHEA system (yellow line in the graph), is always lower, suggesting a higher uptake level in tumour cells rather than in the normal ones. Probably it depends on their differences of the composition and fluidity of the membranes that facilitate the conjugates entrance into MDA-MB231.

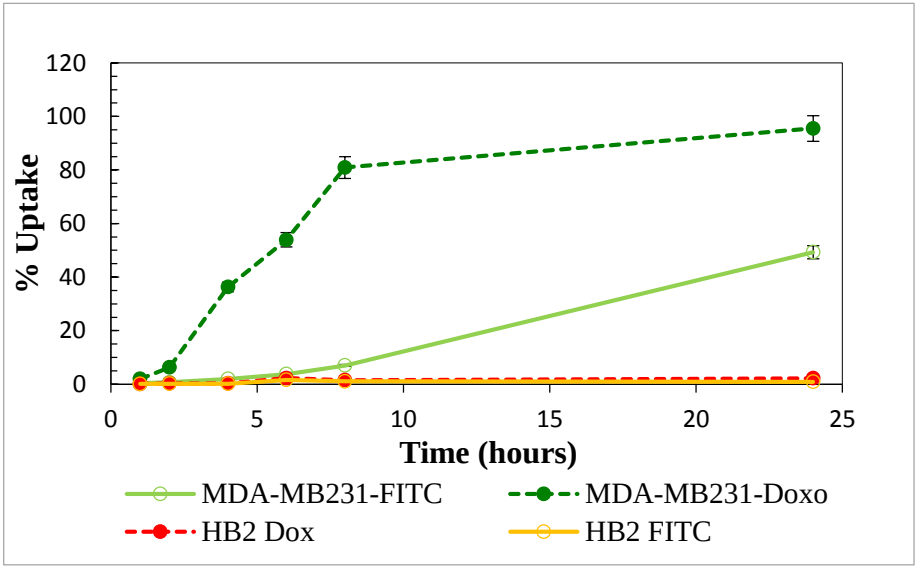

Figure 32. Quantitative uptake of PHEA-EDA-P,C-FITC-Doxo on MDA-MB 231 (Dark and light Green) and HB-2 (Red and Yellow) cell lines: FITC: solid lines; Doxo: dashed lines.

Figure 33 shows the doxo/FITC ratio over time in both cellular samples. In HB-2 the ratio is almost constant over time, suggesting that the unmodified PHEA-EDA-P,C-FITC-Doxo has probably been internalized. By contrast, in MDA-MB231, there is an increase in 8h, but at 24h, the ratio return to 2, the normal Doxo/FITC ratio.

As reported for Inulin systems, the difference of FITC/doxo fluorescence ratios between normal and tumour cells, suggested a possible mechanism of a partial drug release in the tumour microenvironment. Moreover, since Doxo is bound through a pH-sensitive linker to

the copolymer, the lower pH would induce a partial drug release in cancer tissues, permitting the free drug to cross tumour cell membrane, while in the normal tissue the complex remains stable and enters the cells as it is.

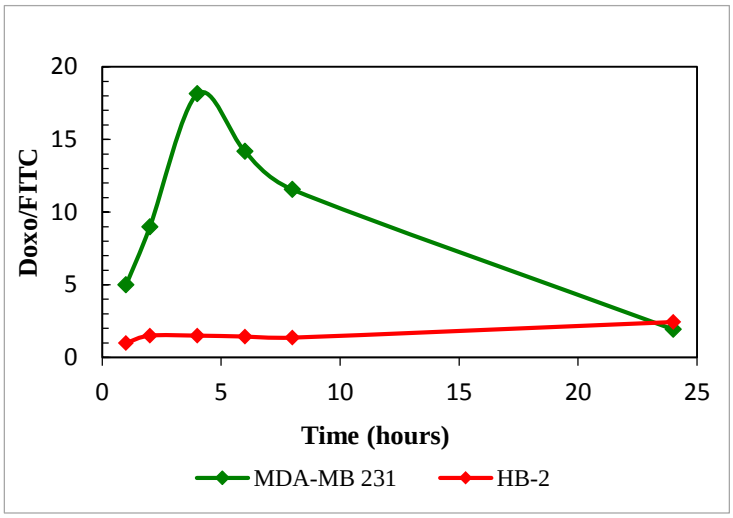

Figure 33. Relative uptake expressed as doxorubicin/FITC fluorescence ratio on MDA-MB 231 (Green) and HB-2 (Red) cell lines.

Co-culture experiments.

To investigate the specific selectivity of PHEA-EDA-P,C-Doxo for tumour cells respect to healthy ones, co-culture experiments were carried out (Figure 34). Firstly, MDA-MB 231 cells were treated with CellTrace CFSE fluorescent dye that conferred them a green fluorescence (b); then, they were mixed with the same amount of unlabelled normal cells (a), seeded in the same plate and incubated with the conjugates. The green fluorescence permitted to distinguish cancer cells from the normal one even if both nuclei were labelled with DAPI, and the possibility to have in the same plate both cell types, would give us more information about the specific action of the complex. In particular, it was possible to identify a selective uptake after only 30 minutes of incubation (15μM PHEA-EDA-P,C-Doxo) as shown in figure 33. In details, the red mark of doxorubicin is present only in the MDA-MB 231 cells, demonstrating that there is an exclusive PHEA-EDA-P,C-Doxo localization inside tumour cells. This is probably due to the different composition of the two cellular types concerning, for example, fatty acid and proteins and determining a diverse membrane fluidity (Meng *et al.*, 2004; Szachowicz –Petelska *et al.*, 2010).

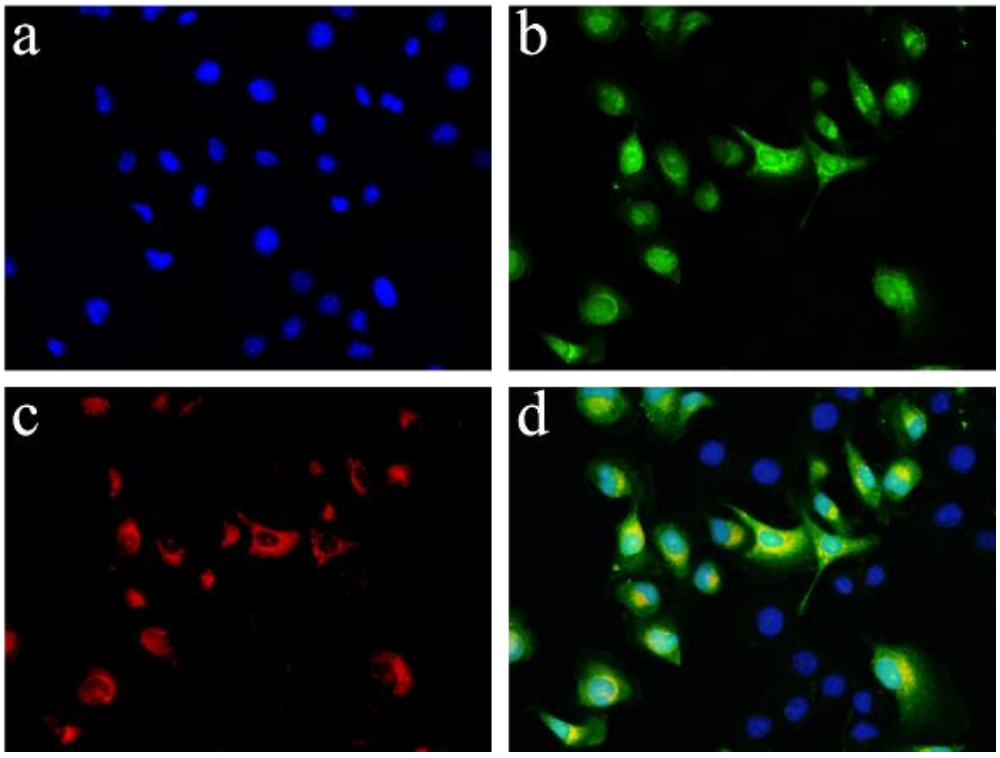

Figure 34. Co-culture of MDA-MB 231 and HB-2 incubated for 30' with 15 μM PHEA-EDA-P,C-Doxo. Blue: nuclei, green: MDA-MB 231, red: Doxo. Magnificence: 40X.

In order to better characterize the uptake kinetic, co-culture experiments were carried out over time (30', 1h, 2h, 6h and 24h), using low PHEA-EDA-P,C-Doxo concentrations and free drug as a control (Figure 35). After short incubation times (30'; 1h; 2h), there is an exclusive localization of the complexes in cancer cells, as suggested by the co-localization of the red and the green signals (a'''; b''' and c'''). Doxorubicin begins to appear in HB-2 cytoplasm only after 6h of treatment (d'''); subsequently (at 24h), the drug is into the nuclei of both cell lines probably because it can enter all cells through a diffusion process (e''') as it has been demonstrated for many nanosystems (Dalmark *et* Hoffmann, 1983).

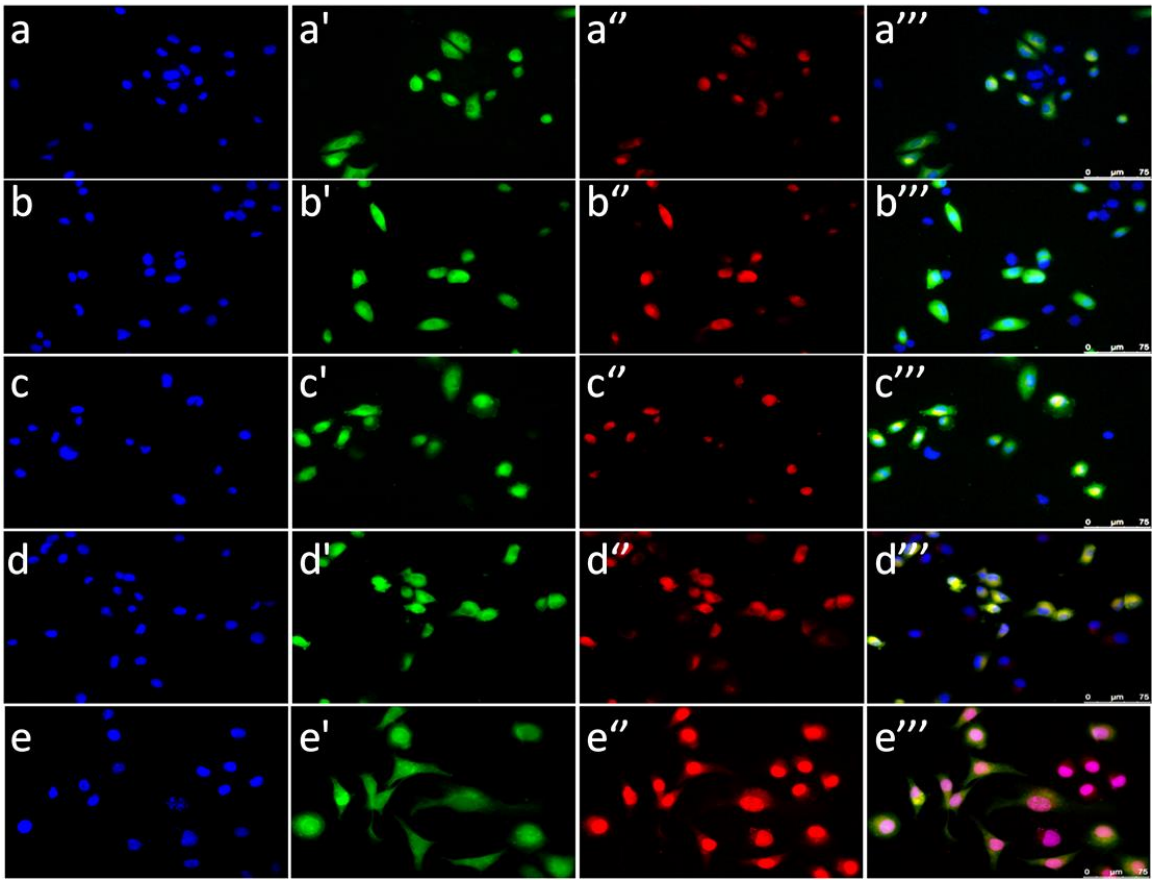

Figure 35. Co-culture of MDA-MB 231 and HB-2 incubated with 10 µM PHEA-EDA-P,C-Doxo for 30' (a-a'''), 1h (b-b'''), 2h (c-c'''), 6h (d-d''') and 24h (e-e'''). Blue: nuclei, green: MDA-MB 231, red: Doxo. Magnificence: 40X.

By contrast, free doxorubicin is inside both normal and tumour cells already after 30 minutes of incubation, demonstrating that the copolymer PHEA is responsible for the specific selectivity for cancer cells (Figure 36).

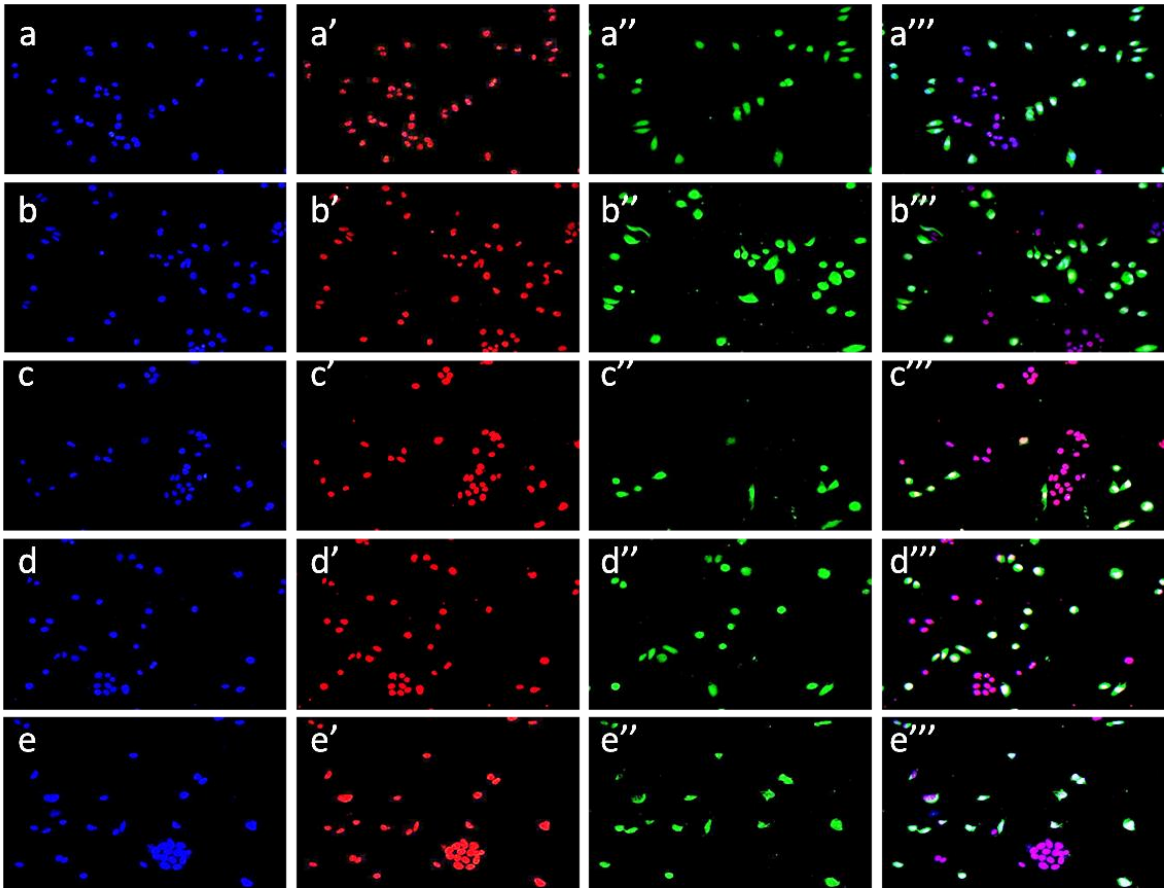

Figure 36. Co-culture of MDA-MB 231 and HB-2 incubated with 10 µM Doxo for 30' (a-a'''), 1h (b-b'''), 2h (c-c'''), 6h (d-d''') and 24h (e-e'''). Blue: nuclei, green: MDA-MB 231, red: Doxo. Magnificence: 20X.

PHEA-EDA-P,C-FITC-Doxo internalization mechanisms.

In most cases, classical drugs constituted by small molecules are internalized into cells through passive diffusion or active transport. It is largely reported in literature that nanosystems, instead, enter cells via endocytosis through different mechanisms involving membrane components or specific cellular pathways, in dependence of kind and nature of the systems (Longfa Kou *et al.*, 2013) (Figure 37). Depending of the proteins involved, endocytosis pathways has been classified in different groups like Phagocytosis, Clathrin-dependent or Caveolae-dependen endocytosis and Macropinocytosis (Gary *et al.*, 2009). To individuate the PHEA-EDA-P,C-FITC-Doxo internalization mechanisms, flow cytometric analysis and confocal microscopy assays were conducted in both cell lines, using three endocytic inhibitors. Ethyl-isopropyl amiloride (EIPA) is a macropinocytosis inhibitor that reduces cytosolic pH and, in this manner, blocks the activation of Rac1 and Cdc42 GTPases

that normally play a key role in the process (Kälin *et al.*, 2010). Phenylarsine oxide (PAO) inhibits clathrin-dependent endocytosis through the inactivation of multiple intracellular targets, including major actin cytoskeleton regulators related to this specific pathway (Di Andrei I. Ivanov, 2008). At last, nystatin is a sterol-binding agent that links and restricts the function of many proteins, like kinases implicated in Caveolae-dependent endocytosis: it disassembles caveolae and cholesterol in the membrane.

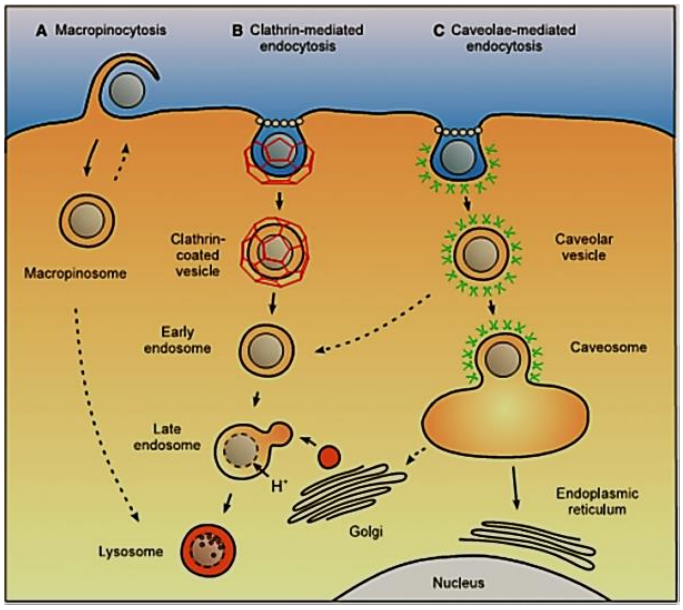

Figure 37. Intracellular nanocarrier trafficking following macropinocytosis, clathrin-mediated endocytosis and caveolae-mediated endocytosis (Hillaireau and P. Couvreur, 2009).

First, each inhibitor was valuated for its effects on cell viability through Cell Counting Kit-8 (CCK-8) (Sigma Aldrich) assay and none was capable of inducing any cytotoxic effect (data not shown). Cells treated with PHEA-EDA-P,C-FITC-Doxo but without inhibitors were used as negative control, while cells incubated at 4°C was used as positive control. Indeed, the low temperature inhibits all the active internalization pathways so that the conjugates would enter only by a passive process (simple diffusion). In all samples, after the treatment with inhibitors, the nanopolymers were incubated for 1 hour. The data concerning flow cytometric studies were collected and related as FITC (relative to nanosystem) or Doxo fluorescence percentage values in figure 38 (Pannel A and B, respectively). The results obtained following the two fluorescence signals were comparable. Indeed, in both cases, MDA-MB-231 or HB-2 cell lines treated with EIPA and PAO show similar values to the negative control ones, suggesting that PHEA internalization is not dependent on

macropinocytosis and clathrin-dependent endocytosis. By contrast, cells inhibited by Nystatin show lower level of fluorescence, comparable to those of the positive control (4°C), strongly suggesting that PHEA-EDA-P,C-FITC-Doxo enters cells by Caveolae-dependent endocytosis and, very slowly, by simple diffusion. It is interesting to underline that nystatinhas a stronger inhibition effect on tumour rather than on normal cells, confirming, another time, the specificity of cancer uptake.

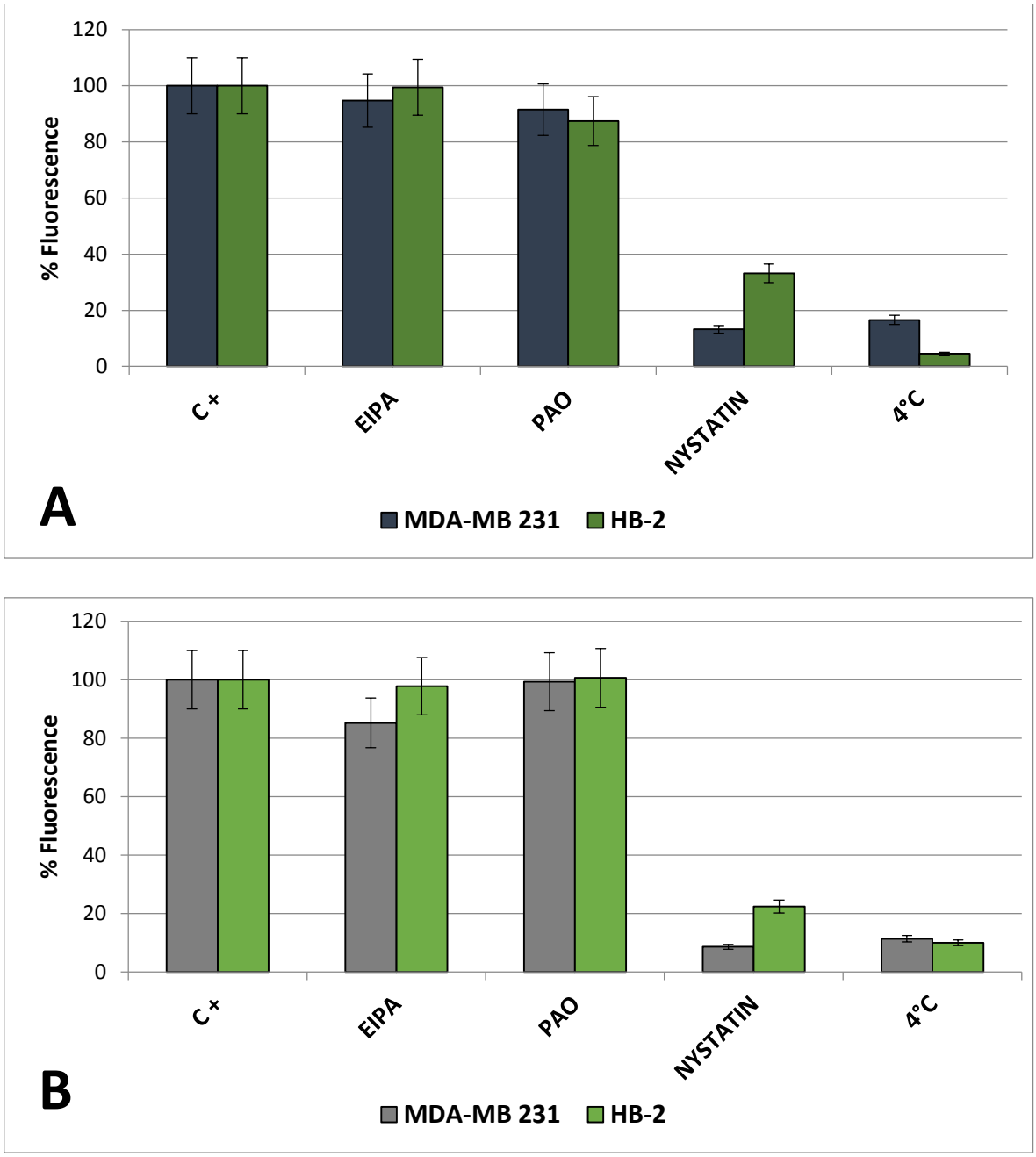

Figure 38. Effect of various endocytic inhibitors on the internalization of 25µM of PHEA-EDA-P,C-FITC-Doxo on MDA-MB 231 and HB-2 cells after 24h (Panel A) and 48h (Panel B) of treatment.

The data above were confirmed by confocal microscopy analysis of MDA-MB231 treated with Nystatin, giving not only quantitative, but also morphologic information (Figure 39). The green fluorescence inside inhibited cells (a) is very low, according with the positive control (b) and it is localized on the cellular surface. By contrast, in not inhibited samples (c), the green dye is diffused in the cytoplasm, demonstrating that the amount of conjugates is higher.

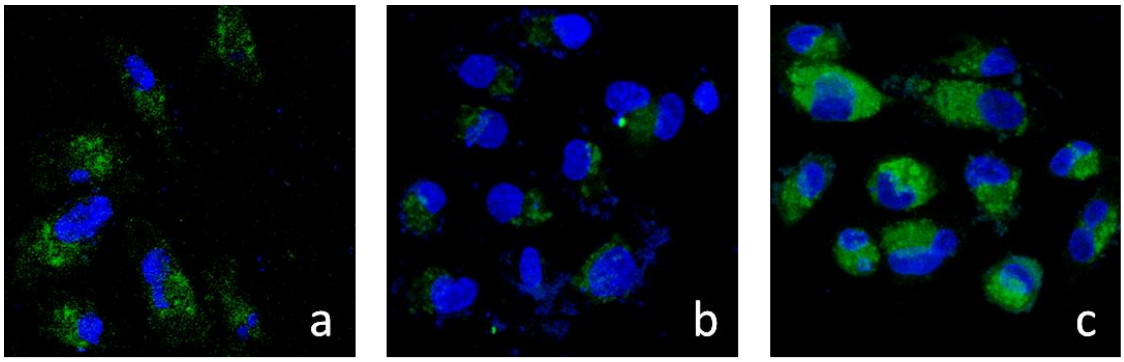

Figure 39. Confocal microscopy images of MDA-MB231 treated with Nystatin and incubated with 25 µM of PHEA-EDA-P,C-Doxo (a). Cells incubated at 4°C (b) are used as positive control and cell without inhibitor (c) as negative control. Blue: nuclei. Green: PHEA. Merge: overlay of 2 fluorescence. Magnificence 60X.

Specific localization studies

Depending of the nature of the molecules, endocytosis via caveolae can involve two divergent mechanisms (Figure 40). For examples, the virus SV40 can enter the cells though this mechanism, but it can escape the lysosomal degradation (Carver and Schnitzer, 2003). Other ligands internalized through a caveolae pathway, instead, are involved in the formation of early endosomes, named caveosomes, that then fuse with lysosomes following the classical endocytic pathway (Kiss and Botos, 2009).

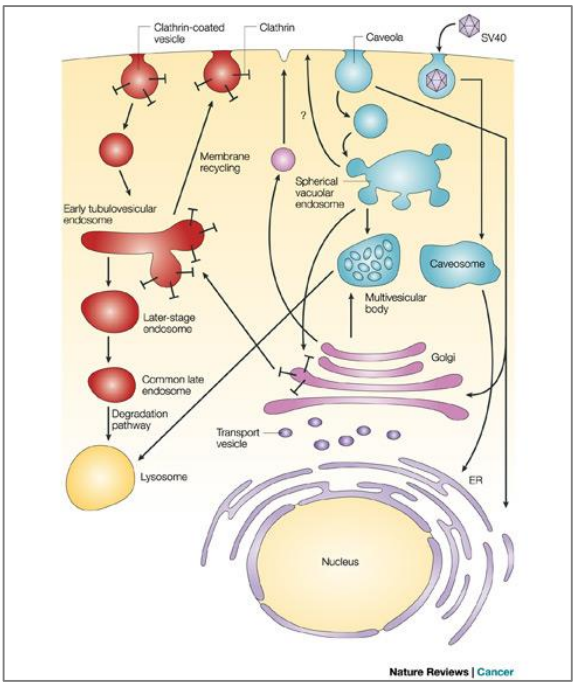

Figure 40. The caveolae vescicular endocytic pathway

To identify the pathways involved in PHEA-EDA-P,C-Doxo internalization, specific localization studies were conducted through confocal microscopy. In particular, MDA-MB231 cells were incubated with the conjugates over time (30', 1h, 2h, 4h, 6h and 24h) and then the lysosomal compartments were labelled with LysoTracker (Figure 41, a'- f') in order to verify if a co-localization occurs. For early times of incubation (30 minutes), the copolymer is still largely diffused in the medium and partially situated in the cell membrane, suggesting that it is going inside the cells (a-a'''). At 1h of treatment, there is a different localization of the green (lysosomes) and red (PHEA-EDA-P,C-Doxo) fluorescences (b-b'''), highlighting that the nanosystem is partially localized in the cytoplasm but not in the lysosomes. Their co-localization is partially observed at 2h (c-c''') and, after 4h (d-d'''), there is a complete co-localization. These data strongly indicates that, once internalized by claveolae mechanism, PHEA localizes in the lysosomal compartment where the low pH would induce the drug release.

Furthermore, at 6h (f-f''') the red mark does not more co-localize with the green one anymore, but it start to appear in the nuclear area, the site of doxorubicin action. At last, at 24h cells have an apoptotic morphology, probably because of the doxorubicin effect.

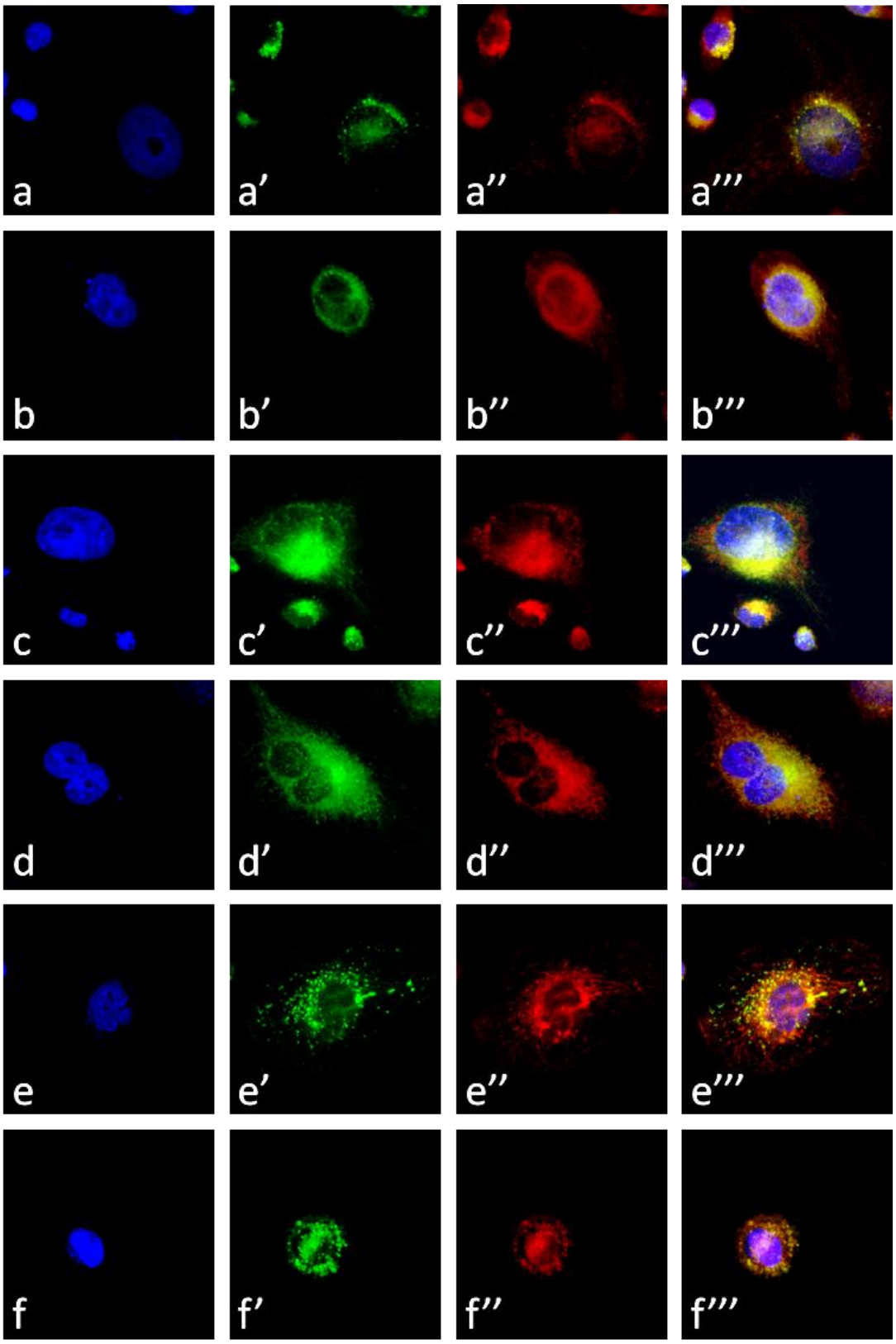

Figure 41. Confocal microscopy images of MDA-MB231 incubated with 10 µM of PHEA-EDA-P,C-Doxo for 30' (a-a'''), 1h (b-b'''), 2h (c-c'''), 4h (d-d'''), 6h (e-e''') and 24h (f-f'''). Blue: nuclei. Green: Lysosomes LysoTracker-labelled. Red: Doxo. Merge: overlay.

All the data have permitted to hypothesize a model in which PHEA-EDA-P,C-DOXO complex would start to release the drug in the tumour microenvironment thanks to lower pH. (Maybe, it can reach the cancer site though the EPR Effect, but this aspect needs to be more investigated). In this way, free doxorubicin would diffuse inside the cells while the nanosystem would be internalized through a caveolae pathway involved lysosomes, following the classical endocytic pathway. It would be supposed that the low pH inside the lysosomes would induce the complete doxorubicin release thanks to the pH-sensitive spacer; once set free, the drug would go into the nuclei and induce the cellular death (Figure 42).

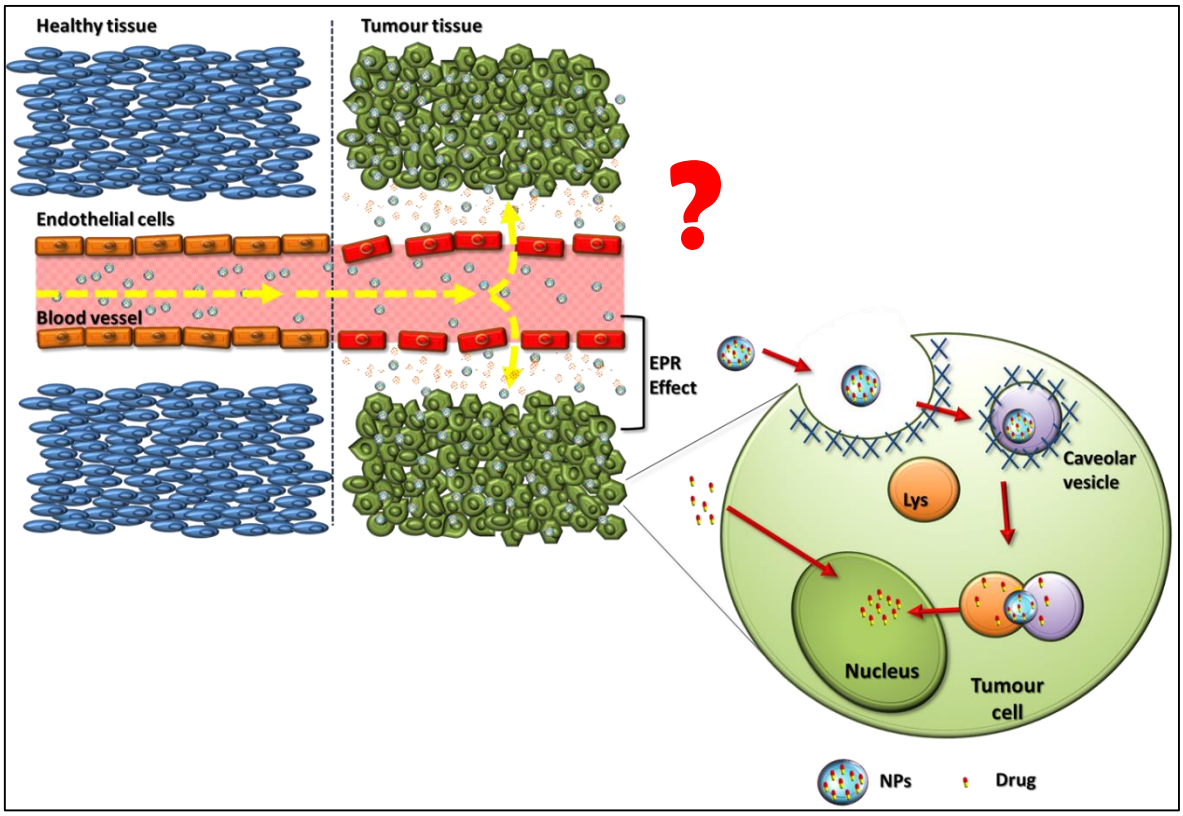

Figure 42. Representation of the model act of PHEA-EDA-P,C-Doxo.

PVP nanogels

PVP nanogels (NGs) were synthesized in collaboration with Professor Dispenza research group (University of Palermo) by high-energy radiation (e-beam irradiation), starting from a dilute aqueous solution of a commercial polyvinylpyrrolidone (PVP K60, Aldrich) and using the linear accelerator at the ICHTJ of Warsaw (Poland), Electronika 10/10. In this way, it was possible to obtain sterile nanoparticles with appropriate size, shape, surface properties and specific chemical functionality. In particular, PVP was functionalized with Acrylic Acid (AA) in order to produce carboxyl-functionalized nanogel systems (Figure 43) that have been characterized by DLS, FTIR and NMR (Dispenza et al.,2012; Dispenza *et al.*, 2013). NGs have been largely characterized and studied by Dr. Adamo (from Professor Ghersi research group). In particular, their fully biocompatibility was demonstrated through *in vitro* studies like cells viability assay, valuation of apoptotic activation and Acridine Orange (AO) stain for DNA damage analysis (Dispenza *et al.*, 2013; Adamo, 2013). Furthermore, the nanoparticles were able to conjugate biological molecules, like doxorubicin, for tumour therapy and/or specific ligands (like monoclonal antibodies) to recognize receptors into the target cells, for targeting activities (Adamo, Campora *et al.*, 2014; Adamo, 2013). Moreover, recent studies had demonstrated also the possibility to link a small oligonucleotide that remained functional after the conjugation process (Dispenza *et al*., 2013).

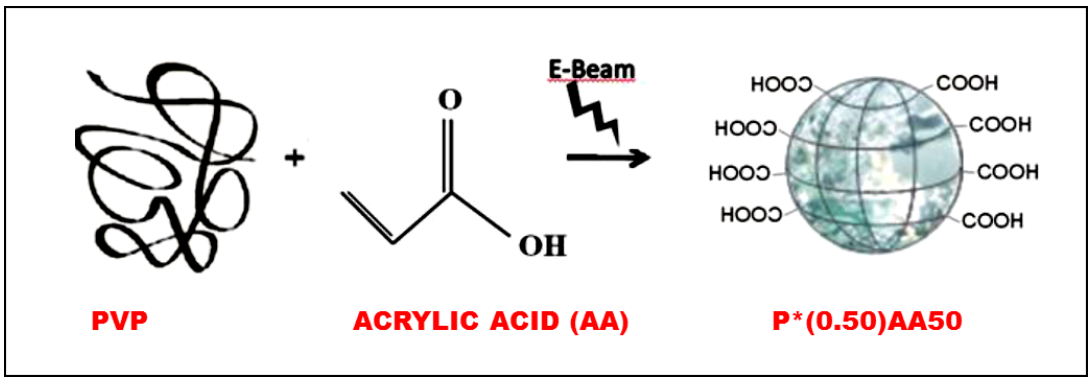

Figure 43. Schematic representation of P*(0.50)AA50 nanogels.

Egr-1 pathway and Egr-1 silencing by siRNA

Egr-1 pathway studies

Patients with hepatocellular carcinoma (HCC) have high serum levels of the hepatocyte growth factor (HGF) that is associated with the progress of the desease. In particular, HGF can induce the activation of the *zinc finger* transcription factor Egr-1 (Early growth response-1) that is involved in the transcription of metalloproteases, like MMP-2 and MMP-9, able to degrade the extracellular matrix (ECM) and to induce tumour metastasis (Ozen *et al.*, 2012) (Figure 44). It is reported that Egr-1 is also implicated in angiogenesis by regulating the transcription of *vegf* gene (Hee Lee et Ryong Kim, 2009). Therefore, Egr-1 would be a good candidate for gene silencing in tumor therapy.

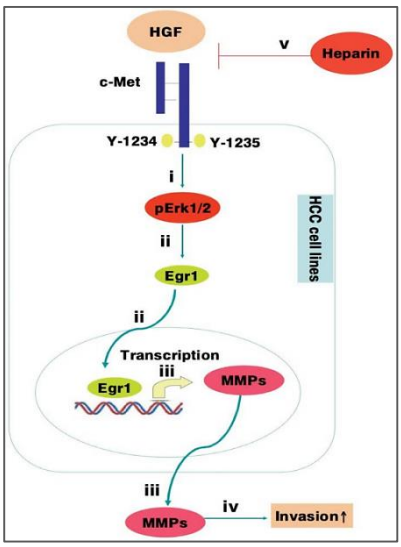

Figure 44. The HGF pathway on HCC cell lines.

In order to determinate the best conditions to induce *Egr-1* expression, the effect of HGF was studied. Fetal bovine serum (FBS) contains many growth factors able to interfere with the expression of genes like *Egr-1*; therefore, SK-HEP-1 cells were subjected to a gradual serum starvation (see material and methods) before the HGF incubation (10 ng/ml).

After 1, 2 and 3hours of treatment, Egr-1 expression was investigate by Western Blot analysis (Figure 45). Data elaborated by ImageJ program, reveals a higher protein expression after 3h of treatment. For longer time, the amount of Egr-1 expressed remains stable (data not shown).

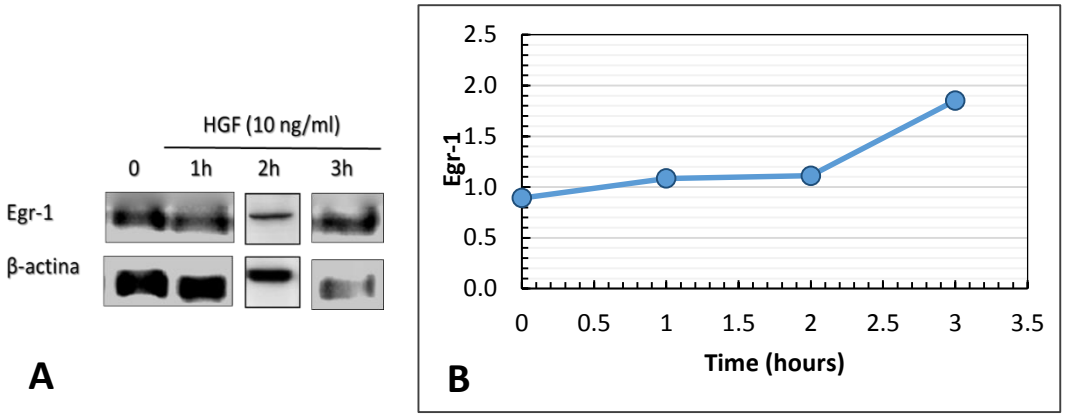

Figure 45. Egr-1 expression after HGF treatment. A:Western Blot analysis of Egr-1 expressed in SK-HEP-1 after 1h, 2h and 3h of HGF treatment. B: Graph of the Egr-1 expression in HGF treatment time-dependent way (ImageJ).

Egr-1 silencing by siRNA using Lipofectamine

Once established the optimal conditions to induce the maximum expression of Egr-1, silencing experiments were conducted. In order to study siRNA efficiency, lipofectamine system was used. As shown in figure 46, *Egr-1* siRNA is able to reduce the expression of the protein both with and without HGF treatment, if compared to untreated cells. Remarkably, after 3 hours of treatment with HGF, the silencing is stronger , suggesting that this is the best condition to perform the other experiments.

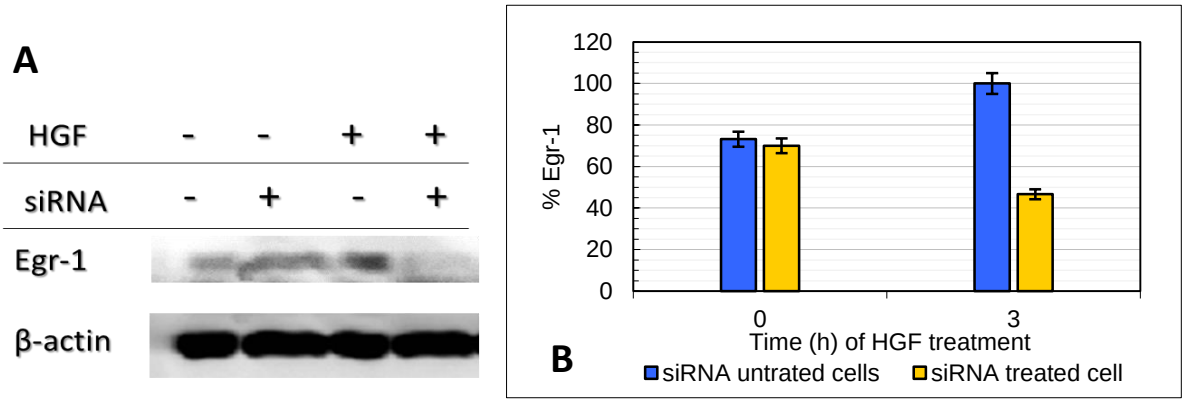

Figure 46. Egr-1 expression after HGF treatment (3h) and/or Egr-1 siRNA treatment (48h). A:Western Blot analysis of Egr-1 expressed in SK-HEP-1. B: Graph of the Egr-1 expression.

Conjugation of modified siRNA to PVP nanoparticles

In order to increase the efficiency of the siRNA against tumour cells, Egr-1 siRNA was conjugated to PVP nanogels functionalized with carboxyl groups. The possibility to functionalize these kind of nanoparticles makes them optimal candidate for siRNA delivery. Indeed, in this contest, a modified siRNA, with an AminoC6linker at 5' end of the sense strand, can be used. The covalent bond stabilizes the siRNA and the nature of the nanogels protects it from the degradation.

A conjugation protocol was developed using EDC and Sulfo-NHS reagents. EDC reacted with carboxylic acid groups of the NGs to form an intermediate that was easily displaced by nucleophilic attack from the primary amino group of the siRNA. The primary amine formed an amide bond with the original carboxyl group, and an EDC by-product was released as a soluble urea derivative. Sulfo-NHS was also added to improve efficiency or create dry-stable (amine-reactive) intermediates. EDC coupled NHS to carboxyl group of PVP, forming an NHS ester that is considerably more stable than the intermediate, and is important to have an efficient conjugation to the amino group of the siRNA at physiologic pH (Figure 47).

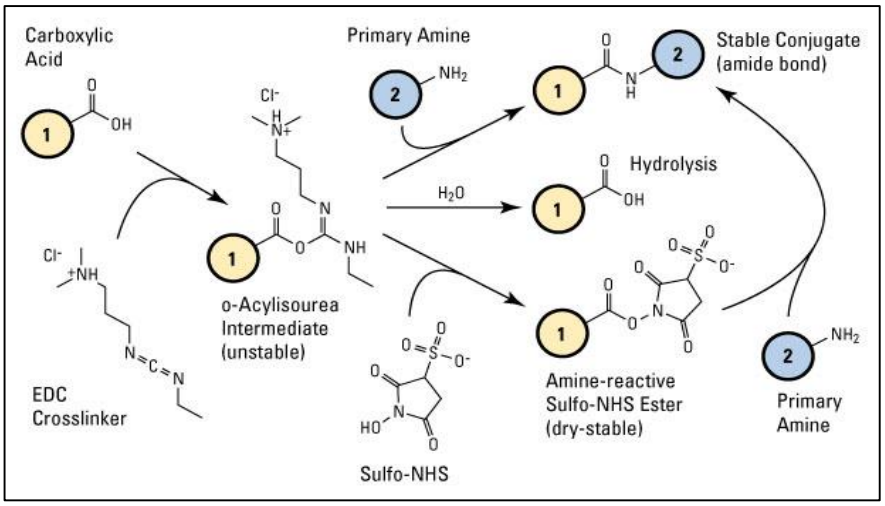

Figure 47. Representation of siRNA- PVP conjugation protocol. Number 1: PVP nanogel; Number 2: 5'-AminoC6linker modified siRNA.

The amount of siRNA conjugated to the nanoparticles was determined by a spectrophometric analysis using the NanoDrop 1000 Spectrophotometer. A standard curve were constructed reading at 260nm the absorbance of serial dilutions of free siRNA (Figure 48). The absorbance relative to PVP nanogels were used as blank to read the conjugated samples. By interpolating their optical density (OD) to the standard trend, it was possible to identify that 6.25 ng/µl of 5'-AminoC6linker modified Egr-1 siRNA were conjugated to PVP.

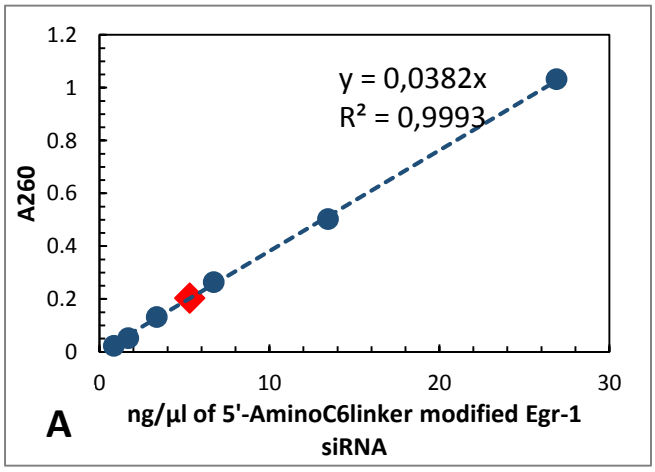

ng/µl free siRNA	OD_{260}
0,84	0,022
1,69	0,051
3,36	0,131
6,72	0,263
13,45	0,502
26,9	1,032

OD_{260} NGs-siRNA (subtracted of OD_{280} of NGs)	0,239
siRNA conjugated to PVP (ng/µl)	**6,256545**

Figure 48. Quantification of siRNA conjugated to PVP nanogels. A: standard curve of serial dilutions of free siRNA.

Egr-1 silencing by siRNA through PVP-siRNA complex

PVP ability to deliver siRNA into cells and the efficiency of the oligonucleotides against their target were tested by treating SK-HEP-1 cells with the complex. Cells were incubated for 48 h with 150 pmol of Egr-1 siRNA-conjugated nanoparticles. Western blot analysis shows that Egr-1 is less expressed in treated cells. Indeed, the densitometric analysis (ImageJ) shows a silencing of 45.9% respect to cell incubated with nanogels alone (Figure 49).

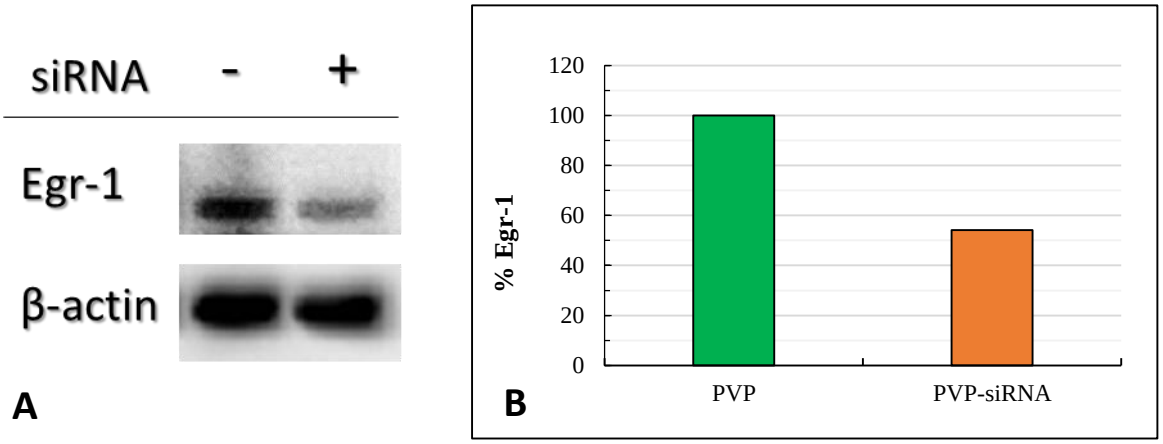

Figure 49. Silencing by siRNA-PVP nanogels. A: Western Blot analysis of Egr-1 expressed in SK-HEP-1 after PVP-siRNA treatment. B: Graph of the Egr-1 expression.

These results demonstrate that PVP nanogels are optimal candidates for siRNA delivery. Therefore, siRNA remains stable when linked to the nanogels, so that the entire complex is able to enter the cells. Then the oligonucleotide is released (probably thanks to a competition mechanism with the Dicer complex), and it can exert its role reducing the expression of its target. In this way, a higher amount of oligonucleotides can reach the target site, thus avoiding the problem of high degradation often observed in tumor therapy.

Bcl-2 silencing by siRNA

Conjugation of modified siRNA to PVP nanoparticles through AEDP

Once established the PVP capacity to target a siRNA for gene delivery, the system was improved on the ability to release the oligonucleotide in a controlled way. Recent studies conducted by Dr Giorgia Adamo of the University of Palermo (Department of "*Scienze e Tecnologie Biologiche Chimiche e Farmaceutiche*"- STEBICEF) have been demonstrated that doxorubicin, linked to PVP nanogels through AEDP spacer, was released in a stimuli-responsive manner into tumour cells. AEDP (3-[(2 aminoethyl)dithio] propionic acid) is a small molecule with a disulphide bridge in the middle, and an amino terminal and a carboxyl terminal. In this manner, it links the carboxyl group of the functionalized nanoparticles at one extremity and, the amino group of the modified siRNA at the other extremity. The presence of the disulphide bridge makes it sensible to the redox state of the microenvironment. When the NG is in the extracellular environment, the cargo remains linked to PVP-AEDP; but when it enters tumour cells, characterized by a high Glutathione (GSH) level the disulphide bride is broken and the drug is released (Adamo, 2013).

PVP-AEDP nanogels, synthetized by Professor Dispenza research group (University of Palermo), were conjugated to Bcl-2 5'-AminoC6linker (see materials and methods) (Figure 50).

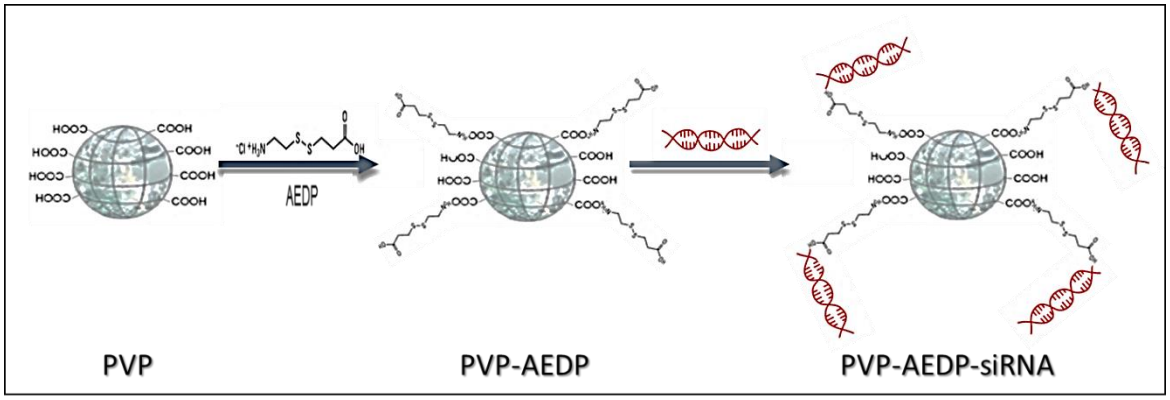

Figure 50. Conjugation of PVP nanogels first to AEDP spacer (PVP-AEDP) and then to Bcl-2 siRNA (PVP-AEDP-siRNA).

The amount of siRNA conjugated was calculated by spectrophotometric analysis using NanoDrop 1000 Specrophotometer, as evaluated before for PVP-Egr-1 siRNA complex. The absorbance values of serial dilutions of siRNA permitted to obtain the standard curve with a coefficient of determination (R^2) of 0.9992 (Figure 51, Table and Panel A). Comparing the spectra of PVP-AEDP and PVP-AEDP-siRNA nanosystems (Figure 51 Table and Panel B), an increase of the absorbance values at 260 nm (typical wavelength to quantify nucleic acids) is evident, suggesting that the siRNA is conjugated to PVP-AEDP. It was obtained a conjugation of 5.6 ng/µL of siRNA.

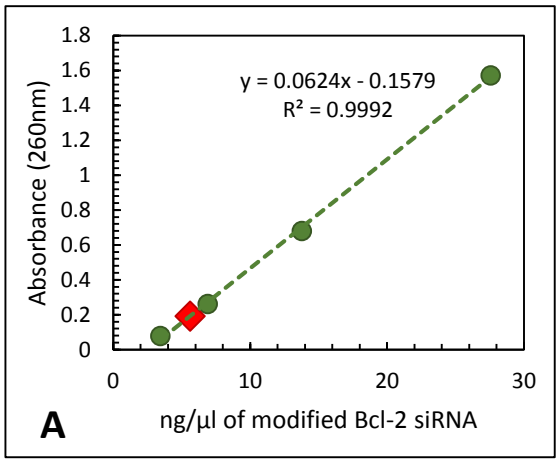

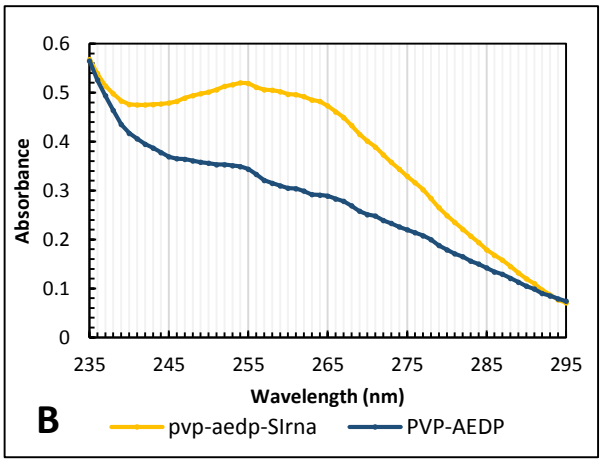

siRNA Bcl-2 ng/µl	OD_{260}
27.566	1.573
13.783	0.681
6.8915	0.262
3.44575	0.078

OD_{260} PVP-AEDP-siRNA (Subtracted of OD_{260} of PVP-AEDP)	0.192
siRNA conjugated to siRNA-PVP-AEDP (ng/µl)	**5.6**

Figure 51. Quantification of siRNA conjugated to PVP nanogels. A: standard curve of serial dilutions of free siRNA. B PVP-AEDP and PVP-AEDP-Bcl-2 siRNA spectra.

Bcl-2 silencing by siRNA through PVP-AEDP-siRNA complex

To test a specific release mechanism mediated by Glutathione (GSH), HeLa cells were seeded in 6-well plates. They were treated with GSH-Oet (Glutathione reduced ethyl ester) that increases the Glutathione concentration inside the cells until 10 mM (GHS typical concentration of tumour cell cytoplasms) (Anderson *et al.*, 1985; Koo *et al.*, 2011). Therefore, the cells were incubated with PVP-AEDP-siRNA nanogels (300 pmol of siRNA for Bcl-2 targeting). Cells treated with PVP-AEDP NGs, were used as control. In order to

clarify the effect of Glutathione, samples were compared with untreated cells and incubated with PVP-AEDP alone or conjugated with the oligonucleotide. Western blot analysis (Figure 52) shows that without GSH-Oet treatment, there is no a significant silencing of the target protein, indeed the intensities of Bcl-2 bands are very similar. By contrast, in samples subjected to the action of the inductor of GSH, substantial difference is evident. Indeed, in the specimen incubated with PVP-AEDP-siRNA NGs, the band relative to Bcl-2 protein is almost totally disappeared respect to the negative control (cells incubated with PVP-AEDP NGs).

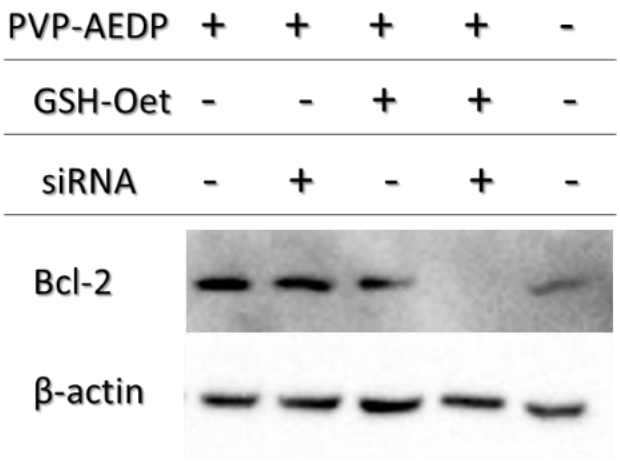

Figure 52. Western blot analysis of Bcl-2 expression in HeLa cells.

These preliminar results suggested that PVP nanoparticles would be used as vehicles for siRNA delivery. In particular, adding the AEDP linker would permit a controlled release of the siRNA glutathione-mediated and therefore a specific action against tumour cells for cancer therapy. Anyway the validation of the data with specific analysis of the RNA expression by RT-Real Time PCR needs to be done.

GRAPHENE

Reduced graphene oxide (**RGO**) consists of carboxyl-graphene carrying some hydroxyl group in the core and carboxyl functions in the "perimeter" that would permit the conjugation to biological molecules, like antibodies. The bi-dimensional and planar nature offers a large surface area for steaking interactions, for examples with nucleic acids, like siRNA. The systems were synthetized in collaboration with Dr. Nicolò Mauro (from Professor Giammona research group, Laboratory of Biocompatible Polymers, Department of "Scienze e Tecnologie Biologiche, Chimiche e Farmaceutiche" (STEBICEF)- University of Palermo) and their characterization was conducted in collaboration with Professor Peter Griffiths research group (Head of Department Pharmaceutical, Chemistry and Environmental Science, University of Greenwich -Medway Campus).

Sterilization and characterization of RGO systems.

RGO had a size more high then 0.2µm, so that it was impossible to sterilize with 0.2 µm filter. Therefore, a sterilization protocol was performed by treating the samples with 70% ethanol (EtOH) in sterile conditions, as described in materials and methods.

To evaluate any possible effects on RGO due to the EtOH treatment, Raman spectroscopy and Differential Scanning Calorimetry (DSC) analyses were carried out. Raman spectroscopy supplies information about the inner atomic structure of the sample through a spectrum analysis. As shown in figure 53, comparing untreated and EtOH treated samples, there are no differences in their spectra . In both cases, two peaks are present: D and G bands correspond to sp^2 and sp^3 carbon stretching modes, suggesting that Ethanol does not change the molecular properties.

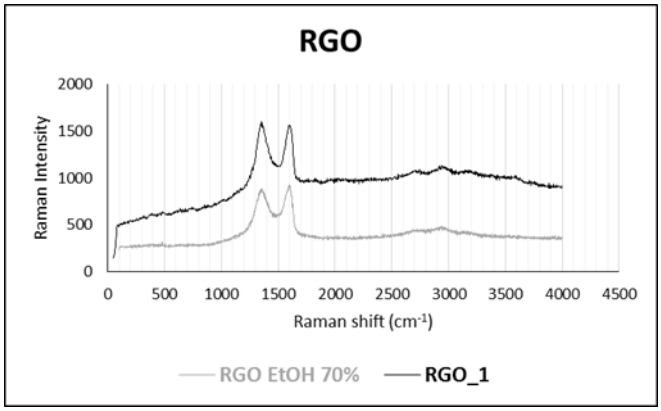

Figure 53. Raman Spectroscopy of RGO untreated (RGO_1) or treated with EtOH 70% (RGO EtOH 70%).

On the other hand, DSC give data relative to the chemical characteristics of the samples, like melting point and enthalpy. Even this analysis did not point out any considerable alterations induced by the treatment. Untreated RGO has a melting temperature of 215 °C, while RGO-EtOH 70% of 216.2 °C, this little difference is considered not significant. The diverse peak areas depend only by the different amount of samples used (Figure 54).

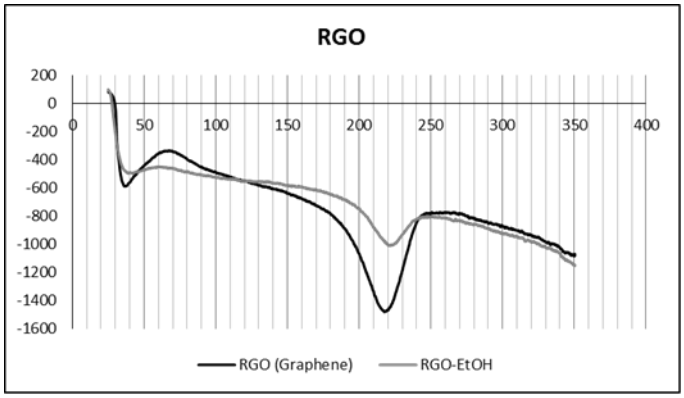

SAMPLES	PEAK AREA (J/g)	T_i (°C)	T_{peak} (°C)	T_f (°C)
RGO	-649	178.9	215	249.3
RGO-EtOH	-483	199.3	216.2	236.3

Figure 54. DSC Thermograms of RGO untreated (RGO_1) or treated with EtOH 70% (RGO EtOH 70%).

Furthermore, the nanosystem shape was investigated through Transmission Electron Microscopy (TEM) (Figure 55). The image clarifies the bidimensional nature of the RGO that appears like lamellar sheets, as expected.

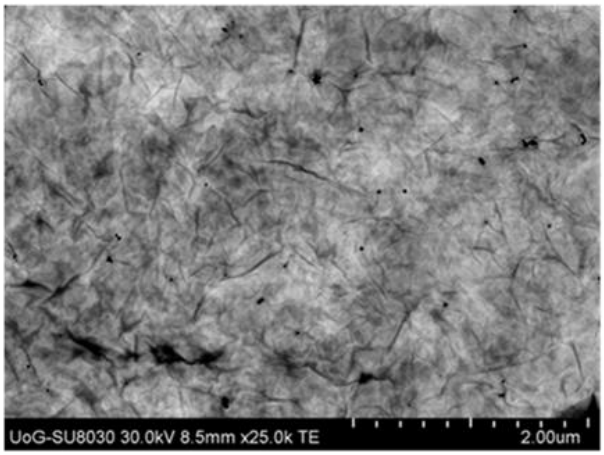

Figure 55. TEM analysis of RGO after EtOH treatment.

Biocompatibility of sterile RGO systems

Biocompatibility of RGO was tested on HepG2 cell lines. The samples were incubated with 6.25, 12.5, 25 and 50 µg/mL of RGO in DMEM medium for 24h, 48h and 72h (Figure 56). Untreated or treated with Polyethylenimine (PEI) (that, in solution, presents a cellular toxic effect) cells were used as negative and positive control respectively. In all cases, the viability is always higher than 80%, even after 72h of incubation with the highest concentration of RGO (50µg/mL), suggesting that the complexes are biocompatible.

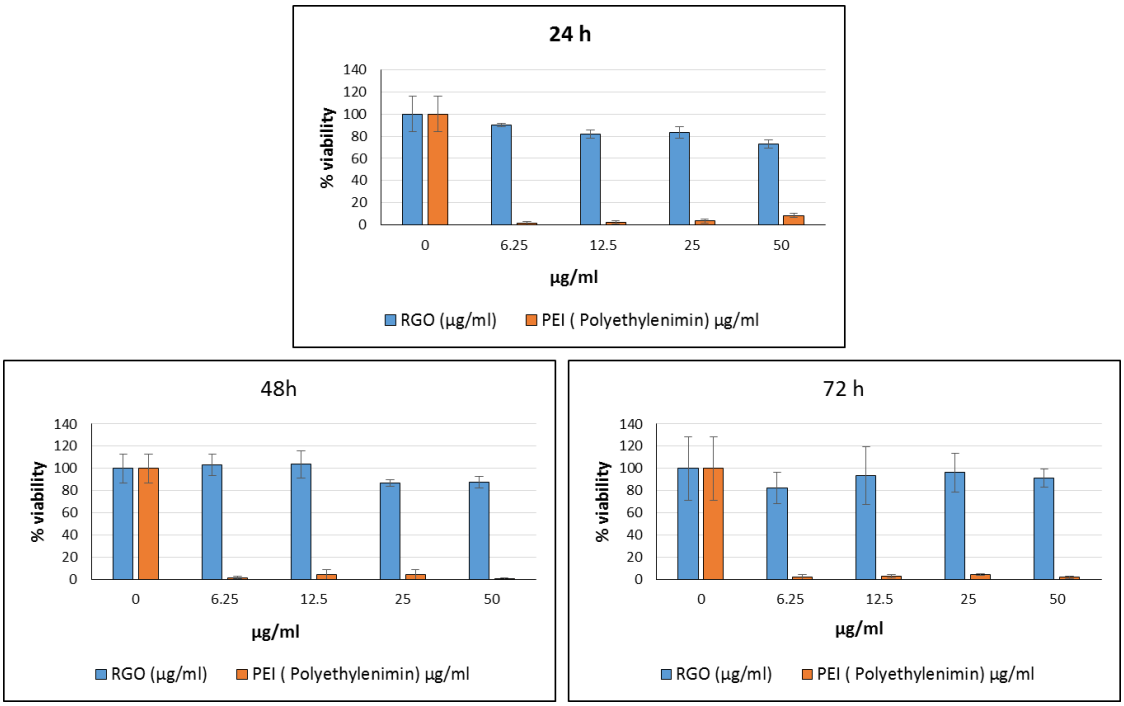

Figure 56. Biocompatibility of RGO systems on HepG2 cells after 24 hours (a), 48 hours (b) and 72 hours (c) of treatment.

RGO conjugated to an antibody: RGOY

In order to optimize its function as vector for drug delivery, the complex was analysed for its capacity to bind biological molecules. For this purpose, an antibody conjugation was performed in collaboration with Dr. Nicolò Mauro (from Prof. Giammona research group): the Seprase antibody was conjugated to the carboxyl groups of RGO to form the RGOY systems (Figure 57).

Samples were suspended in culture medium without Fetal Bovine Serum (FBS), because it contains many factors that facilitate the aggregation of the graphene sheets and, before all the experiments, RGOY was sonicated in 35 kHz Ultrasonic Bath many times (10'x 3times) in order to reduce the stacking interactions.

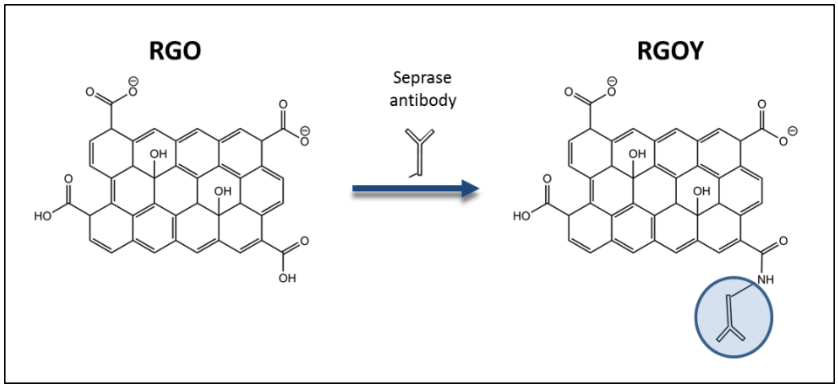

Figure 57. Conjugation of RGO to an antibody to obtain RGOY

To confirm the binding of the antibody to RGO, DSC analysis and Raman Spectroscopy were carried out. Raman Spectroscopy shows the same trend for both samples (Figure 58), but, through DSC analysis, a difference in the melting point peaks is evident: 204 °C and 215°C for RGO and RGOY, respectively. This shift is probably due to the presence of the conjugated antibody (Figure 59).

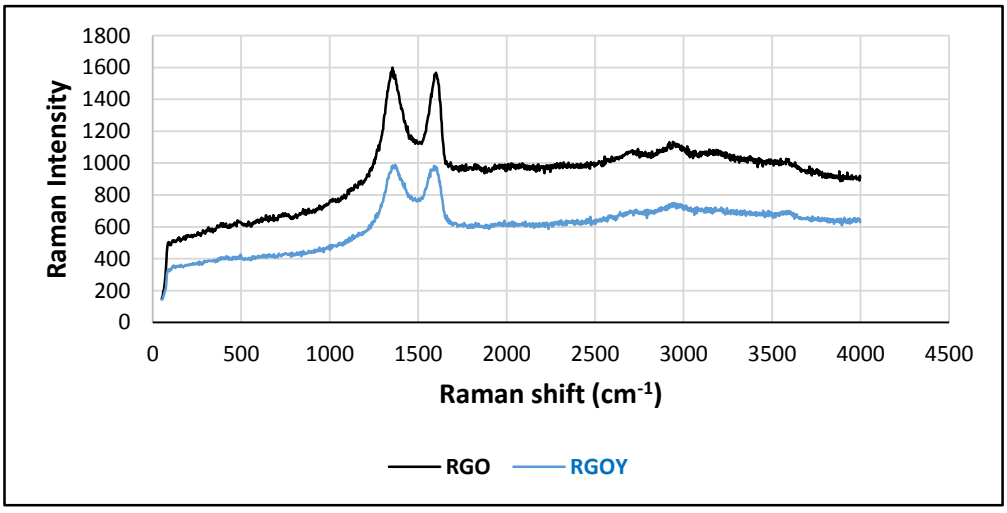

Figure 58. Raman Spectroscopy for RGO and RGOY samples.

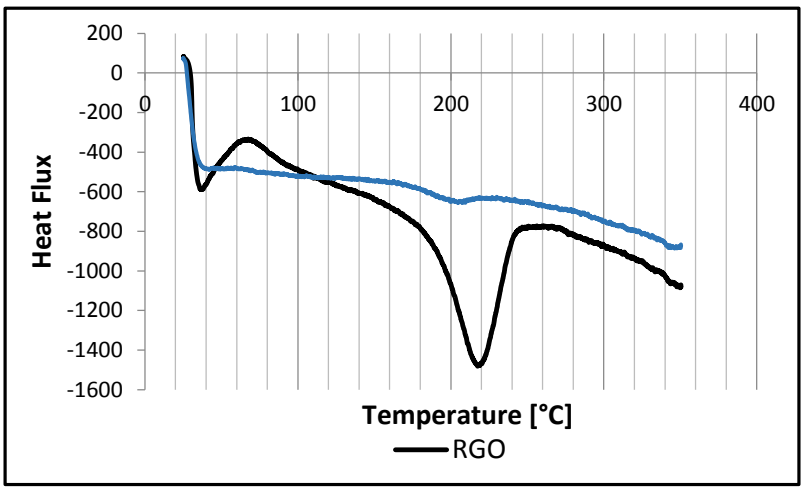

SAMPLES	PEAK AREA (J/g)	T_i (°C)	T_{peak} (°C)	T_f (°C)
RGO	-649	178.9	215	249.3
RGOY	-35.3	160.8	204.5	220.8

Figure 59. DSC Thermograms of RGO and RGOY

In order to obtain information about the size and population distribution of the complex, the Dynamic light scattering (DLS) was performed. Surprisingly, the data reveal a difference in the dispersion grade of the samples in solution: the peak area of RGO is wider than the RGOY one (368.9 *vs.* 263.6, respectively) (Figure 60). This suggests the presence of complexes of different size in RGO solution,probably due to non-specific interactions.In RGOY solution the population is more homogeneous, probably because of the presence of the antibody linked to each complex that limits the stacking interactions.

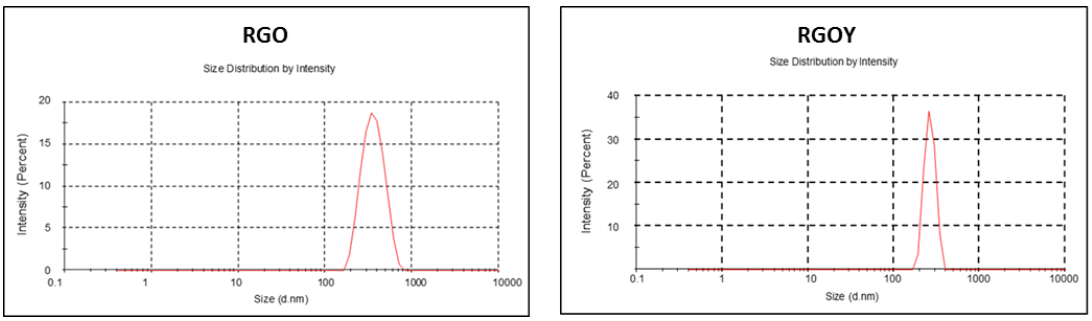

Sample	T (°C)	PdI	Pk1 Mean Int d.nm	Pk1 Area Int Percent
RGO	25	0,164	368,9	100
RGOY	25	0,578	263,6	100

Figure 60. DSL analysis of RGO and RGOY systems

The shape of the system conjugated with antibody was also investigated by TEM (Figure 61). Again, the image reflects the bidimensional nature of the samples.

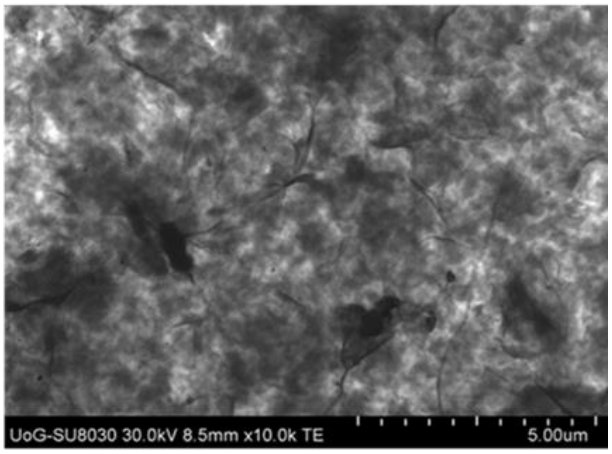

Figure 61. TEM analysis of RGO and RGOY

Cellular biocompatibility and uptake studies of RGOY-AF

In order to investigate the biocompatibility and the cellular uptake, the system was conjugated to the red fluorescence probe Alexa Fluor 647 (RGOY -AF) (Figure 62).

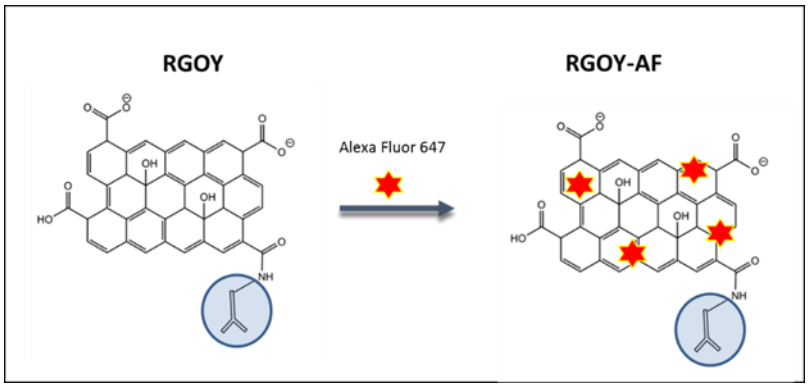

Figure 62. Conjugation of RGOY to Alexa Fluor 647 probe to obtain RGOY-AF

Biocompatibility assay of RGOY-AF was performed on ECV-304 cell line. Cells were incubated for 24h, 48h and 72h with different concentrations of particles: 0.25, 0.5, 1, 2.5, 5, 10, 15, 25, 30 and 50 µg/ml. As shown in figure 63, the viability is 100% (as the untreated cells are considered with 100% of viability). Cells treated with doxorubicin and used as negative control have a higher mortality, in dependence on the treatment duration and the RGOY-AF concentration. Even after 72 hours of incubation with 50 µg/ml of RGOY, cells are 85.5% viable, suggesting that the particles are biocompatible.

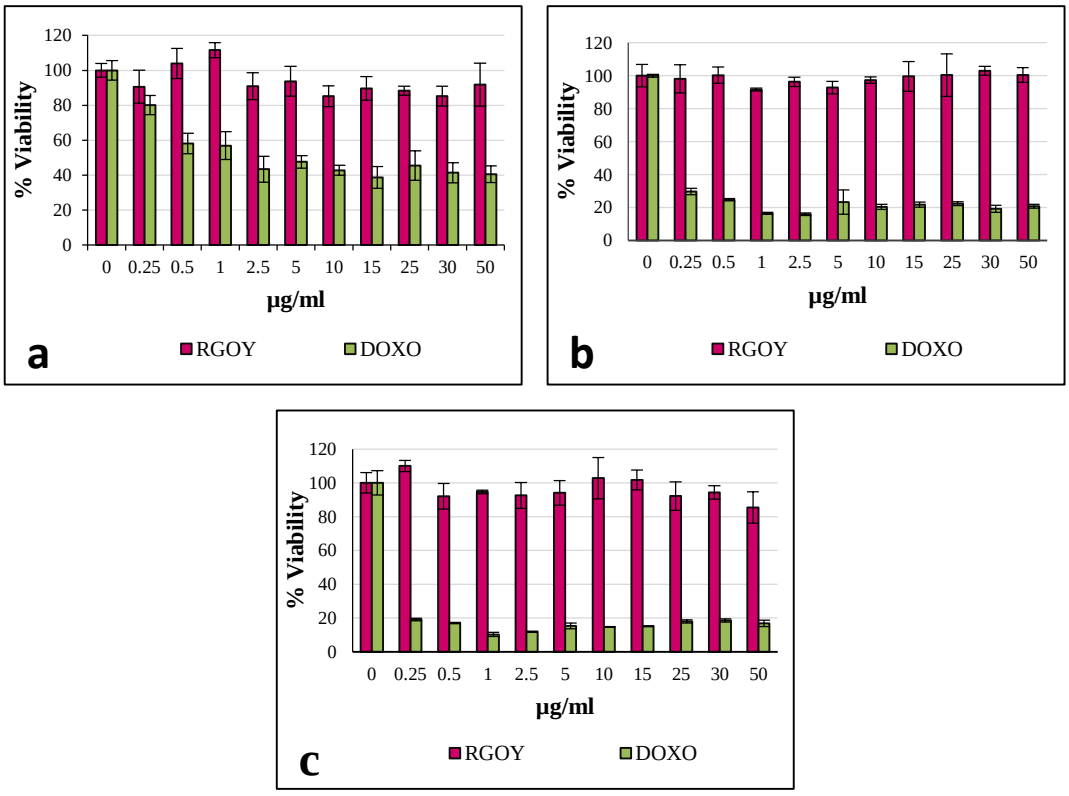

Figure 63. Biocompatibility of RGOY systems on ECV-304 cells after 24 hours (a), 48 hours (b) and 72 hours (c) of treatment.

Once the absence of cytotoxicity of RGOY-AF was established, uptake studies were carried out in order to analyse the specific particles localization inside the cells and their possible effects on the cytoskeleton component over time. For this purpose, ECV-304 cells were stained with phalloidin-FITC, marking the actin cytoskeleton, and with DAPI, to stain the nuclei (Figure 64). After 15 minutes of incubation, the red fluorescence of RGOY-AF is still diffused in the media and is partially present on the cells surface (a’’’). After 1 h (c’’’), the RGOY-AF red signal is higher and it starts to appear also in the cytoplasmic compartment.

The red signal increase with the duration of the treatment 2h (d’’’), suggesting that the particles are internalized in a time- dependent way.

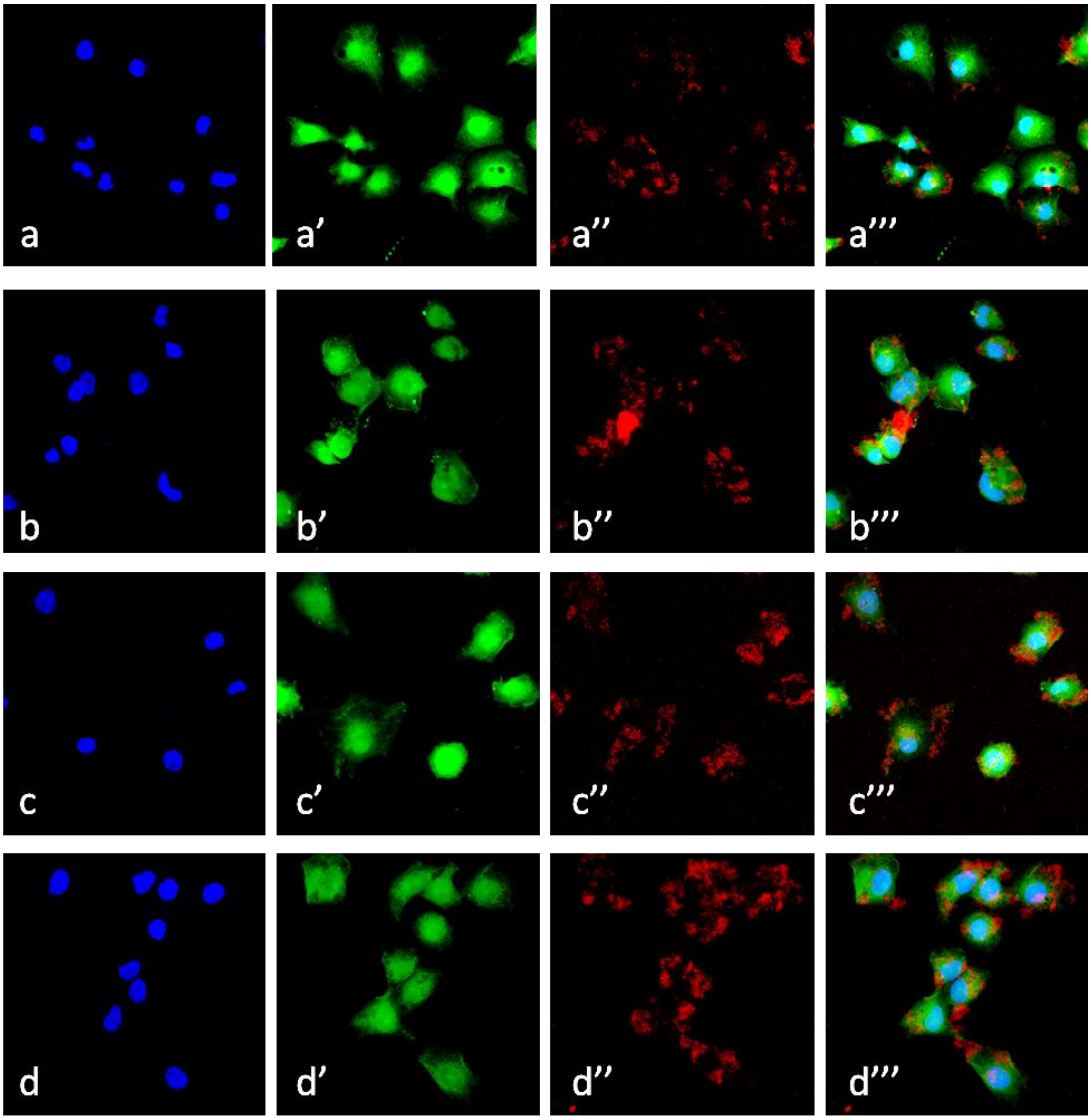

Figure 64. Localization studies of RGOY-AF on ECV-304 after 15’ (a-a’’’), 30’ (b-b’’’), 1h (c-c’’’) and 2h (d-d’’’) of incubation. Blue: nuclei, green: Phalloidin red: RGOY-AF. Magnificence 60 X.

RGOY-siRNA systems

The RGO is synthetized in a very simple manner, starting from graphite, easily obtainable at low cost, and this permits to synthetize a large amount of nanosystems. Furthermore, because of its bidimensional nature, it can offer a very big surface available for stacking interactions with many molecules. For example, the conjugation with planar bases of small oligonuotides like a siRNA is very simple to realize and would permit to link a higher amount of them. Starting from this idea, Dr. N. Mauro (from Prof. Giammona research group) conjugated RGOY systems to Egr-1 siRNA (**RGOY-siRNA**) (Figure 65).

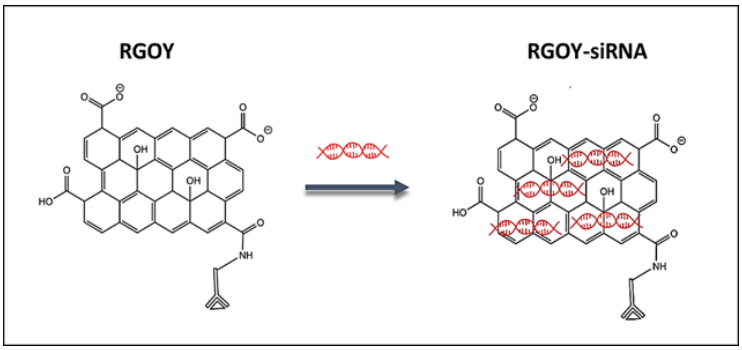

Figure 65. Conjugation of RGOY to Egr-1 siRNA to obtain RGOY-siRNA

The conjugation was confirmed by Electrophoresis assay and Atomic Force Microscopy (AFM) (data not shown, Dr. N. Mauro), and by DSC analysis (Figure 66). As it can be seen from the graph, RGO and RGOY-siRNA samples are characterized by different melting points: 215 °C and 196.2 °C respectively.

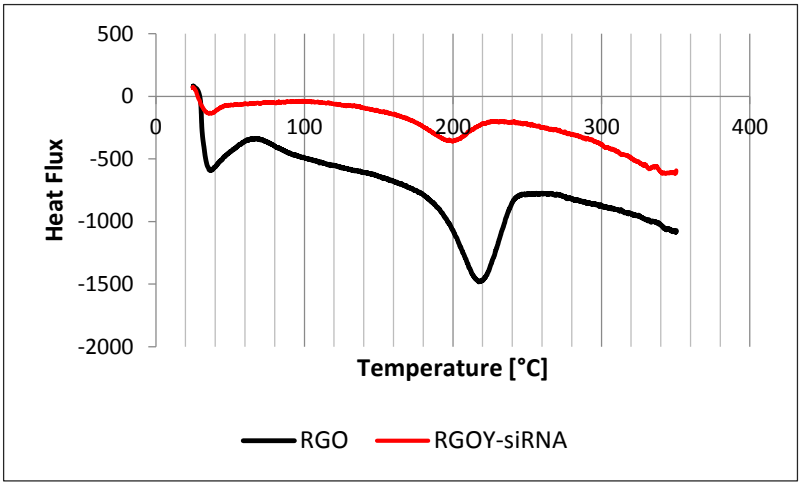

SAMPLES	PEAK AREA (J/g)	T_i (°C)	T_{peak} (°C)	T_f (°C)
RGO	-649	178.9	215	249.3
RGOY-siRNA	-154	164.8	196.2	224.1

Figure 66. DSC Thermograms of RGO and RGOY-siRNA

Furthermore, the complex was also characterized through DLS analysis and Raman spectroscopy (Figure 67). RGOY-siRNA and graphene have the same peculiar two peaks: D and G bands correspond to sp^2 and sp^3 carbon stretching modes (a). Conversely, RGOY-siRNA has a size of 149.7 nm with a good Polydispersity Index (PdI) of 0.516. Stunningly, compared with the RGOY size (263.6 nm), it is evident that the presence of siRNA reduces the size of the complexes (149.7 nm), probably because of its negative charge. Indeed, it is presumable that the repulse force between the negative siRNAs limits the staking interactions of the RGOY sheets, resulting in a lower size of the aggregates.

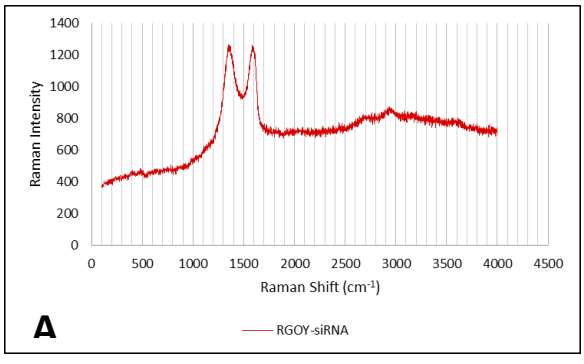

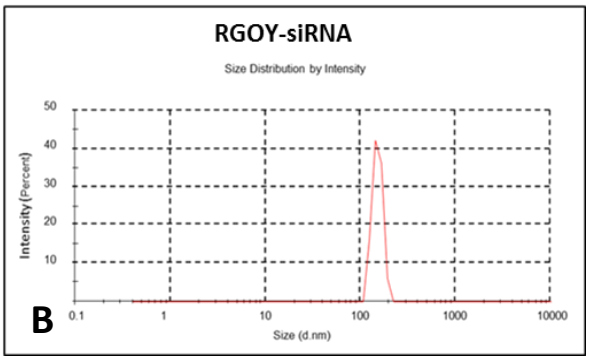

Sample	T(°C)	PdI	Pk1 Mean Int d.nm	Pk1 Area Int Percent
RGOY-siRNA	25	0.516	149.7	100

Figure 67. Raman spectroscopy (a) and DLS analysis (b) for RGOY-siRNA systems

The possibility to link an oligonucleotide as a siRNA, makes the reduced graphene oxide an optimum candidate for gene delivery in tumour therapy. Furthermore, its ability to link an antibody can be used for specific targeting.

RGOY-PVP systems

A high reduction of the staking interactions between the graphene sheets was obtained by conjugating RGOY particles to Polyvinylpyrrolidone (PVP) (**RGOY-PVP**). These systems were synthetized in collaboration with Professor Gaetano Giammona research group that conjugated them to the red fluorescence probe Alexa Fluor 647, to generate the complex RGOY-PVP-AF.

Biocompatibility was tested for the ECV-304 cells using different RGOY-PVP concentrations (0.25, 0.5, 1, 2.5, 5, 10, 15, 25, 30 and 50 µg/ml) (Figure 68). Also using this complex, the viability of cells is about 100% after 24h, 48h and 72h of treatment.

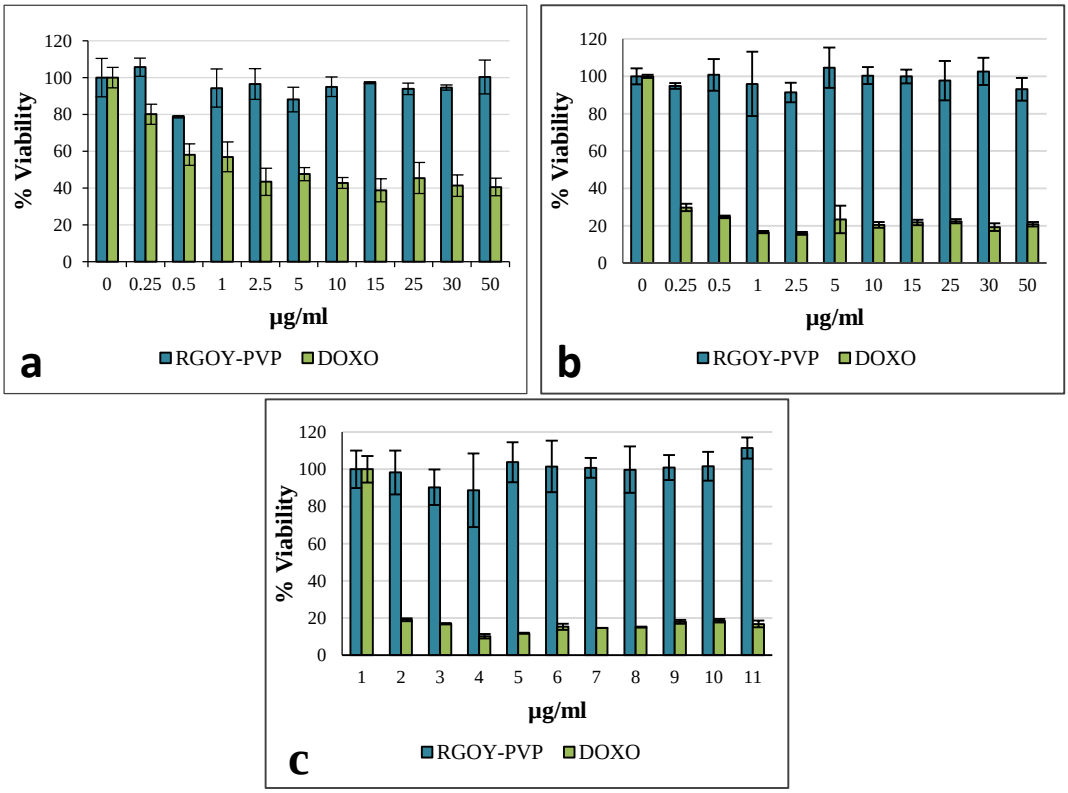

Figure 68. Biocompatibility of RGOY-PVP-AF systems on ECV-304 cells after 24 hours (a), 48 hours (b) and 72 hours (c) of treatment.

The internalization studies were conducted through confocal microscopy and revealed a time-dependent uptake (Figure 69). In particular, after 15 minutes (a’’’), the RGOY-PVP-

AF is still dispersed around the cells and partially localized in correspondence to the plasma membrane. It starts to go inside the cells and situates in the cytoplasm after only 30 minutes or more (1 hour of treatment), when the red fluorescence inside the cells is higher. The signal increases after 2 hours of treatment, when the particles appear localized in the perinuclear area (d''-d'''). For longer incubation times, the red mark is even brighter , and it is especially localized around the nucleus compartment.

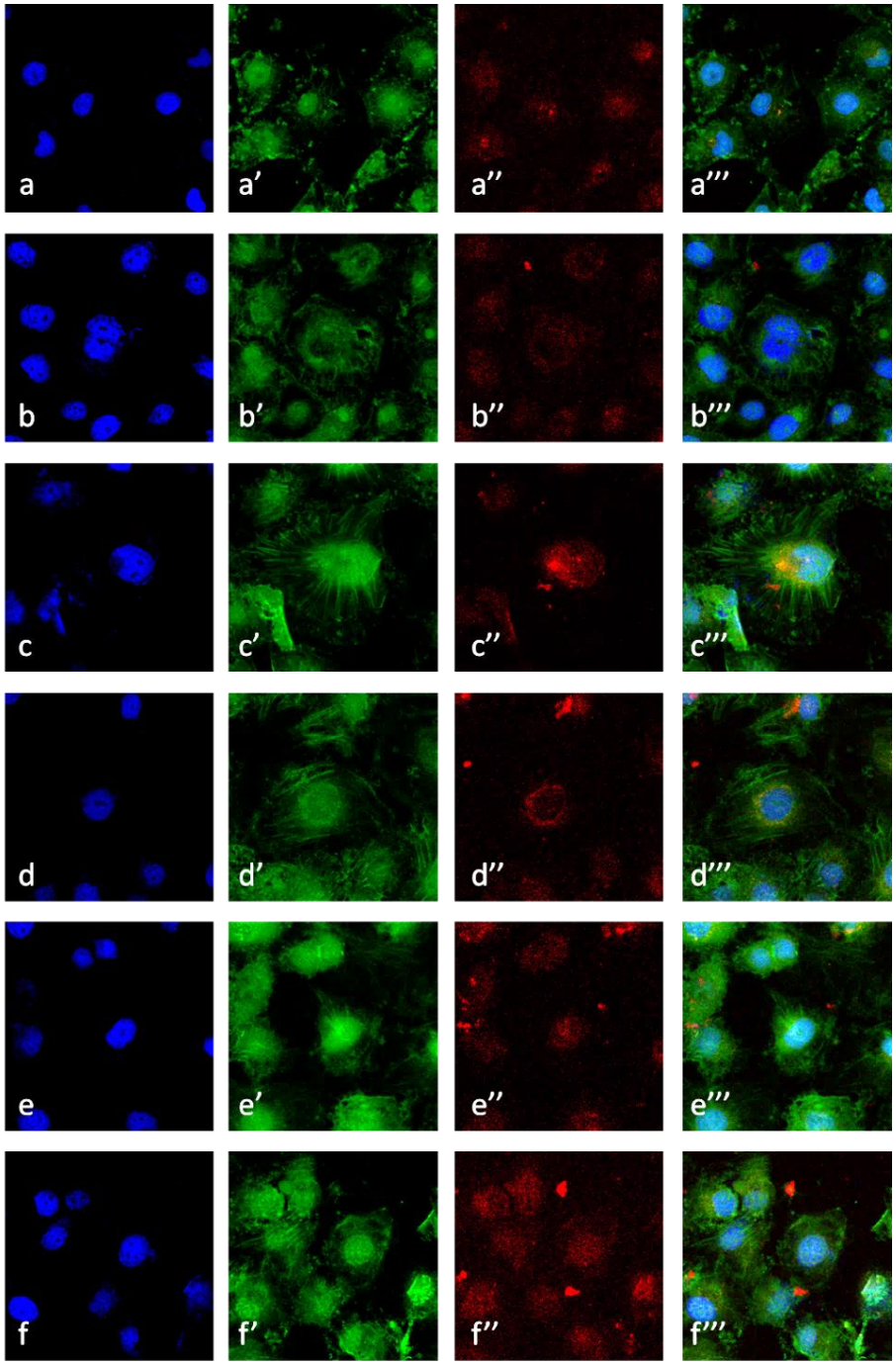

Figure 69. Localization studies of RGO-PVP on ECV-304 after 15' (a-a'''), 30' (b-b'''), 1h (c-c'''), 2h (d-d'''), 4h (e-e''') and 6h (f-f''') of incubation. Blue: nuclei, green: Phalloidin red: RGO-PVP. Magnificence 100 X.

Conclusion

Cancer is one of the most terrible diseases for the majority of world population and the principal cause of death worldwide (Globocan, 2014). The only approach used consists on the traditional anti-tumour drug administration technics, though they present many limitations because of their nonspecific action and consequently of the diffused side effects.

Therefore, in the last decades, Drug delivery system has been object of interest of many researchers. Indeed, it offers the basis for a modern form of tumour therapy thanks to the possibility of using nanocarriers able to recognise the target site and to release the therapeutic agent in a controlled manner.

In this contest, the PhD project has been developed in order to compare four different nanosystems for tumour therapy: **INU-EDA-P,C-DOXO**; **PHEA-EDA-P,C-DOXO**; **PVP-siRNA and RGO-siRNA.**

The polymeric nanocarriers Inulin and PHEA were conjugated to the antineoplastic drug doxorubicin (Doxo) through the same pH sensitive spacer, in order to compare them and individuate the more efficient. Both systems were analysed for their capacity to induce cellular death (using viability assays) and to be internalized (by fluorescence microscopy and flow cytometric analysis) comparing healthy and tumour cells from the same tissue (HB-2 and MDA-MB 231 cell lines, respectively). It is evident that the viability of HB-2 treated with different concentrations of either conjugates is always higher, not only respect to tumour cells, but also if compared with samples treated with the free drug, suggesting that the nanoconjugates confer more selectivity for tumour cells respect to the normal ones, independently of the EPR effect. This specific action is more evident for cancer samples treated with PHEA-EDA-P,C-DOXO as it is evident comparing the two viability graphs (Figure 22 and 28). Indeed, the trends relative to the two cell lines start to diverge at lower concentration of PHEA-EDA-P,C-DOXO (5 µM) compared with those of INU-EDA-P,C-DOXO (25 µM). In particular, MDA-MB 231 cells show the same trend if treated with PHEA or free drug (from 3.5µM to 25µM), suggesting that all the drug conjugated to the nanosystem has been released (Figure 28).

Uptake studies through fluorescence microscopy were conducted using green fluorescence variant of both systems (INU-EDA-P,C-DOXO and PHEA-EDA-P,C-DOXO) so that it was possible to follow them and, simultaneously, to follow the doxorubicin red auto-fluorescence. The images (Figure 23 and 30) show a good internalization of both nanosystems in tumour cells: after 1h of incubation the drug is still bound to the polymers

(indeed, the green and red fluorescence signals from the nanopolymers itself and from the doxorubicin co-localized in the cytoplasm), while after 4h the doxorubicin starts to go inside the nuclear compartment whereas the nanocarriers remainn in the cytoplasm. A different situation were registered for normal cells: in both cases, the green fluorescence appears muffled, punctuate and restricted in peripheral cytosolic area even after 4 hours, thus demonstrating a different uptake grade between normal and tumour cells, probably because of their dissimilar membrane composition.

This difference is more evident looking the quantitative uptake analysis data from flow cytometry. While in HB-2 cells the doxorubicin and polymers (Inulin or PHEA) uptake profiles follow the same tendency, in MDA-MB 231 they are very different (Figure 25 and 32): the red fluorescence (Doxo) inside the cancer cells increases faster than green marck (polymer). Therefore, these data reveal that, probably, there is a partial drug release in the tumour microenvironment. It is widely known that cancer tissue presents a lower pH (6.5) compared to the one of healthy microenvironment (pH 7.4) (Gerweck and Seetharaman, 1996). Therefore, as the drug is bound through a pH-sensitive linker to the copolymers, the lower pH would induce a partial doxorubicin release in cancer tissues, so that it would diffuse into tumour cells; while, the physiological pH of the normal tissue, cannot permit the controlled release so that the entire complexes would go inside the cells. In details, comparing the results of using Inulin and PHEA nanosystems, it is evident that the uptake difference between normal and tumour cells is more prominent in the second one. It is probably due to the different polymeric composition and therefore to the different capacity to be internalized.

In light of these data that support PHEA-EDA-P,C-DOXO as the most efficient nanocarrier, its preferential uptake into tumour cells was further investigated through co-culture experiments: the same number of MDA-MB 231 and HB-2 cells were grown together and incubated with the selected nanosystem (Figure 34-35). Fluorescence microscopy confirms a faster internalization into the cancer line. Furthermore, also the endocytic pathway and the subsequent itinerary inside cells were investigated using specific endocytosis inhibitors (by flow cytometric analysis and confocal microscopy, Figure 38 and 39) and a specific lysosomal probe (byconfocal microscopy, Figure 41) respectively.

Therefore, all the data have permitted to hypothesize a model in which PHEA-EDA-P,C-DOXO complex would start to release the drug in the tumour microenvironment thanks to the low pH. In this way, free doxorubicin would diffuse inside the cells, while the

nanosystem would be internalized through a pathway involving in the formation of caveolae, that progressively would fuse with lysosomes, following the classical endocytic pathway. It would be reasonable to think that the low pH inside the lysosomes would induce the complete doxorubicin release thanks to the pH-sensitive spacer; once set free, the drug would go into the nuclei and induce the cellular death (Figure 42).

Even if the data obtained explain very well the PHEA-EDA-P,C-DOXO action mechanism, this model needs to be more investigated. It is very important to know how the nanocomplex reaches the tumour target site (we would suppose through the EPR Effect). Furthermore, even if it is evident a preferential ability of the complex for tumour cells, it will be possible to add a targeting molecule, able to recognise the specific tumour site to increase its selective character. Collectively, all the data support a PHEA-EDA-P,C-DOXO action model *in vitro*, but needs to be confirmed through *in vivo* experiments.

siRNA delivery studies have been conducted by comparing two different nanosystems conjugated with anti-tumour siRNA: Egr-1 involved in the progress of hepatocarcinoma and Bcl-2 related to the apoptotic pathway in cancer cells.

The choise of these particular nanosystems depends on their nature and their ability to link siRNA. PVP nanoparticles are nanogels with a three-dimensional structure functionalized with carboxyl groups that allow a covalent binding to the amine group of modified siRNA. Its tri-dimensional structure would facilitate the oligonucleotide protection and limit its degradation. Instead, RGO is a two-dimensional system in which the planar conformation would favour the stacking interation with a larger amount of unmodified siRNA and the siRNA release would be promoted by a competition mechanism.

PVP studies had demonstrated their good propensity as siRNA delivery system. Indeed, they are able to link modified siRNA (Figure 48), without any alteration of their functionality, as indicated by western blot analysis (Figure 49). Tumour cells have high cytoplasmic level of GHS compared to normal ones, and this feature can be used to achieve a controlled release mechanism. For this purpose, the introduction of AEDP, with a disulphide bridge in the middle, permits a controlled release GHS-mediate and a higher release grade into the cells (Figure 52).

Western blot analysis suggests a reduction of target protein expressed due to the siRNA action, thus demonstrating the system efficiency, anyway the RNA expression analysis by RT-real time PCR still needs to be done.

Preliminary studies were conducted also with graphene nanosystems. It is such an innovative system as DDS, that only few papers have been already published. Its nature, as well as the possibility to synthesize it at low cost, have made Graphene nanosystems very interesting in tumour therapy in the last years. As it is not very well characterized, the initial approach was very complicated by its aptitude to form aggregates that have limited its sterilization.

Very interesting results were obtained through a collaboration between University of Palermo (Professor Giammona and Professor Ghersi research groups) and Greenwich University (Professor Griffiths research group). Together we developed a sterilization protocol using Ethanol: it does not alter graphene specific features, as demonstrated through DLS and DSC analyses, TEM and Raman spectroscopy. Graphene aptitude as vector for drug delivery is evident thanks to its capability to link antibodies (as possible specific targeting molecules) or siRNA (for tumour therapy). Furthermore, it is biocompatible (Figure 56, 63 and 68) and it is able to enter the cells, as demonstrated by confocal microscopy (Figure 64 and 69).

Even if the preliminary data identifies Graphene as a very good candidate for siRNA delivery, the siRNA effect still needs to be investigated: silencing experiments and consecutive RNA and proteins expression analyses will be performed, as well as the investigation of the targeting capability induced by a conjugated antibody.

Both PVP and RGO nanosystems will be studied also for the Egr-1 or Bcl-2 silencing effects, through migration and invasion experiments (transwell migration or invasion assays) or enzymatic activation assays of specific proteins involved in the apoptotic pathway.

All these preliminary data suggest the possibility to develop an innovative therapeutic approach for tumour therapy. In particular, Inulin and especially PHEA nanopolymers have shown very interesting features with an EPR-mediated passive targeting but also a major affinity for the tumour cell membrane. Furthermore, they are able to induce a pH-controlled drug release in tumour microenvironment and in the lysosomal compartment. For this reason, even their in vivo activity will be investigated. On the other hand, PVP nanogels and graphene seem very good candidates as delivery system thanks to their specific properties that permit to link siRNA without any degradation effect. PVP NGs present high biocompatibility and a GHS-controlled siRNA release; furthermore, precedent studies has demonstrated an active tumour targeting antibody-mediated (Adamo, 2013). Finally,

graphene data are still very preliminary, but they are promising, thus encouraging further studies.

Acknowledgments

This PhD Thesis is the result of three years working in biochemical laboratory of the STEBICEF Department of the University of Palermo. Many people have contributed to realize it. I would like to thank my PhD supervisor, Professor Giulio Ghersi (University of Palermo) for supporting me during this past period and for transmitting me the enthusiasm for the research. All the members of my group lab played a very important and fundamental role: Dr. Salvatrice (Silvia) Rigogliuso, Dr. Silvia Saladino, Lorenzo Volpe (PhD student), Dr. Monica Salamone, Marco Ciappa, Dr. Anna Giardina, Dr. Elvira Di Leonardo, Mariangela Pampalone, Dr. Francesco Carfì Pavia, Dr. Felice Gaetano Caldara, Silvia Greco and Dr. Luca Lo Piccolo (the first one that has believed in me). A special thanks to my colleague and friend Dr. Giorgia Adamo that, always, supports me and has made special and full of smiles these years. She has also contributed to do this work by collaborating in many experiments reported. I would like to thank also my students (Salvatore Mannino, Alessandra Trainito, Francesca Gisone, Simone Scrima, Simone Bonelli and Martina Gruppuso) and my colleagues that have made especially my PhD period: Dr. Sergio Spatafora, Dr. Giuseppe Costa, Dr. Salvatore Manuel Molino, Dr. Silvia Casamirra, Dr. Walter Spinello, Dr. Rosaria (Sara) Tinnirello and Dr. Aldo Nicosia.

I also have to thank the director of PhD programme Professor Renza Vento and the members of my PhD committee for their helpful career advice and suggestions.

I also thank all my partners that supplied the nanosystems used: Dr. Nicolò Mauro, Professor Gaetano Giammona and his team (Dr. Cinzia Scialabba and Dr. Mariano Licciardi) (University of Palermo) that have given me the Inulin, PHEA and Graphene nanosystems; Eng. Celia Dispenza and her group (Dr. Maria Antonietta Sabatino, Dr. Natascia Grimaldi and PhD student Lorena Ditta) (University of Palermo) that have synthetized PVP nanogels.

I will be thankful to Professor Peter Griffiths (University of Greenwich) to give me the possibility to work in his lab, for three months, at Medway Campus (Kent, UK). He was very available to give me support and advices for my research. He and his group (Dr. Beatrice Cattoz, Omar Tarek Abouarab (PhD Student) and Sunit Atwal) have welcomed me as a member of their team. A special thanks also to Dr. Bruce Alexander that helped me with the Raman Spectroscopy, Dr. Ian Slipper for TEM analysis, Shashi Ravi Suman Rudrangi (PhD Student) for DSC assay, Prof. Simon Richardson and Gordon Tang (PhD Student) for the biological assays in Medway Campus. Very special thanks also to Laura Intxaurraga

(PhD student of Universidad de Navarra): she was an optimal companion during my visit in UK.

At last, but not for importance, I will forever be thankful to Dr. Roberta Sanfilippo that supports me so much. She is not only a colleague, but also and especially an optimal friend. A very special thanks to my family that has always been and will always be with me. In general, thanks to all the other colleagues and friends that have supported me during this work experience.

Bibliography

A. Swami , J. Shi , S. Gadde , A. R. Votruba , N. Kolishetti , and O. C. Farokhzad. 2012. Nanoparticles for Targeted and Temporally Controlled Drug Delivery, Nanostructure Science and Technology, Chapter: Multifunctional Nanoparticles for Drug Delivery Applications. Part of the series Nanostructure Science and Technology pp 9-29.

Adamo, 2013. PhD Thesis: Sviluppo di nanocarriers per il "drug release" controllato di biomolecole nella terapia antitumorale. University of Palermo.

Adamo, G., Grimaldi, N., Campora, S., Sabatino, M., Dispenza, C., and Ghersi, G. 2014. Glutathione-sensitive nanogels for drug release. Chem. Eng. Transact, 38:457-462.

Adams, M. L.,Lavasanifar, A., Kwon, G. S., Pharm,J. 2003. Amphiphilic block copolymers for drug delivery. Sci. 92:1343 – 1355.

Al-Ahmady, Z. S., W. T. Al-Jamal, *et al.* 2012. Lipid-peptide vesicle nanoscale hybrids for triggered drug release by mild hyperthermia in vitro and in vivo. ACS Nano, 6(10):9335-9346.

Alexander V. Kabanov *et al.*, 2009. Nanogels as Pharmaceutical Carriers: Finite Networks of Infinite Capabilities. Angew Chem Int Ed Engl, 48(30): 5418–5429.

Alexander V. Kabanov, Serguei V. Vinogradov. 2009. Nanogels as Pharmaceutical Carriers: Finite Networks of Infinite Capabilities. Angew Chem Int Ed Engl. 48(30):5418–5429.

Aluri, S., S. M. Janib, *et al.* 2009. Environmentally responsive peptides as anticancer drug carriers. Adv Drug Deliv Rev, 61(11):940-952.

Anderson M E et. *al.*, 1985. Glutathione monoethyl ester: preparation, uptake by tissues, and conversion to glutathione. Archives of Biochemistry and Biophysics, 239(2): 538-548.

Aruna, U., Rajalakshmi, R., Muzib, Y. I., Vinesha, V., Sushma, M., Vandana, K. R.,Kumar, N. V. 2013. Role of Chitosan Nanoparticles in Cancer Therapy. Inter. J. Inn. Pharm. Res, 4:318 – 324.

Audumbar DM, Ritesh S. 2015. A Review on sustained release drug delivery system. GCC Journal of Science and Technology, 1(4):107-123.

Basavaraj K. Nanjwade, Hiren M. Bechra, Ganesh K. Derkar, F.V. Manvi, Veerendra K. Nanjwade. 2009. Dendrimers: Emerging polymers for drug-delivery systems. European Journal of Pharmaceutical Sciences 38(3):185–196.

Bates, P.J., Laber, D., Miller, D.M., Thomas, S.D., Trent, J.O. 2009. Discovery and development of theG-rich oligonucleotide AS1411 as a novel treatment for cancer. Exp. Mol. Path. 86:151–64.

Bawa, P., V. Pillay, *et al.* 2009. Stimuli-responsive polymers and their applications in drug delivery. Biomed Mater, 4(2):022001.

Bertrand,N., Wu, J., Xu, X., Kamaly, N., Farokhzad, O. C. 2014. Cancer nanotechnology: The impact of passive and active targeting in theera of modern cancer biology. Advanced Drug Delivery Reviews, 66:2-25.

Blanco, M.D., Teijón, C., Olmo, R.M.,Teijón,J.M. 2012. Targeted Nanoparticles for Cancer Therapy in Pharmacology, Toxixology and Pharmaceutical Science, Pharmacology, Recent Advances in Novel Drug Carrier Systems. Chapter 9.

Carver L. A. and J. E. 2003. Caveolae: mining little caves for new cancer targets. Schnitzer Nature Reviews Cancer, 3, 571-581.

Catalina E. Haro Pérez. 2005. Nanoestructuras tridimensionales formadas con liposomas: propiedades estàticas y dinàmicas, Editorial de la Universidad de Granada.

Champion, J.A., Mitragotri, S. 2006. Role of target geometry in phagocytosis. Proc Natl AcadSci U S A. 103(13):4930–4934.

Chen Y., Zhu X., Zhang X., Liu B. and Huang L.. 2010. Nanoparticles Modified With Tumor-targeting scFv Deliver siRNA and miRNA for Cancer Therapy. Molecular Therapy,18(9):1650–1656.

Chen, X., C. P. Ooi, *et al.* 2006. "Effect of ganciclovir on the hydrolytic degradation of poly(lactide-co-glycolide) microspheres." J Biomater Appl 20(3):287-302.

Chen, X., C. P. Ooi, *et al.* 2006. Effect of ganciclovir on the hydrolytic degradation of poly(lactide-co-glycolide) microspheres. J Biomater Appl 20(3):287-302.

Cheng, K., S. Peng, *et al.* 2009. Porous hollow Fe(3)O(4) nanoparticles for targeted delivery and controlled release of cisplatin. J Am Chem Soc 131(30):10637-10644.

Chithrani B. D., W. C.W. Chan. 2007. Elucidating the mechanism of cellular uptake and removal of protein-coated gold nanoparticles of different sizes and shapes. Nano Lett., 7:1542 – 1550.

Chithrani, B.D., Ghazani, A.A., Chan, W.C. 2006. Determining the size and shape dependence of gold nanoparticle uptake into mammalian cells. Nano Lett. 6(4):662–668.

Choe, T.B., Park, I.C., Hong, S.I. 1998. Enhancement of cationic liposome-mediatedtransfection by lactoferrin. Biotechnol Tech 12:577-581.

Colombo, G.,Curnis, F.,De Mori, G.M.S.,Gasparri, A., Longoni, C., Sacchi, A., Longhi, R., Corti, A. 2002. Structure–activity relationships of linear and cyclic peptides containing the NGR tumor-homing motif. J. Biol. Chem. 277:47891–47897.

Couvreur, P. 2013. Nanoparticles in drug delivery: past, present and future. Adv Drug Deliv Rev 65(1):21-23.

Dalmark M and Hoffmann EK. 1983. Doxorubicin (Adriamycin) transport in Ehrlich ascites tumour cells: comparison with transport in human red blood cells. Scand J Clin Lab Invest. 43(3):241-8.

Daniels, D.A., Chen, H., Hicke, B.J., Swiderek, K.M., Gold, L. 2003. A tenascin-C aptamer identified by tumor cell SELEX: systematic evolution of ligands by exponential enrichment. Proc Natl AcadSci U S A. 100(26):15416–15421.

Decuzzi P., Lee S., Bhushan B., Ferrari M.. 2005. A theoretical model for the margination of particles within blood vessels. Ann. Biomed. Eng., 33:179 – 190.

Desai, M.P., Labhasetwar, V., Walter, E., Levy, R.J., Amidon, G. L. 1997. The mechanism of uptake of biodegradable microparticles in Caco-2 cells is size dependent. Pharm Res, 14, 1568-73.

Devarajan, P.V., Jindal, A.B., Patil, R.R., Mulla, F., Gaikwad, R.V., Samad, A. 2010. Particle shape: a new design parameter for passive targeting in splenotropic drug delivery. J Pharm Sci. 99(6):2576–2581.

Di Andrei I. Ivanov. 2008 Exocytosis and Endocytosis. Humana Press.

Dispenza C., G. Adamo, M. A. Sabatino, N. Grimaldi, D. Bulone, M. L. Bondı, S. Rigogliuso, G. Ghersi. 2013. Oligonucleotides-Decorated-Poly(N-vinyl pyrrolidone) Nanogels for Gene Delivery. J. APPL. POLYM. SCI. 131(2): 39774-39782.

Dispenza C., M. A. Sabatino, N. Grimaldi, D. Bulone, M. L. Bondì, M. P. Casaletto, S. Rigogliuso, G. Adamo, and G. Ghersi. 2012. Minimalism in Radiation Synthesis of Biomedical Functional Nanogels. Biomacromolecules, 13 (6): 1805–1817.

Dispenza C., Sabatino M. A., Grimaldi N., Spadaro G., Bulone D., Bondi M. L., Adamo G., Rigogliuso S., 2012, Large-scale Radiation Manufacturing of Hierarchically Assembled Nanogels, Chemical Engineering transactions, 27:229-234.

Du, H., Chandaroy, P., Hui, S.W. 1997. Biochim. Biophys. ActaBiomembr. 1326:236 – 248.

Duncan, R. 2009. Development of HPMA copolymer-anticancer conjugates: clinical experience and lessons learnt. Adv Drug Deliv Rev, 61(13):1131-1148.

E. S. Papazoglou and A. Parthasarathy. 2007. BioNanotechnology. Morgan & Claypool Publishers.

Eric Drexler, 1986. “Engines of creation: the coming era of nanotechnology”.

F. Alexis, E. M. Pridgen, R. Langer, O. C. Farokhzad. 2009. Nanoparticle Technologies for Cancer Therapy. Chapter Drug Delivery Volume 197 of the series Handbook of Experimental Pharmacology pp 55-86.

Ferrari. 2005. Cancer nanotechnology: opportunities and challenges. Nat Rev Cancer, 5(3):161-71.

Fleige, E., M. A. Quadir, *et al.* 2012. Stimuli-responsive polymeric nanocarriers for the controlled transport of active compounds: concepts and applications. Adv Drug Deliv Rev, 64(9):866-884.

Frey NA, Peng S, Cheng K, Sun S. 2009. Magnetic nanoparticles: synthesis, functionalization, and applications in bioimaging and magnetic energy storage. Chem Soc Rev. 38(9):2532-42.

Gary J. Doherty and Harvey T. McMahon. 2009. Mechanisms of Endocytosis. Annu. Rev. Biochem. 78:31.1–31.46.

Gerweck L. E. and Seetharaman K.. 1996. Cellular pH gradient in tumor versus normal tissue: potential exploitation for the treatment of cancer. Cancer Res., 55(6): 1194–1198.

Gibas I., Janik H., 2010. Review: synthetic polymer hydrogels for biomedical applications, Chemistry & chemical technology 4:4.

Globocan 2012, 2015.

Gopferich, A. 1996. Mechanisms of polymer degradation and erosion. Biomaterials 17(2):103-114.

Haba, K., M. Popkov, *et al.* 2005. Single-triggered trimeric prodrugs. Angew Chem Int Ed Engl 44(5):716-720.

Harris, J. M.,Martin, N. E.,Modi, M. 2001. Pegylation: a novel process for modifying pharmacokinetics. Clin. Pharmacokinet. 40:539 – 551.

Haun J. B., 2010. Bioorthogonal chemistry amplifies nanoparticle binding and enhances the sensitivity of cell detection. Nat Nanotechnol, 5(9): 660–665.

Hillaireau H. and P. Couvreur. 2009. Nanocarriers' entry into the cell: relevance to drug delivery. Cell. Mol. Life Sci, 66: 2873.

Huang et El-Sayed. 2010. Gold nanoparticles: Optical properties and implementations in cancer diagnosis and photothermal therapy. Journal of Advanced Research. 1(1):13–28.

Jain, K. K. 2010. Advances in the field of nanooncology, BMC Med. 8:83.

Jesus and Grazu. 2012. Nanobiotechnology- Inorganic Nanoparticles vs Organic Nanoparticles. Elsevier., ISBN: 978-0-12-415769-9.

Jiang, J., Tong X., *et al.* 2005. A new design for light-breakable polymer micelles. J Am Chem Soc 127(23):8290-8291.

João Conniot *et al.*, 2014. Cancer immunotherapy: nanodelivery approaches for immune cell targeting and tracking. Front Chem, 2: 105.

Kälin S., Amstutz B., Gastaldelli M., Wolfrum N., Boucke K., Havenga M., DiGennaro F., Liska N., Hemmi S., and Greber U. F.. 2010. Macropinocytotic Uptake and Infection of Human Epithelial Cells with Species B2 Adenovirus Type 35. Journal of virology, p. 5336–5350.

Kamaly, N., Xiao, Z., Valencia, P. M., Radovic-Moreno, A. F., Farokhzad, O. C. 2012. Targeted polymeric therapeutic nanoparticles: design, development and clinical translation. Chem. Soc. Rev. 41(7):2971 – 3010;

Kisley, L.R., Barrett, B.S., Bauer, A.K., Dwyer-Nield, L.D., Barthel, B., Meyer, A.M., Thompson, D.C., Malkinson, A.M. 2002. Genetic ablation of inducible nitric oxide synthase decreases mouse lung tumorigenesis. Cancer research, 62(23):6850-6.

Kiss A. L. and Botos E. 2009.J. Endocytosis via caveolae: alternative pathway with distinct cellular compartments to avoid lysosomal degradation? Cell. Mol. Med., 13(7):1228-1237.

Konios D. *et al.*, 2014. Dispersion behaviour of graphene oxide and reduced graphene oxide. Journal of Colloid and Interface Science. 430: 108-112.

Koo *et al.*, 2011. Tumoraccumulation and antitumor efficacy of docetaxel-loaded core-shell-corona micelles with shell-specific redox-responsive cross-links. Biomaterials, 33(5):1489-1499.

Kroll, R.A., Pagel, M.A., Muldoon, L.L., Roman-Goldstein, S., Fiamengo, S.A., Neuwelt, E.A. 1998. Improving drug delivery to intracerebral tumor and surrounding brain in a rodent model: a comparison of osmotic versus bradykinin modification of the blood-brain and/or blood-tumor barriers. Neurosurgery. 43(4):879-86.

Ku, S. H., Kim K., *et al.* 2014. Tumor-targeting multifunctional nanoparticles for siRNA delivery: recent advances in cancer therapy. Adv Healthc Mater, 3(8):1182-1193.

Ladj R., H. *et al.* Elaissari A. 2013. Individual inorganic nanoparticles: preparation, functionalization and in vitro biomedical diagnostic applications. J. Mater. Chem. B, 1381-1396.

Law B. , and Tung C. H.. 2009. Proteolysis: a biological process adapted in drug delivery, therapy, and imaging. Bioconjug Chem 20(9):1683-1695.

Lee C. C., Gillies E. R., *et al.* 2006. A single dose of doxorubicin-functionalized bow-tie dendrimer cures mice bearing C-26 colon carcinomas. Proc Natl Acad Sci U S A, 103(45):16649-16654.

Lee K- Hee and Jae-Ryong Kim. 2009. Hepatocyte growth factor induced up-regulations of VEGF through Egr-1 in hepatocellular carcinoma cells. Clin Exp Metastasis, 26:685–692.

Lee K., Bae K. H., *et al.* 2010. Pluronic/polyethylenimine shell crosslinked nanocapsules with embedded magnetite nanocrystals for magnetically triggered delivery of siRNA. Macromol Biosci, 10(3):239-245.

Leroux J. C., Allemann E., DeJaeghere F., Doelker E., Gurny R. J.. 1996. Controlled Release, 39:339-350.

Liu, J., H. Lee, *et al.* 2006. Liposome formulation of a novel hydrophobic aryl-imidazole compound for anti-cancer therapy. Cancer Chemother Pharmacol 58(3):306-318.

Longfa Kou, Jin Sun, Yinglei Zhai, Zhonggui He. 2013. The endocytosis and intracellular fate of nanomedicines: Implication for rational design. Asian Journal of Pharmaceutical Sciences 8(1): 1–10.

Lotan, R., Raz, A. 1988.Lectins in cancer cells.Ann N Y Acad Sci. 551:385-96.

Luk, B.T., Hu, C.M., Fang, R.H., Dehaini, D., Carpenter, C., Gao, W., Zhang, L. 2014. Interfacial interactions between natural RBC membranes and synthetic polymeric nanoparticles. Nanoscale.6(5):2730–2737.

Ma K.,. Wang D. D, Lin Y., Wang J., Petrenko V., Mao C.. 2013. Synergetic Targeted Delivery of Sleeping-Beauty Transposon System to Mesenchymal Stem Cells Using LPD Nanoparticles Modified with a Phage-Displayed Targeting Peptide. Adv. Funct. Mater. 23:1172 – 1181.

Ma, Y., Zheng Y., *et al.* 2011. Novel docetaxel-loaded nanoparticles based on PCL-Tween 80 copolymer for cancer treatment. Int J Nanomedicine 6:2679-2688.

Manzoor Ahmad Gatoo *et al.*, 2014. Physicochemical Properties of Nanomaterials: Implication in Associated Toxic Manifestations, Biomed Res Int 498420.

Marrache, S.,Dhar, S. 2012. Engineering of blended nanoparticle platform for delivery ofmitochondria-acting therapeutics. Proc. Natl. Acad. Sci. U. S. A. 109:16288–16293.

Martin, 2014. The role of tight junctions in cancer metastasis. Semin Cell Dev Biol. 36:224-31.

Matsumura, Y., Maeda, H. 1986. A New Concept for Macromolecular Therapeutics in Cancer Chemotherapy: Mechanism of Tumoritropic Accumulation of Proteins and the Antitumor Agent Smancs.Cancer Research: 46:6387-6392.

Mauro N., Campora S., Scialabba C., Adamo G., Licciardi M., Ghersi G. and Giammona G. 2015. Self-organized environment-sensitive inulin–doxorubicin conjugate with a selective cytotoxic effect towards cancer cells, RSC Advances, 5: 32421-32430.

Meng X, Riordan NH, Riordan HD, Mikirova N, Jackson J, González MJ, Miranda-Massari JR, Mora E, Trinidad Castillo W. 2004. Cell membrane fatty acid composition differs between normal and malignant cell lines. P R Health Sci J., 23(2):103-6.

Miyata T., Uragami T., and Nakamae K. 2002. Biomolecule-sensitive hydrogels. Adv.Drug Deliv.Rev. 54:79-98.

Miyata, K., Y. Kakizawa, *et al.* 2004. Block catiomer polyplexes with regulated densities of charge and disulfide cross-linking directed to enhance gene expression. J Am Chem Soc 126(8):2355-2361.

Miyata, T., Uragami, T., and Nakamae, K. 2002. Biomolecule-sensitive hydrogels. Adv.Drug Deliv.Rev. 54:79-98.

Mohanraj, V. J.,Chen, Y. 2006. Nanoparticles- A Review. Trop. J. Pharm. Res. 5 (1):561 – 573.

Mrinmoy De, Partha S. Ghosh, Vincent M. Rotello. 2008. Applications of Nanoparticles in Biology, Adv. Mater. 20:4225–4241.

Mura, S., J. Nicolas, *et al.* 2013. Stimuli-responsive nanocarriers for drug delivery. Nat Mater, 12(11):991-1003.

Nagavarma B VN, Hemant K. S.Yadav, Ayaz A, Vasudha L.S, Shivakumar H.G, 2012. Different techniques for preparation of polymeric nanoparticles- a review, Asian Journal of Pharmaceutical and Clinical Research, 5(3): 0974-2441.

Nemunaitis, J.M.,Nemunaitis, J, 2008. Potential of Advexin®: a p53 gene-replacementtherapy in Li–Fraumeni syndrome, Future Oncol. 4:759–768.

Neri, D., Bicknell, R. 2005. Tumour vascular targeting. Nat. Rev. Cancer, 5:436 – 446.

Neu, M., O. Germershaus, *et al.* 2007. Crosslinked nanocarriers based upon poly(ethylene imine) for systemic plasmid delivery: in vitro characterization and in vivo studies in mice. J Control Release 118(3):370-380.

Nimjee, S.M., Rusconi, C.P., Sullenger, B.A. 2005. Aptamers: An emerging class of therapeutics.Ann Rev Med 56:555-83.

Oishi, M., Hayashi, H., Iijima, Y., Nagasaki, M. 2007. Endosomal release and intracellular delivery of anticancer drugs using pH-sensitive PEGylated nanogels, J. Mater. Chem, 17:3720–3725.

Okuzaki A., S. Kida, J. Watanabe, Z. Hirasawa, Y. Tabei. 2013. Efficient plastid transformation in tobacco using small gold particles (0.07–0.3μm). Plant Biotechnology 30: 65–72.

Owen, S. C., A. K. Doak, *et al.* 2012. Colloidal aggregation affects the efficacy of anticancer drugs in cell culture. ACS Chem Biol 7(8):1429-1435.

Ozen *et al.*, 2012. Heparin inhibits Hepatocyte Growth Factor induced motility and invasion of hepatocellular carcinoma cells through early growth response protein 1. PLoS One. 7(8):e42717.

Pang, Z., Feng, L., Hua, R., Chen, J., Gao, H., *et al.*, 2010. Lactoferrin-conjugatedbiodegradable polymersome holding doxorubicin and tetrandrine for chemotherapy of glioma rats. Mol Pharm 7:1995-2005.

Park, J.H., Von Maltzahn, G., Zhang, L., Derfus, A.M., Simberg, D., Harris, T.J., Ruoslahti, E., Bhatia, S.N., Sailor, M.J. 2009. Systematic surface engineering of magnetic nanoworms for in vivo tumor targeting. Small. 5(6):694–700.

Peppas N. A. and Bures C. D.. 2013. Glucose-Responsive Hydrogels. Encyclopedia of Biomaterials and Biomedical Engineering.

Peppas N.A., Bures P., Leobandung W., Ichikaw H.. 2000. Hydrogels in pharmaceutical formulations. European Journal of Pharmaceutics and Biopharmaceutics 50:27±46.

Prucek R., Tuček J., Kilianová M., Panáček A., Kvítek L., Filip J., Kolář M., Tománková K., Zbořil R.. 2011. The targeted antibacterial and antifungal properties of magnetic nanocomposite of iron oxide and silver nanoparticles. Biomaterials, 32(21):4704-13.

Ranganathan R *et al.*, 2012. Nanomedicine: towards development of patient-friendly drug-delivery systems for oncological applications. International Journal of Nanomedicine, **7**:1043–1060.

Ranganathan R *et al.*, 2012. Nanomedicine: towards development of patient-friendly drug-delivery systems for oncological applications. International Journal of Nanomedicine, 7:1043–1060.

Rashmi H Prabhu *et al.*, 2015. Polymeric nanoparticles for targeted treatment in oncology: current insights. Int J Nanomedicine,10: 1001–1018.

Robitzki, A. A. and Kurz R.. 2010. Biosensing and drug delivery at the microscale : novel devices for controlled and responsive drug delivery. Handb Exp Pharmacol, (197):87-112.

Ruoslahti, E. 2002. Specialization of tumour vasculature. Nat. Rev. Cancer. 2(2):83–90.

Ryman-Rasmussen JP., Riviere JE., Monteiro-Riviere NA. 2006. Penetration of Intact Skin by Quantum Dots with Diverse Physicochemical Properties. Toxicol. Sci. 91(1):159-165.

Salata OV. 2004. Applications of nanoparticles in biology and medicine. Journal of Nanobiotechnology, 2:3.

Sambruy, Y., Ferruzza, S., Ranaldi, G., De Angelis, I. 2001. Intestinal cell culture models: applications in toxicology and pharmacology. Cell BiolToxicol.17(4–5):301–317.

Schmidt, D. J., J. S. Moskowitz, *et al.* 2010. Electrically Triggered Release of a Small Molecule Drug from a Polyelectrolyte Multilayer Coating. Chem Mater, 22(23):6416-6425.

Seymour, L. W., Ferry, D. R., Anderson, D., Hesslewood, S., Julyan, P. J., Poyner, R., Doran, J., Young, A. M., Buetles, S., Kerr, D. J., Cancer Research Campaign Phase I/II

Clinical Triels committee. 2002. Hepatic Drug Targeting: Phase I Evaluation of Polymer-Bound Doxorubicin. J ClinOncol. 20(6):1668-76.

Siddiqui M. R. *et al,* 2015. Synthesis of Silver Nanoparticle: A New Analytical Approach for the Quantitative Assessment of Adrenaline, Anal Sci. 31(5):437-43.

Smith, R.A.J.,Porteous, C.M.,Gane, A.M.,Murphy, M.P. 2003. Delivery of bioactive moleculesto mitochondria in vivo. Proc. Natl. Acad. Sci. U. S. A. 100:5407–5412.

Srikanth M.*et al.,* 2012. Nanotechnology-novel therapeutics for CNS disorders. Nat Rev Neurol, 8(6): 307–318.

Sun, T., Y. S. Zhang, *et al.* 2014. Engineered nanoparticles for drug delivery in cancer therapy. Angew Chem Int Ed Engl 53(46):12320-12364.

Swami, A., Shi, J., Gadde, S., Votruba, A. R., Kolishetti, N., Farokhzad, O. C. 2012. Nanoparticles for Targeted and Temporally Controlled Drug Delivery, inSvenson, S., Prud'homme, R. K., Multifunctional Nanoparticles for Drug Delivery Applications. Part of the series Nanostructure Science and Technology, 9-29.

Szachowicz-Petelska B., I. Dobrzynska, S. Sulkowski and Z. Figaszewski. 2010. Characterization of the cell membrane during cancer transformation Journal of Environmental Biology 31(5): 845-850.

Taniguchi, Norio. 1974. On the Basic Concept of 'Nano-Technology', Proc. Intl. Conf. Prod. Eng. Tokyo, Part II, Japan Society of Precision Engineering.

Tianmeng Sun, Yu Shrike Zhang, Bo Pang, Dong Choon Hyun, Miaoxin Yang, and Younan Xia. 2014. Engineered Nanoparticles for Drug Delivery in Cancer Therapy. Nanomedicine, 53(46):12320-12364.

Tiwari M., 2012, Nano cancer therapy strategies. Journal of Cancer Research and Therapeutics, 8(1):19-22.

Torchilin, V. P., A. N. Lukyanov, *et al.* 2003. Immunomicelles: targeted pharmaceutical carriers for poorly soluble drugs. Proc Natl Acad Sci U S A 100(10):6039-6044.

Van der Zee M., J. H. Stoutjesdijk, P. A. A. W. van der Heijden and D. J. de Wit, J. Environ. 1995. Structure-biodegradation relationships of polymeric materials. 1. Effect of degree of oxidation on biodegradability of carbohydrate polymers. Polym. Degrad, 3(4): 235–242.

Van Vlierberghe S, *et al.,* 2011. Biopolymer-based hydrogels as scaffolds for tissue engineering applications: a review. Biomacromolecules, 12(5):1387-408.

Vaupel, P., F. Kallinowski, *et al.* 1989. Blood flow, oxygen and nutrient supply, and metabolic microenvironment of human tumors: a review. Cancer Res, 49(23):6449-6465.

Wang Y. C., S.Shim M., Sung H.W., Xia Y. 2014. Stimuli-Responsive Materials for Controlled Release of Theranostic Agents. Adv. Funct. Mater., 24:4206 –4220.

West, K. R. and S. Otto. 2005. Reversible covalent chemistry in drug delivery. Curr Drug Discov Technol 2(3):123-160.

Woodrow, K. A., Y. Cu, *et al.* 2009. Intravaginal gene silencing using biodegradable polymer nanoparticles densely loaded with small-interfering RNA. Nat Mater 8(6):526-533.

Xia, X. H.,Yang, M. X.,Wang, Y. C.,Zheng, Y. Q.,Li, Q. G.,Chen, J. Y.,Xia, Y. 2012. Quantifying the coverage density of poly(ethylene glycol) chains on the surface of gold nanostructures.ACS Nano 6:512 – 522.

Xing Y., Zhao J., Conti P. S., Chen K.. 2014. Radiolabeled Nanoparticles for Multimodality Tumor Imaging. Theranostics. 4(3):290-306.

Yamane S., Sasaki Y. and Akiyoshi K.. 2008. Siloxane-crosslinked Polysaccharide Nanogels for Potential Biomedical Applications. Chemistry Letters, 37(12):1282- 1283.

Yang, K., Ma, Y. Q. 2010. Computer simulation of the translocation of nanoparticles with different shapes across a lipid bilayer.Nat. Nanotechnol. 5:579 – 583.

Yun Y., *et al.*, 2012. Nanoparticles for oral delivery: Targeted nanoparticleswith peptidic ligands for oral protein delivery, Adv. Drug Deliv. Rev. 65(6):822-32.

Zhang, L., Zhu, D., Dong, X., Sun, H., Song, C., Wang, C., Kong, D. 2015. Folate-modified lipid–polymer hybrid nanoparticles for targeted paclitaxel delivery.Int J Nanomedicine, 10:2101–2114.

Zhu, L., P. Kate, *et al.* 2012. Matrix metalloprotease 2-responsive multifunctional liposomal nanocarrier for enhanced tumor targeting. ACS Nano 6(4):3491-3498.

Zuleger S., Lippold B. C.. 2001. Polymer particles erosion controlling drug release. I. Factors influencing drug release and characterization of the release mechanism. Int. J. Pharm., 217:139 – 152.